Properties of Non-Equilibrium States: Dense Colloidal Suspensions under Steady Shearing

Dissertation

zur Erlangung des akademischen Grades des Doktors der Naturwissenschaften an der Universität Konstanz im Fachbereich Physik, Lehrstuhl Prof. Dr. Matthias Fuchs,

vorgelegt von

Matthias Helmut Günter Krüger

Tag der Einreichung: 9. Februar 2009
Tag der mündlichen Prüfung: 9. April 2009

1. Referent: Prof. Dr. Matthias Fuchs
2. Referent: Prof. Dr. Jörg Baschnagel

Acknowledgments

A lot of people contributed to this thesis in different ways. First, I would like to thank Prof. Matthias Fuchs for the opportunity to work under his supervision. I profitted enormously from his instructions and our discussions. He was always available when I needed help. I also thank him for being very exacting concerning my results, which forced me to optimize my arguments and helped me to separate helpful from meaningless ideas.

I am grateful to Prof. Jörg Baschnagel, the second referee of the thesis, for various discussions. He made it possible for me to spend two inspiring months in his group at the Institut Charles Sadron in Strasbourg for which I thank him.

I acknowledge financial support from the "Deutsche Forschungsgemeinschaft" in the International Research Training Group (IRTG) "Soft Condensed Matter". The IRTG gave me the opportunity to participate in various seminars and workshops. I would also like to thank the "Studienstiftung des deutschen Volkes" for its support and the possibility to participate in several seminars for doctoral students.

I acknowledge the discussions with Dr. Joseph M. Brader on all kinds of topics as well as the competitions on the badminton court. It was simply good to hear his opinion about things. I also thank Dr. Thomas Voigtmann. For me, he is the "MCT-encyclopedia" on two legs and he immediately understands my points in our discussions.

Special thanks go to all my colleagues in the group who enriched the daily life. Dr. Thomas Voigtmann, Dr. Joseph M. Brader and Christof Walz are acknowledged for a critical reading of the manuscript. I thank Fabian Weyßer for discussions within our beginning theory-simulation collaboration.

I also acknowledge discussions with Prof. Jean-Louis Barrat, Prof. Michael E. Cates, Prof. Udo Seifert, Dr. Andrea Gambassi, Dr. Patrick Ilg and Dr. Igor Gazuz. They helped me find my way through the FDT-violation jungle.

The members of the Baschnagel-group in Strasbourg made my stay there a great pleasure for which I thank especially the young generation. I also acknowledge the inspiring discussions with Dr. Joachim Wittmer.

My parents, Dr. Ekkehard und Gisela Krüger, supported me in uncountable many ways for which I want to thank them.

Final and special thanks go to Anja Ging for her support, especially during the last weeks. She is also acknowledged for a critical reading of the manuscript and comments from the literature-studies point of view.

Contents

1 Introduction

1.1 Preamble

Paul is very drunk. He has lost control over his feet and his steps are random and uncorrelated. Because of this, it seems likely that Paul will move into the wrong direction and not find his way home. But since he is a physicist, he takes advantage of a very fortunate coincidence: The street has a slight gradient pointing directly to his home. He knows he is safe because, due to this gradient in the street, his walk is not completely random. He will adopt a small mean velocity which will eventually lead him home. After some time he reaches a pedestrian crossing, where lots of people cross the street, their velocities being perpendicular to his. The density of the pedestrians is very high over an appreciably wide band. Paul enters the pedestrian band (he has no means to prevent it). In the band he encounters many collisions with the pedestrians, they are pushing him in arbitrary directions. Sometimes they even push him uphill, away from his home. He realizes that his dynamics is now *very fast* due to the pushes by the pedestrians. But these pushes seem to be hardly influenced by the gradient of the street, his average velocity *remains roughly unchanged*. He starts wondering: "Am I violating some fundamental physics law?"

The expert reader has noticed that in the example above, the drunken walker misses the heat bath, which is one of the important essences of the law he is violating; the fluctuation dissipation theorem (FDT). It is indeed a fundamental law that describes the relation between thermal fluctuations (the random steps of the drunken walker) and the response to a small external force (the mean velocity due to the gradient in the street). The law holds in equilibrium. In systems out of equilibrium, it does not hold in general. The drunken walker realizes that his fluctuations are stronger when he enters the (driven) pedestrian region, while his average velocity is roughly unchanged. The ratio of response and fluctuations is different compared to the case without the pedestrians.

In this thesis, we will investigate the violation of the fluctuation dissipation theorem for dense Brownian particles under shear near the glass transition. The study is motivated by simulations [1] of this system, where a very peculiar violation of the theorem was found: The non-equilibrium state seems to be characterized by a so called effective temperature that replaces the real temperature in the fluctuation dissipation theorem. During the theoretical investigation of this phenomenon, it turned out that the description involves different correlation functions describing the fluctuations in the sheared system. After a general introduction of the system in this chapter, we will hence first study these different correlation functions and investigate their similarities and differences. Following this, we will study a specific class of observables, namely the

fluctuations of a tagged particle and its mean squared displacement. These variables were the focus of investigation in the simulations in Ref. [1]. In Chap. 3, we will study their dynamics which is necessary to be able to study their FDT version in Chap. 4. Considering the dynamics, we will additionally encounter an interesting effect, the particle motion parallel to the shear direction is not diffusive at long times. This is known as Taylor dispersion for low particle densities. But how will this relation look near the glass transition? In Chap. 4 we will finally turn to the fluctuation dissipation theorem and study its version for the system under shear. To a first approximation we find a universal law for glassy states, which has intriguing similarities to the ones that were found in non-equilibrium spin models. Our studies will yield results which are in good agreement with the simulation results, differing only in one detail. This detail is important though, since our findings contradict the interpretation of this violation in terms of an effective temperature. After this approximative treatment of the response functions, a more general and exact relation is derived in Chap. 5. It shows that the violation of the equilibrium FDT is connected to the non-Hermiticity of the time evolution operator and gives further insights into the system under shear. In the last chapter finally, the physical reason for the violation of the equilibrium FDT will be illuminated. The chapter closes with the study of a very simple toy model which allows to illustrate many phenomena encountered in this thesis, thus contributing to their understanding.

1.2 The System: Dense Colloidal Particles under Shear

The system under consideration is a suspension of over-damped spherical Brownian particles, so called colloids, interacting with each other via – in the simplest case – a hard sphere potential. At high density, this suspension is one of the most simple viscoelastic systems, i.e., under external deformation it exhibits both dissipative behavior, like a Newtonian fluid, and elastic behavior, like a solid [2]. It is therefore often referred to as soft (metastable) solid and shows many interesting phenomena which will be briefly discussed below.

The Brownian particles are typically in the size range from a few nm to μm, i.e., they are much larger than water molecules but still small enough to feel the thermal fluctuations. Since the observation timescale of the colloids is much larger than the timescale on which the water molecules fluctuate, one can introduce an idealized picture, where the colloids are subject to short, random forces. The colloids thus perform random walks. Quantum effects play no role. Due to their mutual interactions, their motion is hindered and the dynamics is slowed down in comparison to an isolated particle. This effect is the more drastic the higher the density of particles. At a certain density, the particles hinder each other so much that they cannot get past each other any more and the system freezes in; it undergoes a transition from an ergodic to a non-ergodic state, called the glass transition, which was verified for colloidal particles experimentally [3–9]. If the system is monodisperse, i.e., all particles have the same size, it will crystallize before the glass transition density is reached. To avoid crystallization, one can for example use particles with a small degree of polydispersity. In the glassy state, each

particle is trapped in a cage formed by the surrounding particles. It is very hard or even impossible to calculate the transition density exactly because it is a collective phenomenon and cannot be treated by considering the motion of a single particle while keeping the other ones fixed. An approximate theory that very successfully describes the glass transition is the mode coupling theory (MCT) [10].

Another phenomenon connected to the glass transition is aging; if the density of the particles is increased rapidly ("quenched") to the glassy phase (or if, for soft particles the temperature is rapidly decreased below the transition temperature), the system falls out of equilibrium. It is not in the global energy minimum which it can reach only very slowly due to its glassy nature. The outcome of measurements will depend on the amount of time elapsed since the quench; the system changes slowly with time, it "ages". The described phenomenology can be found e.g. in Ref. [11].

While the glass transition of hard spheres (or of super-cooled liquids) has been studied for many years, it is still a great challenge to describe systems close to the glass transition under external driving. We will consider the simplest external driving, namely a steady homogeneous shear flow. This is currently also the subject of experimental studies [12–14]. We will consider space translationally invariant systems, where the gradient of the flow velocity of the particles is constant, i.e., we do not consider phenomena like shear banding [15], where this is not the case. Also, the increase of the viscosity at higher shear rates, the so called shear thickening [16] attributed to hydrodynamic interactions, and the jamming transition at somewhat higher densities and shear rates [11, 17] will not be issues for our small-shear studies. For small shear rates, one usually observes shear thinning, i.e., the viscosity decreases with shear rate. Aging effects are absent in the time translationally invariant steady state under shear. See e.g. the reviews in Refs. [18, 19].

The sheared system under consideration hence reaches a steady state, but it is out of equilibrium. This causes many new and interesting phenomena. The system under shear is ergodic even when the un-sheared system is glassy, i.e., due to the shear, the particles can explore all (phase-) space. The dynamics of the system is governed by shear at arbitrary small shear rates. Due to this, many observables are non analytic in shear rate which leads to non-trivial limiting values. The most famous example is the yield stress, which will be introduced in Sec. 1.6.4. As we will see in Chap. 4, the violation of the fluctuation dissipation theorem also shows such a non-trivial limit in glassy states.

1.3 Microscopic Starting Point

We consider a system of N spherical particles of diameter d, dispersed in a solvent, see Fig. 1.1. The system has volume V. The particles have bare diffusion constants $D_0 = k_B T \mu_0$, with mobility μ_0 and $k_B T$ is the thermal energy. The interparticle force acting on particle i ($i = 1 \dots N$) at position $\mathbf{r}_i$ is given by $\mathbf{F}_i = -\partial/\partial \mathbf{r}_i U(\{\mathbf{r}_j\})$, where U is the total potential energy. In an experimental system, also hydrodynamic interactions between the particles are present [20]; if particle i moves, it causes the surrounding solvent to move as well. The moving solvent affects the motion of the other particles,

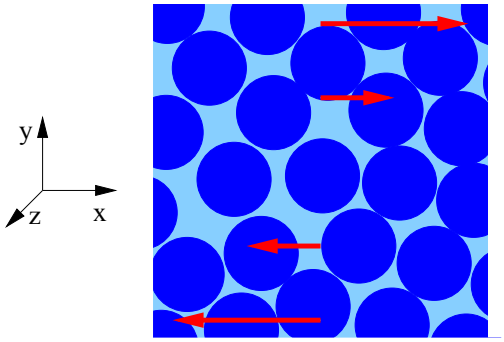

Figure 1.1: The considered system: A dense colloidal suspension under shear. The spacial directions are referred to as flow (x), gradient (y) and neutral (z) direction.

which in turn affects the solvent velocity and on this way particle i again. We will neglect hydrodynamic interactions to keep the theoretical description as simple as possible. Also, one assumes that they are less important for the slow glassy systems under consideration [18]. We will compare our results mostly to computer simulations, where hydrodynamic interactions are absent.

The external driving, viz. the shear, acts on the particles via the solvent flow velocity $v(\mathbf{r}) = \dot{\gamma} y \hat{\mathbf{x}}$, i.e., the flow points in x-direction and varies in the y-direction. $\dot{\gamma}$ is the shear rate. Due to the solvent velocity, the friction force of the solvent on particle i is not proportional to its velocity, but proportional to the difference of this velocity to the solvent velocity at $\mathbf{r}_i$. This leads to the equation of motion for the particles, namely the Langevin equation that misses in the over-damped system an inertia term,

$$\frac{\partial \mathbf{r}_i}{\partial t} - \mathbf{v}(\mathbf{r}_i) = (\mathbf{F}_i + \mathbf{f}_i)\,\mu_0. \tag{1.1}$$

Different particles are coupled by the forces $\mathbf{F}_i$. $\mathbf{f}_i$ is the random force, representing the thermal activations by the solvent molecules. It satisfies (α and β denote directions)

$$\left\langle f_i^\alpha(t) f_j^\beta(t') \right\rangle = 2\frac{k_B T}{\mu_0}\delta_{\alpha\beta}\delta_{ij}\delta(t-t'). \tag{1.2}$$

Eq. (1.2) expresses that the random forces in different directions, on different particles, and at different times are uncorrelated. The pre-factor must be chosen such that the random force obeys the fluctuation dissipation theorem. One can show that from Eq. (1.2) the mean squared displacement of a free particle equals $2D_0t$. For the theoretical description of the system it is more handy to use an equivalent formulation to Eq. (1.1), namely the Smoluchowski equation. It is an equation for the particle distribution func-

tion $\Psi(\Gamma \equiv \{\mathbf{r}_i\}, t)$ [20, 21],

$$\begin{aligned} \partial_t \Psi(\Gamma, t) &= \Omega\, \Psi(\Gamma, t), \\ \Omega &= \Omega_e + \delta\Omega = \sum_i \boldsymbol{\partial}_i \cdot [\boldsymbol{\partial}_i - \mathbf{F}_i - \boldsymbol{\kappa} \cdot \mathbf{r}_i], \end{aligned} \tag{1.3}$$

with $\boldsymbol{\kappa} = \dot{\gamma}\hat{\mathbf{x}}\hat{\mathbf{y}}$ for the case of simple shear. Ω is called the Smoluchowski operator (SO) and it is built up by the equilibrium SO, $\Omega_e = \sum_i \boldsymbol{\partial}_i \cdot [\boldsymbol{\partial}_i - \mathbf{F}_i]$ of the system without shear and the shear term $\delta\Omega$. We introduced dimensionless units $d = k_B T = D_0 = 1$, which will be used throughout the thesis unless stated otherwise. In contrast to Eq. (1.1), Eq. (1.3) has the advantage that it contains no random element. Nevertheless, it cannot be solved exactly for the many particle system [22]. Without shear, the system reaches the equilibrium distribution Ψ_e, i.e., $\Omega_e \Psi_e = 0$. Under shear, the system is assumed to reach the stationary distribution Ψ_s with $\Omega\Psi_s = 0$. Ensemble averages in equilibrium and in the stationary state are denoted

$$\langle \dots \rangle = \int d\Gamma \Psi_e(\Gamma) \dots, \tag{1.4a}$$

$$\langle \dots \rangle^{(\dot{\gamma})} = \int d\Gamma \Psi_s(\Gamma) \dots, \tag{1.4b}$$

respectively. In the stationary state, the distribution function is constant but the system is still not in thermal equilibrium due to the non-vanishing probability current $\mathbf{j}_i^s$ [21],

$$\mathbf{j}_i^s = [-\boldsymbol{\partial}_i + \mathbf{F}_i + \boldsymbol{\kappa} \cdot \mathbf{r}_i]\Psi_s. \tag{1.5}$$

In thermal equilibrium at $\dot{\gamma} = 0$ the probability current vanishes, i.e., the system obeys detailed balance [21]. In the steady state only the divergence of the current vanishes, not the current itself,

$$\sum_i \boldsymbol{\partial}_i \cdot \mathbf{j}_i^s = -\Omega\Psi_s = 0. \tag{1.6}$$

1.3.1 Low Density Limit – Taylor Dispersion

For the case of a single particle under shear, the Smoluchowski equation for the probability density $P(\mathbf{r}, \mathbf{r}_0, t)$ can be solved and shall be shortly sketched here because we will compare some of our results to the low density case. It reads (with restored units) [20]

$$\frac{\partial}{\partial t} P(\mathbf{r}, \mathbf{r}_0, t) = \left(D_0 \boldsymbol{\partial} \cdot \boldsymbol{\partial} - \dot{\gamma} y \frac{\partial}{\partial x} \right) P(\mathbf{r}, \mathbf{r}_0, t). \tag{1.7}$$

For initial condition $P(\mathbf{r}, \mathbf{r}_0, 0) = \delta(\mathbf{r} - \mathbf{r}_0)$ one finds analytically,

$$\begin{aligned} P(\mathbf{r}, \mathbf{r}_0, t) = \frac{1}{8\pi^{3/2}\sqrt{{D_0}^3 t^3 \left(\frac{\dot{\gamma}^2 t^2}{12} + 1\right)}} \exp\Bigg(& \frac{-\left(\frac{\dot{\gamma}^2 t^2}{3} + 1\right)(y - y_0)^2}{4D_0 t \left(\frac{\dot{\gamma}^2 t^2}{12} + 1\right)} \\ & + \frac{\dot{\gamma} t (x - x_0 - \dot{\gamma} t y_0)(y - y_0) - (x - x_0 - \dot{\gamma} t y_0)^2}{4D_0 t \left(\frac{\dot{\gamma}^2 t^2}{12} + 1\right)} - \frac{(z - z_0)^2}{4D_0 t} \Bigg). \end{aligned} \tag{1.8}$$

From this one can determine the mean squared displacements (MSDs) of the particle in the different directions,

$$\left\langle (z-z_0)^2 \right\rangle^{(\dot\gamma)} = \left\langle (y-y_0)^2 \right\rangle^{(\dot\gamma)} = 2\,D_0\,t, \tag{1.9a}$$

$$\left\langle (x-x_0)^2 \right\rangle^{(\dot\gamma)} = 2\,D_0\,t + y_0^2\,\dot\gamma^2 t^2 + \frac{2}{3}\,D_0\,\dot\gamma^2\,t^3. \tag{1.9b}$$

$$\left\langle (x-x_0)(y-y_0) \right\rangle^{(\dot\gamma)} = D_0\,\dot\gamma\,t^2. \tag{1.9c}$$

The mean squared displacements in directions perpendicular to the shear flow are unaffected by it. In x-direction the MSD is not diffusive but grows with power t^3 for long times. The physical reason is that a fluctuation of the particle in gradient direction leads to an increase of the velocity in x-direction, because the flow velocity is a function of y. The MSD in x-direction also contains a ballistic term due to the average velocity of the particle of $\dot\gamma y_0$. The non-diffusive motion in flow direction is called Taylor dispersion [23–26]. There is an additional correlation between the x- and y-direction as seen in (1.9c), which is not present without shear. In Chap. 3 we will derive the Taylor dispersion for systems near the glass transition.

1.4 Integration Through Transients (ITT) Approach

In contrast to the equilibrium distribution, $\Psi_e \propto e^{-U/k_BT}$, the stationary distribution is not known, and stationary averages will be calculated with the following trick [21]. Considering instantaneous switch-on of the external shearing, we have

$$\Omega(t) = \begin{cases} \Omega_e & \text{before switch-on,} \\ \Omega & \text{after switch-on.} \end{cases} \tag{1.10}$$

The formal solution of the Smoluchowski equation (1.3) for the distribution at time t_w after switch-on of the rheometer is then given by

$$\Psi(t_w) = e^{\Omega t_w}\,\Psi_e = \Psi_e + \int_0^{t_w} ds\, e^{\Omega s}\,\Omega\,\Psi_e. \tag{1.11}$$

When averaging with $\Psi(t_w)$, one can perform partial integrations to get

$$\int d\Gamma \Psi(t_w) \cdots = \int d\Gamma \Psi_e \cdots + \int_0^{t_w} ds \int d\Gamma \Psi_e \sigma_{xy} e^{\Omega^\dagger s} \ldots. \tag{1.12}$$

$\sigma_{xy} = -\sum_i F_i^x y_i$ is a microscopic stress tensor element and $\Omega^\dagger = \sum_i [\boldsymbol{\partial}_i + \mathbf{F}_i + \mathbf{r}_i \cdot \boldsymbol{\kappa}^T] \cdot \boldsymbol{\partial}_i$ is the adjoined SO that arose from partial integrations. In Eq. (1.12) it acts on everything which is averaged with $\Psi(t_w)$. Averages in the stationary state are finally obtained by letting t_w go to infinity,

$$\langle \ldots \rangle^{(\dot\gamma)} = \int d\Gamma \Psi_e \cdots + \int_0^{\infty} ds \int d\Gamma \Psi_e \sigma_{xy} e^{\Omega^\dagger s} \ldots. \tag{1.13}$$

The stationary distribution is hence expressed as integration over the transient dynamics.

1.5 Correlation Functions

The time dependent correlation of the fluctuation δf of a function $f(\{\mathbf{r}_i\})$, $\delta f = f - \langle f \rangle$[1], with the fluctuation of a function $g(\{\mathbf{r}_i\})$ is a measure for the dynamics of the system. We will mostly consider auto-correlations, $\delta g = \delta f$, but give the definitions in general terms. General correlations will carry subscripts fg, auto-correlations the single subscript f. The following correlation functions are derived via the joint probability $W_2(\Gamma\, t, \Gamma'\, 0)$ that the system is at point (Γ, t), after it was in a state Γ' at $t = 0$. It is given by [21]

$$W_2(\Gamma\, t, \Gamma 0) = P(\Gamma t|\Gamma' 0)\Psi_0(\Gamma') = e^{\Omega(\Gamma)t}\delta(\Gamma - \Gamma')\Psi_0(\Gamma'), \tag{1.14}$$

because the conditional probability P obeys the Smoluchowski equation [22]. $\Psi_0(\Gamma')$ denotes the distribution at the time when the correlation is started ($t = 0$). The so far unspecified correlation function $C_{\mathrm{fg}}^{(0)}$ of f and g is then given by

$$C_{\mathrm{fg}}^{(0)}(t) = \int d\Gamma \int d\Gamma' W_2(\Gamma\, t, \Gamma'\, 0)\delta f^*(\Gamma')\delta g(\Gamma). \tag{1.15}$$

In the time translationally invariant stationary state, we measure the time dependent correlation following from $\Psi_0(\Gamma') = \Psi_s(\Gamma')$,

$$C_{\mathrm{fg}}(t) = \left\langle \delta f^* e^{\Omega^\dagger t}\delta g \right\rangle^{(\dot\gamma)}. \tag{1.16}$$

It is the correlation which is mostly considered in experiments and simulations of sheared suspensions. At this point, we would like to introduce three more correlation functions, which will appear in this thesis. The first is the transient correlator $C_{\mathrm{fg}}^{(t)}$, which is observed when the external shear is switched on at $t = 0$. For it, we have $\Psi_0(\Gamma') = \Psi_e(\Gamma')$ in Eq. (1.14) leading to

$$C_{\mathrm{fg}}^{(t)}(t) = \left\langle \delta f^* e^{\Omega^\dagger t}\delta g \right\rangle. \tag{1.17}$$

It probes the dynamics in the transition from equilibrium to steady state and is the central object of the MCT-ITT approach for colloidal suspensions under shear [21, 27]. It is a nontrivial statement that the expression in Eq. (1.17) is actually the quantity observed in experiments or simulations when switching on the shear at $t = 0$. Intuitively, one would expect that the distribution with which to average in (1.17) must be time dependent. This intuition is wrong. In the general case, where the correlation is started a period t_w, namely the waiting time, after the rheometer was switched on, one observes the two-time correlator $C_{\mathrm{fg}}(t, t_w)$, see Fig. 1.2. We have $\Psi_0(\Gamma') = \Psi(\Gamma', t_w)$ in Eq. (1.14) and with Eq. (1.12), $C_{\mathrm{fg}}(t, t_w)$ follows,

$$C_{\mathrm{fg}}(t, t_w) = \left\langle \delta f^* e^{\Omega^\dagger t}\delta g \right\rangle + \dot\gamma \int_0^{t_w} ds \left\langle \sigma_{xy} e^{\Omega^\dagger s}\delta f^* e^{\Omega^\dagger t}\delta g \right\rangle. \tag{1.18}$$

[1] The average of f is taken with the respective distribution of the correlation, e.g. with Ψ_s for the stationary correlation.

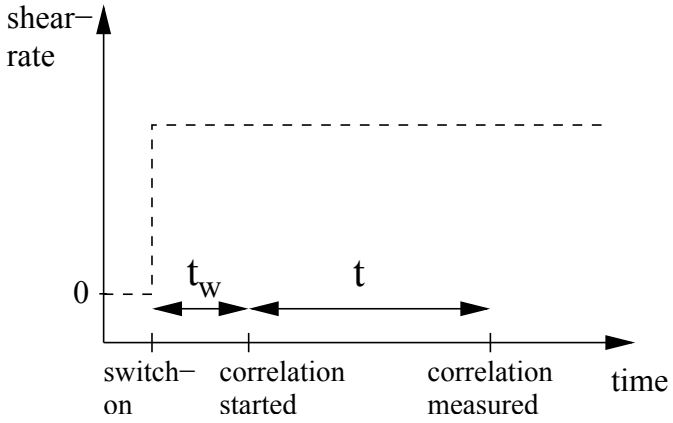

Figure 1.2: Definition of the waiting time t_w and the correlation time t after switch-on of the rheometer.

This correlator will be discussed in Chap. 2. Without shear, one finally observes the equilibrium correlation derived from setting Ω to Ω_e and $\Psi_0(\Gamma') = \Psi_e(\Gamma')$,

$$C_{\mathrm{fg}}^{(e)} = \left\langle \delta f^* e^{\Omega_e^\dagger t} \delta g \right\rangle . \tag{1.19}$$

We will see in Sec. 1.6 that this correlator does in general not decay to zero in glassy states, it reflects the non ergodicity of the system.

1.6 Mode Coupling Theory: Dynamics and Shear Stress

In this section we will discuss the dynamics of colloidal suspensions near the glass transition under shear and shortly sketch the equations of motion and the major properties of their solutions.

1.6.1 Density Correlations

The central quantity in mode coupling theory (MCT) is the density $\varrho_{\mathbf{q}} = \sum_i e^{i\mathbf{q}\cdot\mathbf{r}_i}$ with particle positions $\mathbf{r}_i$, the Fourier transform of the particle density in real space $\varrho(\mathbf{r}) = \sum_i \delta(\mathbf{r} - \mathbf{r}_i)$. It is assumed to be the relevant variable to describe the glassy dynamics of the system. In the MCT-ITT approach for colloidal suspensions under shear [21, 27, 28], see also the recent review [18], the starting point is the normalized transient correlator for the densities, $\delta f = \delta g = \varrho_{\mathbf{q}}$, which reads

$$\Phi_{\mathbf{q}}(t) = \frac{1}{N S_q} \left\langle \varrho_{\mathbf{q}}^* e^{\Omega^\dagger t} \varrho_{\mathbf{q}(t)} \right\rangle . \tag{1.20}$$

$S_q = \langle \varrho_{\mathbf{q}}^* \varrho_{\mathbf{q}} \rangle / N$ is the static structure factor of the system without shear [29]. $\Phi_{\mathbf{q}}(t)$ is called the *coherent* density correlator, coherent denoting the fact that the densities contain sums over all particles. $\Phi_{\mathbf{q}}(t)$ is hence a collective quantity. The *incoherent*

density correlator in contrast contains only the density of one tagged particle. On the right hand side one uses the advected wavevector,

$$\mathbf{q}(t) = \mathbf{q} - \mathbf{q} \cdot \boldsymbol{\kappa} t, \tag{1.21}$$

which appears due to translational invariance of the considered infinite system [21]. Note that the correlator for non-interacting particles with zero diffusivity, $D_0 = 0$, is unity for all times [18], i.e., via the advected wavevector the average shear-motion of the particles is subtracted. The equation of motion for $\Phi_{\mathbf{q}}(t)$ is derived within the Zwanzig-Mori projection operator formalism [30–33], see Ref. [34]. It is generally used to separate the slow degrees of freedom of the system from the fast degrees which simplifies the description of the relevant slow dynamics. Consider the motion of a single colloid in water. In principle, one would have to take into account the movement of each single water molecule and its interaction with the colloid. But if we are interested in the dynamics of the colloid only, i.e., in the slow dynamics, we can rewrite the set of numerous coupled equations into one single equation for the colloid, namely into the Langevin equation, where the motion of the water molecules is implemented as random force, see Eq. (1.1). In MCT, one assumes that the important slow variables of the system are the density fluctuations and therefore uses the projector

$$P = \varrho_{\mathbf{q}} \rangle \langle \varrho_{\mathbf{q}}^* \varrho_{\mathbf{q}} \rangle^{-1} \langle \varrho_{\mathbf{q}}^* \tag{1.22}$$

which projects on the subspace containing the slow variables. P has complement $Q = 1 - P$. After some calculation steps which will be demonstrated in more detail in Chap. 3 for the incoherent case, this leads to the following equation of motion [21, 27]

$$\partial_t \Phi_{\mathbf{q}}(t) + \Gamma_{\mathbf{q}}(t) \left\{ \Phi_{\mathbf{q}}(t) + \int_0^t dt' \, m_{\mathbf{q}}(t,t') \partial_{t'} \Phi_{\mathbf{q}}(t') \right\} = 0, \tag{1.23}$$

where

$$\Gamma_{\mathbf{q}}(t) = -\frac{\left\langle \varrho_{\mathbf{q}(t)}^* \Omega_e^\dagger \varrho_{\mathbf{q}(t)} \right\rangle}{S_q} = \frac{q^2(t)}{S_q} \tag{1.24}$$

is the initial decay rate, which is time dependent under shear. From Eq. (1.23) we have $\partial_t \Phi_{\mathbf{q}}(t)|_{t=0} = -\Gamma_{\mathbf{q}}(0)$. The memory function $m_{\mathbf{q}}(t,t')$ causes the slow decay of the correlator at high densities. Under shear, it decays to zero also for glassy states due to the advection of the wavevectors. It depends explicitely on t and t' instead of $t - t'$ as in MCT for the quiescent system [35, 36]. It is approximated as functional of the correlator itself to close the equation

$$m_{\mathbf{q}}(t,t') = \mathcal{F}_{\mathbf{q}}(t,t',\Phi(t-t')). \tag{1.25}$$

Then the only input parameter to the theory is the equilibrium structure factor S_q. The MCT approach for systems without shear is reviewed in Refs. [37–42]. A slightly different equation of motion for the dynamics under shear within MCT was derived in Refs. [43, 44].

1.6.2 Glass Transition and β-Analysis

Eq. (1.23) and the version without shear have been subject of intense research over the last decades. They contain the glass transition from an ergodic to a non-ergodic system. The transition density was found to be at packing fraction of $\phi_c = n_c \frac{\pi}{6} d^3 \approx 0.52$ [35], with number density $n = N/V$. This is quite close to the experimental finding of $\phi_c \approx 0.58$. While this transition is a collective effect, i.e., it happens for all wavevectors q at the same density, the shape of $\Phi_{\mathbf{q}}(t)$ (for both with and without shear) depends on $\mathbf{q}$. For densities below the glass transition, the correlator for the system without shear decays to zero with time scale τ, the so called α-relaxation time. The effect of shear does then depend on the dressed Peclet or Weissenberg number $Pe = \dot{\gamma}\tau$. For small shear rates, the effect vanishes,

$$\lim_{\dot{\gamma}\to 0} \Phi_{\mathbf{q}}(t) \to \Phi_q^{(e)}(t), \qquad \text{liquid.} \tag{1.26}$$

Above or at the critical density, the correlator without shear stays on the plateau characterized by the non-ergodicity parameter f_q,

$$\lim_{t\to\infty} \Phi_q^{(e)}(t) = f_q, \qquad \text{glass.} \tag{1.27}$$

At the transition, f_q jumps discontinuously from zero to a finite value. The system under shear is always ergodic and $\Phi_{\mathbf{q}}(t)$ decays to zero for any finite $\dot{\gamma}$. Since glassy systems are frozen in without shear, the final decay from the plateau to zero is governed solely by shear, for arbitrarily small $\dot{\gamma} \to 0$. The dressed Peclet number is always infinity because τ is formally infinity. This brings about the interesting phenomena observed for shear molten glasses.

The bare Peclet number $Pe_0 = \dot{\gamma}\, d^2/D_0$ (or $\dot{\gamma}/\Gamma$ in the schematic model introduced below) describes the separation of the short time decay onto the plateau from the long time decay to zero. For $Pe_0 \to 0$, the two dynamics are well separated. In the following, $\dot{\gamma} \to 0$ refers to $Pe_0 \to 0$ in glassy and to $Pe \to 0$ in liquid states.

The so called β-analysis provides more insight into the dynamics near the critical plateau f_q^c. For ϕ near ϕ_c and $\dot{\gamma} \to 0$, the transient correlator is expanded around the critical plateau value f_q^c [21],

$$\Phi_{\mathbf{q}}(t) = \Phi_q(t) = f_q^c + h_q \mathcal{G}(t). \tag{1.28}$$

$\mathcal{G}(t)$ is called β-correlator. It is a nontrivial finding that the correlator in Eq. (1.28) is isotropic in space under shear. Inserting this into Eq. (1.23), one finds for $|\mathcal{G}(t)| \ll 1$ the β-equation of motion,

$$\tilde{\varepsilon} - c^{(\dot{\gamma})}(\dot{\gamma}t)^2 + \lambda \mathcal{G}^2(t) = \frac{\partial}{\partial t} \int_0^t dt' \mathcal{G}(t-t')\mathcal{G}(t'). \tag{1.29}$$

Where $\tilde{\varepsilon} = C\varepsilon = C(\phi - \phi_c)/\phi_c$ with $C \approx 1.3$ describes the distance from the transition point and the other parameters, $\lambda \approx 0.73$ and $c^{(\dot{\gamma})} \approx 0.7$ can be directly calculated from the functional $\mathcal{F}_{\mathbf{q}}$ and the static equilibrium structure factor. Note that the terms of

order $\mathcal{G}^0$ and $\mathcal{G}^1$ cancel in Eq. (1.29) at the critical point. This is explained in great detail in Ref. [10]. The short time behavior of $\mathcal{G}(t)$ must be matched to the short time dynamics of the correlator, $\mathcal{G}(t \to 0) = (t_0/t)^a$, where the matching time t_0 is determined by the initial decay rate Γ_q. The critical exponent a obeys (with the Γ-function) $\lambda = \Gamma^2(1-a)/\Gamma(1-2a)$. From Eq. (1.29), we see that the β-correlator is of order $\sqrt{\varepsilon}$ and $\dot\gamma t$, a fact which we will use in Chap. 3 when expanding the incoherent correlator around the critical plateau. See Ref. [27] for more details on the two parameter scaling relation for $\dot\gamma t$ and ε. The β-correlator takes for $\varepsilon = 0$ the solution for long times [27],

$$\mathcal{G}(\varepsilon = 0, t \gg t_0) = -\sqrt{\frac{c^{(\dot\gamma)}}{\lambda - \frac{1}{2}}}|\dot\gamma| t \equiv -\tilde t, \tag{1.30}$$

Eq. (1.30) describes the initialization of the final shear induced decay from the plateau to zero. For $\varepsilon > 0$, one has to consider two time regimes. For intermediate times, one has

$$\mathcal{G}(\varepsilon > 0, t_0 \ll t \ll t_b) = \sqrt{\frac{\tilde\varepsilon}{1-\lambda}}\left[1 - \frac{c^{(\dot\gamma)}}{2}\left(\frac{t}{t_b}\right)^2 + \dots\right], \tag{1.31}$$

describing the initial decay from the plateau of height $f = f^c + h_q\sqrt{\tilde\varepsilon/(1-\lambda)}$ down to zero. $t_b = \sqrt{\varepsilon}/|\dot\gamma|$ is the upper limit of this regime, where the expansion in (1.31) breaks down. For longer times, the β-correlator merges into a law equivalent to the one for $\varepsilon = 0$,

$$\mathcal{G}(\varepsilon > 0, t \gg t_b) = -\tilde t. \tag{1.32}$$

The shear independent decay from the plateau for the liquid case can be found in Refs. [10, 45, 46].

1.6.3 α-Scaling

We saw that the β-correlator $\mathcal{G}(t)$ for $\varepsilon \geq 0$, $\dot\gamma \to 0$ and $\dot\gamma t = const.$ is a function of $\tilde t \propto |\dot\gamma| t$, i.e., the timescale for the final decay is linear in inverse shear rate and independent of the initial decay rate (i.e. D_0). The correlator $\Phi_{\mathbf{q}}(t)$ reaches a scaling function $\Phi^+_{\mathbf{q}}(\tilde t)$. Approximating $m_{\mathbf{q}}(t,t') \approx \tilde m_{\mathbf{q}}(t-t')$, the scaling equation for $\Phi^+_{\mathbf{q}}(t)$ is found after partial integrations [27],

$$\Phi^+_{\mathbf{q}}(\tilde t) = \tilde m^+_{\mathbf{q}}(\tilde t) - \frac{d}{d\tilde t}\int_0^{\tilde t} d\tilde t' \tilde m^+_{\mathbf{q}}(\tilde t - \tilde t')\Phi^+_{\mathbf{q}}(\tilde t'). \tag{1.33}$$

Here $\tilde m^+_{\mathbf{q}}(\tilde t)$ is given by $\tilde m_{\mathbf{q}}(t-t')$ evaluated with $\Phi^+_{\mathbf{q}}(\tilde t)$. The initial condition for Eq. (1.33) is $\Phi^+_{\mathbf{q}}(\tilde t = 0) = f_q$. Eqs. (1.30-1.32) give the short time terms for $\Phi^+_{\mathbf{q}}(\tilde t)$, and one has for $\varepsilon = 0$,

$$\Phi^+_{\mathbf{q}}(\tilde t \to 0) = f^c_q - h_q \tilde t. \tag{1.34}$$

The linear scaling of the final relaxation time with $\dot\gamma^{-1}$ is called yield scaling, because it leads to the yield stress as described in Sec. 1.6.4 below. In Chap. 3, where we discuss the incoherent correlator, we will derive an α-scaling equation without approximating $m^{(s)}_{\mathbf{q}}(t,t')$ as function of $t-t'$.

1.6.4 Shear Stress

One of the central quantities to be measured in rheological experiments is the shear stress σ [13, 47, 48] that is related to the shear viscosity η by

$$\sigma = \dot{\gamma}\eta. \tag{1.35}$$

σ is the average value of the stress tensor element $\sigma_{xy} = -\sum_i F_i^x y_i$,

$$\sigma = \frac{1}{V}\left\langle \sigma_{xy} \right\rangle^{(\dot{\gamma})}. \tag{1.36}$$

Via the ITT approach (1.13), this leads to an exact non-linear Green Kubo [49] relation,

$$\sigma = \dot{\gamma}\int_0^\infty dt\ \frac{1}{V}\left\langle \sigma_{xy} e^{\Omega^\dagger t}\sigma_{xy}\right\rangle \equiv \dot{\gamma}\int_0^\infty dt\, g(t). \tag{1.37}$$

It is non-linear because the shear modulus

$$g(t) = \frac{1}{V}\left\langle \sigma_{xy} e^{\Omega^\dagger t}\sigma_{xy}\right\rangle \tag{1.38}$$

contains the shear rate in any order. In liquid states, the stress reaches the linear response result for small shear rates, $\sigma = \dot{\gamma}\eta(\dot{\gamma}=0)$, where the SO in Eq. (1.38) is replaced by the equilibrium operator. In the glass, no linear response exists because $\langle \sigma_{xy} e^{\Omega_{eq}^\dagger t}\sigma_{xy}\rangle$ does not decay to zero and the integral in Eq. (1.37) does not exist. In mode coupling approximations, $g(t)$ is approximated as function of the transient correlator $\Phi_{\mathbf{q}}(t)$ [27],

$$\sigma \approx \frac{\dot{\gamma}}{2}\int_0^\infty dt \int \frac{d^3k}{(2\pi)^3}\frac{k_x^2 k_y(-t)k_y}{kk(-t)}\frac{S_k' S_{k(-t)}'}{S_k^2}\Phi^2_{\mathbf{k}(-t)}(t). \tag{1.39}$$

The scaling of the correlator $\Phi^+_{\mathbf{q}}(\tilde{t})$ for $\varepsilon \geq 0$ leads to a constant stress in Eq. (1.39) for $\dot{\gamma}\to 0$, the yield stress σ^+. It follows because $\int_0^\infty dt\, f(\dot{\gamma}t) = \dot{\gamma}^{-1}\int_0^\infty dt\, f(t)$. Eq. (1.39) was recently generalized for time dependent shear [50] and arbitrary flow fields [51].

1.6.5 Schematic Models

It is convenient to consider a simplified version of Eq. (1.23), the so called $F_{12}^{(\dot{\gamma})}$-model, where the q-dependence is neglected and the schematic correlators $\Phi^{(e)}(t)$ and $\Phi(t)$ for the quiescent and the sheared system are derived. The equation of motion reads [27]

$$\dot{\Phi}(t) + \Gamma\left\{\Phi(t) + \int_0^t dt' m(\dot{\gamma}, t-t')\dot{\Phi}(t')\right\} = 0, \tag{1.40}$$

where the only information about the shear rate is hidden in the memory function,

$$m(\dot{\gamma},t) = \frac{1}{1+(\dot{\gamma}t/\gamma_c)^2}\left[\left(v_1^c + \varepsilon\frac{1-f^c}{f^c}\right)\Phi(t) + v_2^c\Phi^2(t)\right]. \tag{1.41}$$

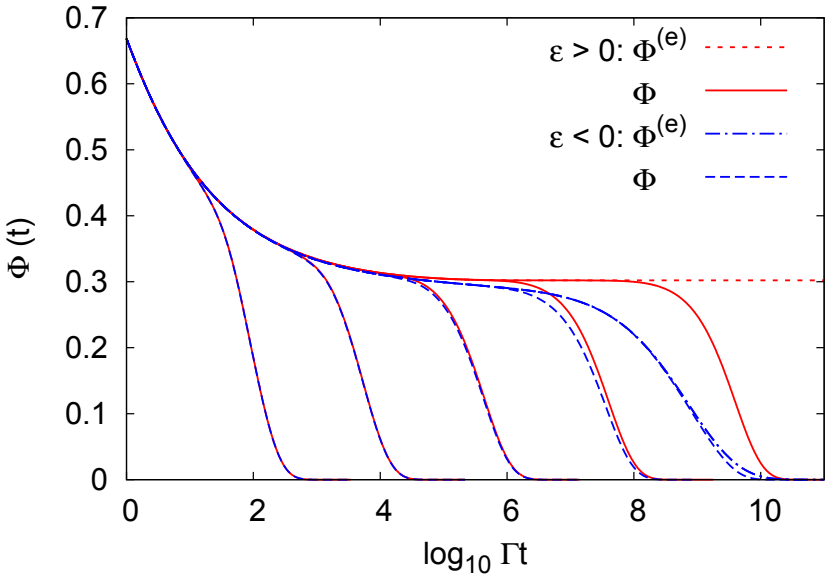

Figure 1.3: Normalized transient correlators in the $F_{12}^{(\dot\gamma)}$-model for a glassy ($\varepsilon = 10^{-4}$) and a fluid state ($\varepsilon = -10^{-4}$). Shear rates are $\dot\gamma/\Gamma = 10^{-10,-8,-6,-4,-2}$ from right to left. Also the equilibrium correlators $\Phi^{(e)}$ are shown.

$m(0,t)$ is used to calculate quiescent correlators [52]. For finite $\dot\gamma$ the memory function will eventually decay to zero due to the $\dot\gamma$-dependent pre-factor. Throughout the text, we will use the much studied values of $v_2^c = 2$ and $v_1^c = v_2^c(\sqrt{4/v_2^c} - 1) \approx 0.828$ giving a critical non-ergodicity parameter of $f^c = 0.293$ and $(1-f^c)/f^c = 2.41$. Positive values of ε correspond to glassy, negative values to liquid states. The parameter γ_c in Eq. (1.41) has been introduced recently in order to adjust the strain, at which the cages of the arrested state break due to the shear. It is necessary in comparisons with experiments [13]. In most parts of this thesis, γ_c is an unimportant rescaling of the shear rate $\dot\gamma$, and we will use $\gamma_c = 1$ if not stated otherwise. In Chap. 3, the initial decay rate will introduce another timescale into the mean squared displacements and the shape of the curves will then depend on γ_c. The numerical algorithm to solve the above equation has been developed many years ago in the group of W. Götze. It is described in Refs. [53–56]. Fig. 1.3 shows $\Phi^{(e)}(t)$ and $\Phi(t)$ for a glassy and a fluid state close to the glass transition. We see that for large shear rates, $\dot\gamma \gg \tau^{-1}$, the fluid and glassy correlators are almost identical. For small shear rates, $\dot\gamma \ll \tau^{-1}$, the fluid curves collapse onto the un-sheared curve, while in the glass, the final relaxation is governed solely by shear and the un-sheared curve stays on the plateau forever. For short times the curves are independent of shear for not too large shear rates.

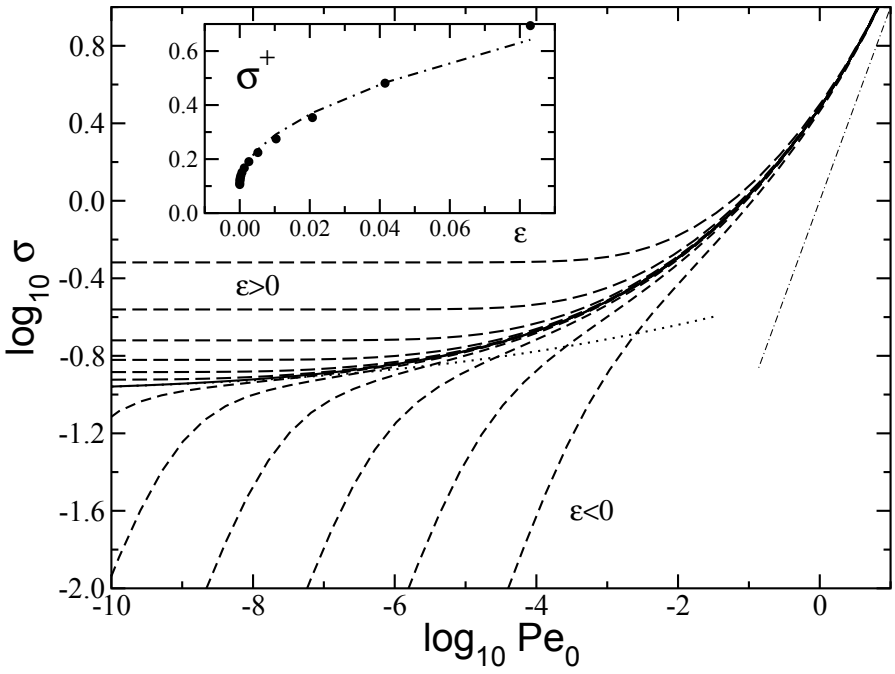

Figure 1.4: Steady shear stress σ as function of bare Peclet number $Pe_0 = \dot{\gamma}/\Gamma$ in the $F_{12}^{(\dot{\gamma})}$-model. Shown are $\varepsilon = 0$ (solid line) and $\varepsilon = \pm 4^n \varepsilon_1$ with $n = -1, 0, \ldots, 4$ and $\varepsilon_1 = 10^{-3.79}$. From Ref. [27].

In this schematic model, Eq. (1.39) for the steady shear stress is simplified to

$$\sigma = v_\sigma \dot{\gamma} \int_0^\infty dt \Phi(t)^2. \tag{1.42}$$

Fig. 1.4 shows the resulting flow curves, i.e., the shear stress σ as function of shear rate for different separations ε. The discussed properties are observed, i.e. a linear response regime with $\sigma = \dot{\gamma}\eta(\dot{\gamma} = 0)$ in the fluid and the non analytic behavior, characterized by a yield stress in the glass.

Another model introduced in Ref. [27] is the isotropically sheared hard sphere model (ISHSM). In this model, the dynamics is assumed to be isotropic in space for the considered small shear rates. This simplifies the analysis of (1.23) and can compared to the $F_{12}^{(\dot{\gamma})}$-model predict the wavevector dependence of the density correlators.

This closes the introductory chapter and we will turn to the phenomena studied by the author during the last three years.

2 Transient, Two-Time, and Stationary Correlators

In Sec. 1.6, we introduced the properties of the transient (density) correlator, measuring the fluctuations after switch-on of the rheometer at $t = 0$. It is the quantity which enters the generalized Green Kubo relation for the stress in Eq. (1.39). In this chapter we discuss its difference to the stationary correlator $C_{\mathrm{fg}}(t)$ which measures fluctuations in the steady state. We will therefore derive an approximation for the general waiting time dependent correlator $C_{\mathrm{fg}}(t, t_w)$, which for zero waiting times equals the transient, and for very long waiting times equals the stationary correlator, compare Fig. 1.2,

$$C_{\mathrm{fg}}(t, 0) = C_{\mathrm{fg}}^{(t)}(t), \qquad C_{\mathrm{fg}}(t, \infty) = C_{\mathrm{fg}}(t). \tag{2.1}$$

For the following approximations, we will restrict ourselves to the case of $f = g$ for functions without explicit advection, $f = f(\{y_i, z_i\})$.

2.1 Approximating the Exact Starting Point

In simulations of super-cooled soft spheres [14], the dependence of $C_{\mathrm{f}}(t, t_w)$ on the waiting time was explicitly tested. Before discussing the findings, we want to point out the difference between the simulated system and our Smoluchowski dynamics. In the simulations, the external shear was implemented by the Lees Edwards boundary conditions [57] of the simulation box only, i.e., after switch-on, the shear velocity diffuses into the system. In our equations, the shear velocity profile is switched on instantaneously throughout the system. This difference can be important for the effects after switch on. Apart from that, the dependence on waiting time was found to be largest at intermediate times. Also, $C_{\mathrm{f}}(t, t_w)$ decreases with t_w for fixed t. These findings are contained in our equations, as we shall see. The exact expression for the two-time correlator is given in Eq. (1.18). We will apply an identity obtained in the Zwanzig-Mori projection operator formalism (see Eq. 11 in Ref. [58] and also Ref. [59]) with[1] $P_{\mathrm{f}} = \delta f \rangle \langle \delta f^* \delta f \rangle^{-1} \langle \delta f^*$ and complement Q_{f} to get

$$\begin{aligned} C_{\mathrm{f}}(t, t_w) &= C_{\mathrm{f}}^{(t)}(t) + \dot\gamma \int_0^{t_w} ds \left\langle \sigma_{xy} e^{\Omega^\dagger s} \delta f^* \delta f \right\rangle \frac{1}{\langle \delta f^* \delta f \rangle} C_{\mathrm{f}}^{(t)}(t) \\ &\quad + \int_0^t dt' \dot\gamma \int_0^{t_w} ds \frac{\left\langle \sigma_{xy} e^{\Omega^\dagger s} \delta f^* Q_{\mathrm{f}} e^{Q_{\mathrm{f}} \Omega^\dagger Q_{\mathrm{f}} (t-t')} Q_{\mathrm{f}} \Omega^\dagger \delta f \right\rangle}{\langle \delta f^* \delta f \rangle} C_{\mathrm{f}}^{(t)}(t'). \end{aligned} \tag{2.2}$$

[1] We use this projector instead of the density projector (1.22) to achieve expressions which hold for arbitrary slow variable f.

The identity thus gave us two contributions to the difference of the two correlators. The first represents the renormalization at $t = 0$ proportional to the change of the initial value $\langle \delta f^* \delta f \rangle^{(\dot\gamma, t_w)} - \langle \delta f^* \delta f \rangle$. In the case of coherent density fluctuations and $t_w \to \infty$ it corresponds to the distorted structure factor [60, 61]. In Ref. [60], only this term for the difference of the correlators is considered. It vanishes for example for incoherent density fluctuations, since $\delta f^* \delta f = \varrho^{s*}_{\mathbf{q}} \varrho^{s}_{\mathbf{q}} = 1$ holds, see Chap. 3. The author is not aware of any other theoretical approach for the difference between the considered correlators.

For the second term, the t-dependent difference between the correlators, we use the Hermitian and idempotent projector on the stresses,

$$P_\sigma = \sigma_{xy} \rangle \langle \sigma_{xy} \sigma_{xy} \rangle^{-1} \langle \sigma_{xy}. \tag{2.3}$$

With it, Eq. (2.2) is approximated to

$$\begin{aligned} C_{\mathrm{f}}(t, t_w) \;\approx\; & C_{\mathrm{f}}^{(t)}(t) + \dot\gamma \int_0^{t_w} ds \left\langle \sigma_{xy} e^{\Omega^\dagger s} \delta f^* \delta f \right\rangle \frac{1}{\langle \delta f^* \delta f \rangle} C_{\mathrm{f}}^{(t)}(t) \\ & + \int_0^t dt' \dot\gamma \int_0^{t_w} ds \frac{\left\langle \sigma_{xy} e^{\Omega^\dagger s} \sigma_{xy} \right\rangle}{\langle \sigma_{xy} \sigma_{xy} \rangle} \frac{\left\langle \sigma_{xy} \delta f^* Q e^{Q\Omega^\dagger Q (t-t')} Q \Omega^\dagger \delta f \right\rangle}{\langle \delta f^* \delta f \rangle} C_{\mathrm{f}}^{(t)}(t'). \end{aligned} \tag{2.4}$$

We factorized the s- and t-dependent average into a product of an s-dependent part and a t-dependent part. The last term can be simplified by using the identity which gave us Eq. (2.2), but now backwards. The right hand side of Eq. (2.4) is exactly given by

$$\begin{aligned} C_{\mathrm{f}}(t, t_w) \;=\; & C_{\mathrm{f}}^{(t)}(t) + \dot\gamma \int_0^{t_w} ds \left\langle \sigma_{xy} e^{\Omega^\dagger s} \delta f^* \delta f \right\rangle \frac{1}{\langle \delta f^* \delta f \rangle} C_{\mathrm{f}}^{(t)}(t) \\ & + \dot\gamma \int_0^{t_w} ds \frac{\left\langle \sigma_{xy} e^{\Omega^\dagger s} \sigma_{xy} \right\rangle}{\langle \sigma_{xy} \sigma_{xy} \rangle} \left\langle \sigma_{xy} \delta f^* e^{\Omega^\dagger t} \delta f \right\rangle. \end{aligned} \tag{2.5}$$

The performed projection with P_σ can be interpreted as "coupling at $s = 0$" in the integrand, i.e., Eq. (2.5) is exact in first order in t_w which will be shown in Sec. 2.2.

Let us have a closer look at the second term, the time dependent difference between the correlators, which was observed in the mentioned simulations. We see that the first factor is the normalized integrated shear modulus

$$\tilde\sigma(t_w) \equiv \dot\gamma \int_0^{t_w} ds \frac{\langle \sigma_{xy} e^{\Omega^\dagger s} \sigma_{xy} \rangle}{\langle \sigma_{xy} \sigma_{xy} \rangle}, \tag{2.6}$$

containing as numerator the familiar stationary shear stress, see Eq. (1.38) and Refs. [13, 21, 47, 48, 62]. For hard spheres, the instantaneous shear modulus diverges [27] giving $\tilde\sigma = 0$ and Eq. (2.5) predicts that transient and stationary correlators agree up to the renormalization at $t = 0$. This remains a paradox because the term in first order in t_w does not vanish for hard spheres. One can avoid this problem by introducing a small short-time cut-off. It might be possible to find a way to repair this divergence by letting the cut-off go to zero at the end [63]. In the following, we will approximate the

s-dependent normalized shear modulus by the transient correlator of the $F_{12}^{(\dot\gamma)}$-model in Eq. (1.40) [64],

$$\frac{\langle\sigma_{xy}e^{\Omega^\dagger s}\sigma_{xy}\rangle}{\langle\sigma_{xy}\sigma_{xy}\rangle}\approx\frac{\Phi(s)}{3}, \tag{2.7}$$

where the factor of three accounts for the different plateau heights of the respective normalized functions. We will abbreviate $\tilde\sigma(t_w=\infty)=\tilde\sigma$ throughout the thesis. The second term, the time dependent contribution,

$$\left\langle\sigma_{xy}\delta f^* e^{\Omega^\dagger t}\delta f\right\rangle, \tag{2.8}$$

will be important in Chap. 4 again. Since it is a central term of this thesis we will dedicate the following section to it.

2.2 The Waiting Time Derivative

The term (2.8) was the focus of study of the author. In the following, it will be referred to as *waiting time derivative*, because from Eq. (1.18) follows exactly

$$\dot\gamma\,\left\langle\sigma_{xy}\delta f^* e^{\Omega^\dagger t}\delta f\right\rangle=\frac{\partial}{\partial t_w}C_{\mathrm{f}}(t,t_w)\bigg|_{t_w=0}. \tag{2.9}$$

The term describes the initial change of the two-time correlator with t_w. We now see that Eq. (2.5) is exact for small t_w,

$$C(t,t_w)=C_{\mathrm{f}}^{(t)}+\dot\gamma\,\left\langle\sigma_{xy}\delta f^* e^{\Omega^\dagger t}\delta f\right\rangle\,t_w+\mathcal{O}(t_w^2). \tag{2.10}$$

In this order, the static renormalization vanishes since

$$\langle\sigma_{xy}\delta f^*\delta f\rangle=0. \tag{2.11}$$

$\delta f^*\delta f$ is symmetric, while σ_{xy} is antisymmetric in x and y. We will now turn to approximating the waiting time derivative. Via partial integrations, one can show (recall $\delta\Omega^\dagger\delta f=0$)

$$\dot\gamma\,\left\langle\sigma_{xy}\delta f^* e^{\Omega^\dagger t}\delta f\right\rangle=\left\langle\delta f^*\,\delta\Omega^\dagger\,e^{\Omega^\dagger t}\delta f\right\rangle=\dot C_{\mathrm{f}}^{(t)}(t)-\left\langle\delta f^*\,\Omega_e^\dagger\,e^{\Omega^\dagger t}\delta f\right\rangle. \tag{2.12}$$

Eq. (2.12) shows the connection of the waiting time derivative to time derivatives of correlation functions. The full time derivative of the transient correlator is split into two terms, one containing the equilibrium operator $\Omega_e^\dagger$, the other one containing the shear term $\delta\Omega^\dagger$. We will reason the following: The term containing $\Omega_e^\dagger$ is the derivative of the short time, shear independent dynamics of the transient correlator down on the plateau, i.e., the derivative of the dynamics governed by the equilibrium SO Ω_e. The term containing $\delta\Omega^\dagger$, i.e., the waiting time derivative, follows then as the time derivative with respect to the shear governed decay down to zero.

The equilibrium derivative $\Omega_e^\dagger \delta f^*$ in the last term of (2.12) is not conserved and decorrelates quickly as the particles loose memory of their initial motion even without shear. In this case, the latter term is the time derivative of the equilibrium correlator, $C_\mathrm{f}^{(e)}(t)$. A shear flow switched on at $t = 0$ should make the particles forget their initial motion even faster, prompting us to use the approximation $e^{\Omega^\dagger t} \approx e^{\Omega_e^\dagger t} P_\mathrm{f} e^{-\Omega_e^\dagger t}\, e^{\Omega^\dagger t}$. We then find

$$\left\langle \delta f^* \Omega_e^\dagger e^{\Omega^\dagger t} \delta f \right\rangle \approx \left\langle \delta f^* \Omega_e^\dagger e^{\Omega_e^\dagger t} \delta f \right\rangle \frac{1}{\langle \delta f^* \delta f \rangle} \left\langle \delta f^* e^{-\Omega_e^\dagger t} e^{\Omega^\dagger t} \delta f \right\rangle. \tag{2.13}$$

The last average in this equation is not known. Applying the same approximation to the transient correlator, we have

$$\left\langle \delta f^* e^{\Omega^\dagger t} \delta f \right\rangle \approx \left\langle \delta f^* e^{\Omega_e^\dagger t} \delta f \right\rangle \frac{1}{\langle \delta f^* \delta f \rangle} \left\langle \delta f^* e^{-\Omega_e^\dagger t} e^{\Omega^\dagger t} \delta f \right\rangle. \tag{2.14}$$

Combining the two equations, we find for the last term in Eq. (2.12)

$$\left\langle \delta f^* \Omega_e^\dagger e^{\Omega^\dagger t} \delta f \right\rangle \approx \dot{C}_\mathrm{f}^{(e)}(t) \frac{C_\mathrm{f}^{(t)}(t)}{C_\mathrm{f}^{(e)}(t)}. \tag{2.15}$$

This term is then assured to decay faster than in equilibrium[2]. Now we can give the final formula for the waiting time derivative,

$$\left\langle \delta f^* \delta \Omega^\dagger e^{\Omega^\dagger t} \delta f \right\rangle = \frac{\partial}{\partial t_w} C_\mathrm{f}(t, t_w)\Big|_{t_w=0} \approx \dot{C}_\mathrm{f}^{(t)}(t) - \dot{C}_\mathrm{f}^{(e)}(t) \frac{C_\mathrm{f}^{(t)}(t)}{C_\mathrm{f}^{(e)}(t)}. \tag{2.16}$$

The author regards this equation as very precise for small shear rates in glassy states as will be argued in Sec. 2.5. Eq. (2.16) is the central approximation of this thesis from which further relations will follow in Chap. 4. We see the properties of the two terms in (2.12). For the fast decay of the transient correlator onto the plateau, we have $C_\mathrm{f}^{(t)}(t) = C_\mathrm{f}^{(e)}(t) + \mathcal{O}(\dot\gamma t)$. The last term in (2.12) is hence equal to the time derivative of the correlator for these short times and the waiting time derivative is zero. This is physically expected: The short time decay is independent of t_w for small t_w. For the final shear induced decay down to zero, the equilibrium correlator stays on the plateau and its derivative is negligible. The last term in (2.12) is hence zero and the waiting time derivative is equal to the time derivative of the transient correlator. This connection between the two derivatives is nontrivial and unexpected. To emphasize this, we call the two terms *short time* and *long time* derivative, respectively,

$$\dot{C}_\mathrm{f}^{(t,s)} \equiv \langle \delta f^*\, \Omega_e^\dagger\, e^{\Omega^\dagger t} \delta f \rangle \approx \dot{C}_\mathrm{f}^{(e)}(t) \frac{C_\mathrm{f}^{(t)}(t)}{C_\mathrm{f}^{(e)}(t)}, \tag{2.17}$$

$$\dot{C}_\mathrm{f}^{(t,l)} \equiv \langle \delta f^*\, \delta \Omega^\dagger\, e^{\Omega^\dagger t} \delta f \rangle \approx \dot{C}_\mathrm{f}^{(t)}(t) - \dot{C}_\mathrm{f}^{(e)}(t) \frac{C_\mathrm{f}^{(t)}(t)}{C_\mathrm{f}^{(e)}(t)}. \tag{2.18}$$

[2] In liquid states with $\dot\gamma \gg \tau^{-1}$, the fraction accounts for the fact that the term in (2.15) decays faster than in equilibrium.

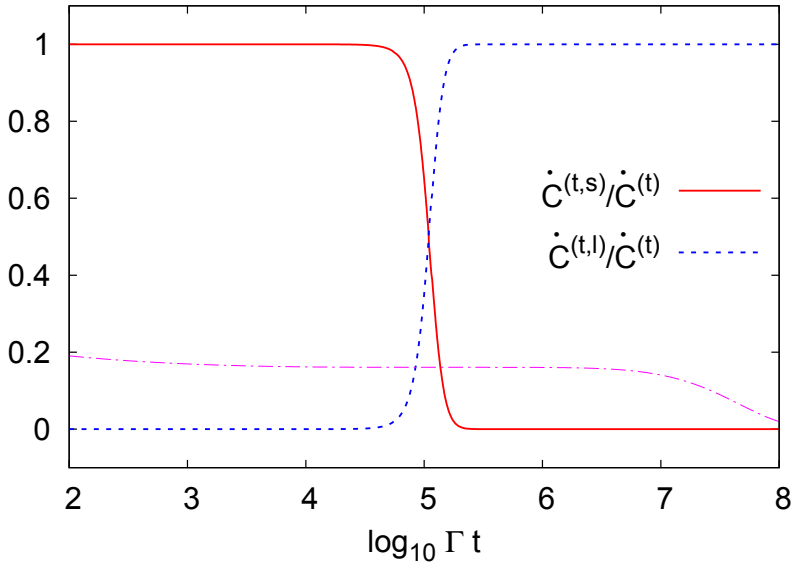

Figure 2.1: Short and long time derivatives normalized by the full time derivative for a glassy state ($\varepsilon = 10^{-3}$) and $\dot{\gamma}/\Gamma = 10^{-8}$. The dashed dotted line shows for comparison the transient correlator divided by 2.

In Fig. 2.1, we show the short and long time derivatives for a glassy state ($\varepsilon = 10^{-3}$) and shear rate $\dot{\gamma}/\Gamma = 10^{-8}$. The transient and equilibrium correlators were calculated via Eq. (1.40). One sees that the full time derivative is equal to the short time derivative at short times and equal to the long time derivative at long times. There is a sharp transition region. For small shear rates the position of this transition seems to depend on the timescale of the internal relaxation onto the plateau rather than on shear rate. With Eq. (2.11) we see that the short time derivative is zero at $t = 0$. Since the anti-symmetric terms in $\delta f^* \exp(\Omega^\dagger t)\delta f$ grow with $\dot{\gamma}t$, it is clear that the waiting time derivative is small for $\dot{\gamma}t \ll 1$, just as is expressed by Eq. (2.18).

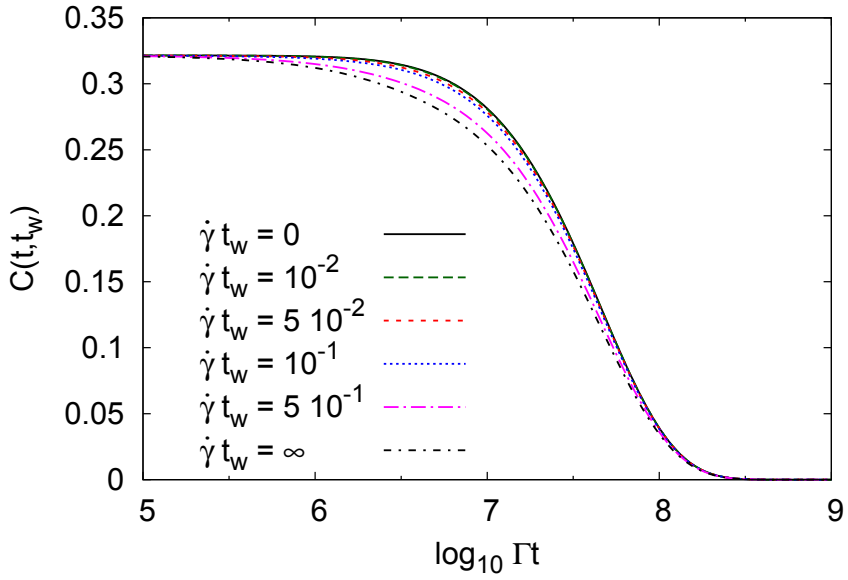

Figure 2.2: The two-time correlator via Eq. (2.19) for a glassy state ($\varepsilon = 10^{-3}$) at shear rate $\dot{\gamma}/\Gamma = 10^{-8}$.

2.3 Discussion of the Two-Time Correlator

Now we are able to study the waiting time dependence of the two-time correlator $C_\mathrm{f}(t, t_w)$. Its final approximation is given by

$$\begin{aligned} C(t,t_w) &\approx C_\mathrm{f}^{(t)}(t) + \dot{\gamma}\int_0^{t_w} ds \frac{\left\langle \sigma_{xy} e^{\Omega^\dagger s}\delta f^* \delta f\right\rangle}{\langle \delta f^* \delta f\rangle} C_\mathrm{f}^{(t)}(t) + \frac{\tilde{\sigma}(t_w)}{\dot{\gamma}} \frac{\partial}{\partial t_w} C(t,t_w)\Big|_{t_w=0}, \\ &\approx C_\mathrm{f}^{(t)}(t) + \dot{\gamma}\int_0^{t_w} ds \frac{\left\langle \sigma_{xy} e^{\Omega^\dagger s}\delta f^* \delta f\right\rangle}{\langle \delta f^* \delta f\rangle} C_\mathrm{f}^{(t)}(t) + \frac{\tilde{\sigma}(t_w)}{\dot{\gamma}} \left(\dot{C}_\mathrm{f}^{(t)} - \dot{C}_\mathrm{f}^{(e)}(t) \frac{C_\mathrm{f}^{(t)}(t)}{C_\mathrm{f}^{(e)}(t)} \right). \end{aligned} \tag{2.19}$$

In Fig. 2.2, we show the final decay of the two-time correlator for different waiting times. For this we again use the transient correlator from the $F_{12}^{(\dot{\gamma})}$-model, Eq. (1.40), and calculate $\tilde{\sigma}(t_w)$ via (2.7). The waiting time dependence at $t = 0$ is neglected. One sees that the two-time correlator and the transient correlator agree for $\dot{\gamma} t_w \ll 1$, and that the stationary correlator is reached on a timescale $\dot{\gamma} t_w = \mathcal{O}(1)$. Note that this dependence on waiting time is another example for a nonanalytic quantity in the glass, since it does not vanish for $\dot{\gamma} \to 0$. The dependence on waiting time is in good agreement with the simulations in Ref. [14]. Neglecting the correction at $t = 0$, we have

$$C_\mathrm{f}(t,t_1) \geq C_\mathrm{f}(t,t_2) \qquad t_1 \leq t_2, \tag{2.20}$$

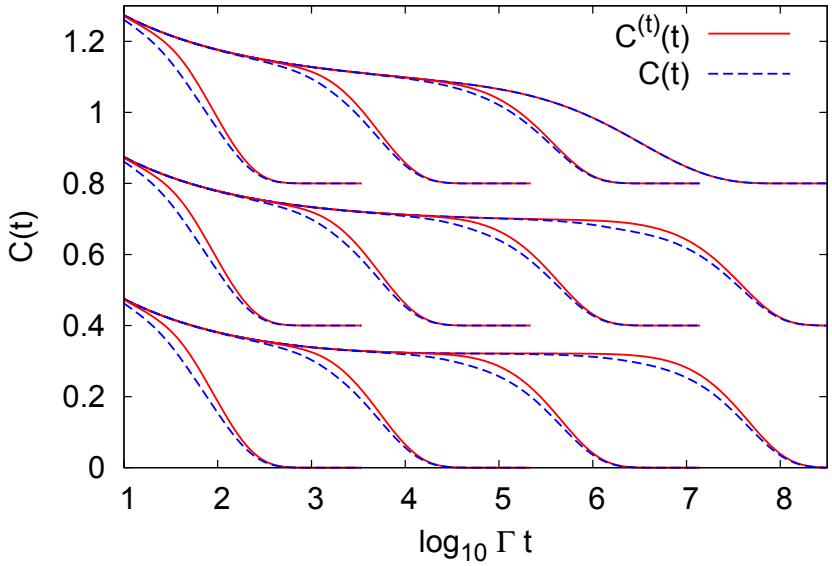

Figure 2.3: The transient and stationary correlators for separation parameters $\varepsilon = -10^{-3}, 0, 10^{-3}$ from top to bottom and shear rates $\dot{\gamma}/\Gamma = 10^{-2n}$ with $n = 1, 2, 3, 4$. The upper and middle curves are shifted by 0.8 and 0.4 respectively.

from our approximations. This follows because the waiting time derivative is negative[3]. Eq. (2.20) is attributed to the fact that in the case of the transient correlator, all particles are mobilized simultaneously at a certain strain. In the steady state, the particles escape their cages every now and then, uncorrelated to the correlation time t. The steady correlator decays hence earlier from the glassy plateau. We would like to comment on the fact that the shear modulus in the microscopic approximation in (1.39) is slightly negative for long times [14, 27], which together with Eq. (2.19) would yield a correlator *smaller* than the stationary one for a short window in t_w with $\dot{\gamma} t_w \lesssim 1$. It would be interesting to see whether this can be observed in simulations.

In Fig. 2.3 we show the transient and the stationary correlators for different densities and shear rates. The glassy and critical curves are qualitatively similar, the difference between the correlators is nonanalytic. In the liquid, the difference vanishes as $\dot{\gamma} \to 0$.

2.4 Plotting the Waiting Time Dependent Curves Differently: Hypothesis of No Crossings

In this section, we will speculate. We saw that the waiting time dependent correlator $C_{\mathrm{f}}(t, t_w)$ as approximated in Eq. (2.5) obeys Eq. (2.20). Here we show $C(t - t_w, t_w)$

[3] This holds because the derivative of the transient correlator is smaller than the time derivative of the equilibrium correlator. While this is reasonable, it cannot be shown rigorously.

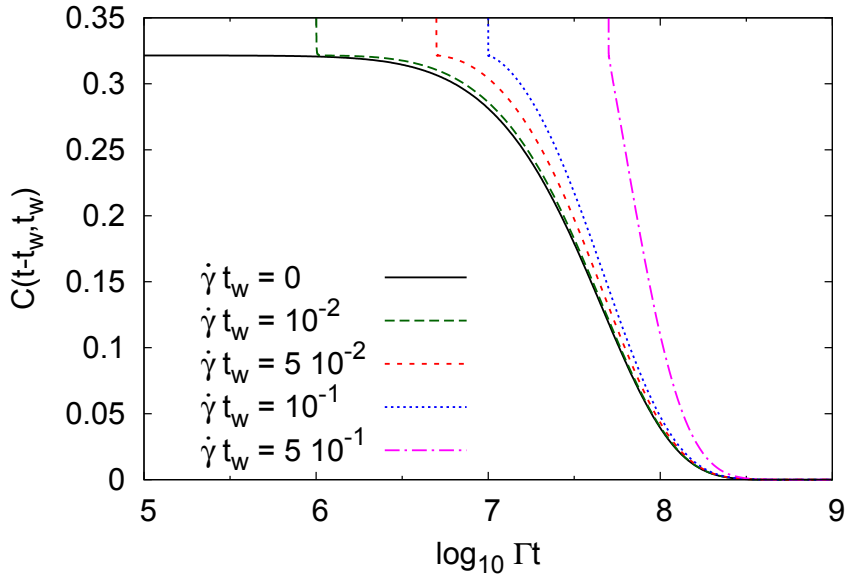

Figure 2.4: The two-time correlator $C(t-t_w, t_w)$ via Eq. (2.19) for a glassy state ($\varepsilon = 10^{-3}$) at shear rate $\dot{\gamma}/\Gamma = 10^{-8}$. The short time decay of the curves for $t_w > 0$ is compressed due to the logarithmic axis.

instead of $C(t, t_w)$, see Fig. 2.4. The different curves do not cross each other and we have from the plot

$$C_\mathrm{f}(t - t_1, t_1) \leq C_\mathrm{f}(t - t_2, t_2) \qquad t_1 \leq t_2, \tag{2.21}$$

i.e., the curves are ordered in opposite manner compared to Fig. 2.2. The author believes that Eq. (2.21) is true due to the following argument: Fig. 2.4 shows the functions as they appear in reality: We switch on the shear and start measuring the transient correlator. Then, after a time t_w, we start measuring $C_\mathrm{f}(t - t_w, t_w)$. At any time t, both correlators describe the *same system in the same state, i.e., the very same particles* and there is good reason to believe that the correlator which was started first will always be smaller[4]. The particles cannot "overtake" themselves. Despite this intuitive reasoning, the author was not able to prove Eq. (2.21), although it seemed possible at the beginning [63]. But why do we care so much about this relation? This will become clear in Sec. 2.5.1, where we will see that we can learn more about the waiting time derivative assuming that Eq. (2.21) holds.

[4] We assume that the correlators are positive with negative derivative.

2.5 The Waiting Time Derivative Reconsidered

2.5.1 Constraint for $\frac{\partial}{\partial t_w} C_\mathrm{f}(t,t_w)\Big|_{t_w=0}$

We will show that the waiting time derivative is bound by the time derivative of the transient correlator. Its definition is given by

$$\frac{\partial}{\partial t_w} C_\mathrm{f}(t,t_w)\Big|_{t_w=0} = \lim_{\delta t\to 0} \frac{C_\mathrm{f}(t,\delta t) - C_\mathrm{f}(t,0)}{\delta t}. \tag{2.22}$$

For comparison, the time derivative of the transient correlator is given by

$$\frac{\partial}{\partial t} C_\mathrm{f}(t,0) = \lim_{\delta t\to 0} \frac{C_\mathrm{f}(t+\delta t,0) - C_\mathrm{f}(t,0)}{\delta t}. \tag{2.23}$$

From Eq. (2.21) we conclude that

$$C_\mathrm{f}(t+\delta t,0) \leq C_\mathrm{f}(t,\delta t). \tag{2.24}$$

From this relation we see that the waiting time derivative is larger than the time derivative,

$$\frac{\partial}{\partial t_w} C_\mathrm{f}(t,t_w)\Big|_{t_w=0} \geq \frac{\partial}{\partial t} C_\mathrm{f}(t,0). \tag{2.25}$$

Note that this means that the absolute value of the waiting time derivative is smaller than the time derivative, if both are negative. In our approximation in (2.18), the greater than or equal to sign in (2.25) becomes an equals sign at long times in glassy states and the constraint is perfectly obeyed. In Fig. 2.1, the dashed line is always smaller than or equal to unity.

2.5.2 Small-Shear Derivation Supporting the Approximation in Sec. 2.2

The author tried to prove that the waiting time derivative is equal to the time derivative of the transient correlator for long times at small shear rates in the glass as displayed by Eq. (2.16). A rigorous proof might not exist, but a convincing derivation shall be presented here. Again, the term of consideration reads

$$\left\langle \delta f^* \, \delta\Omega^\dagger \, e^{\Omega^\dagger t} \delta f \right\rangle. \tag{2.26}$$

The following derivation starts by considering the variance of $\dot{C}_\mathrm{f}^{(t)}$ upon a small change in shear rate *while keeping* $\dot{\gamma}t$ *fixed*,

$$\begin{aligned} \dot{C}_\mathrm{f}^{(t)}(\dot{\gamma}+\delta\dot{\gamma}, t-\frac{t}{\dot{\gamma}}\delta\dot{\gamma}) &= \left\langle \delta f^* \, (\Omega_e^\dagger + \frac{\dot{\gamma}+\delta\dot{\gamma}}{\dot{\gamma}}\delta\Omega^\dagger) \, e^{(\Omega_e^\dagger + \frac{\dot{\gamma}+\delta\dot{\gamma}}{\dot{\gamma}}\delta\Omega^\dagger)(t-\frac{t}{\dot{\gamma}}\delta\dot{\gamma})} \delta f \right\rangle \\ &\overset{\delta\dot{\gamma}\ll\dot{\gamma}}{=} \left\langle \delta f^* \, (\Omega_e^\dagger + \frac{\dot{\gamma}+\delta\dot{\gamma}}{\dot{\gamma}}\delta\Omega^\dagger) \, e^{\Omega_e^\dagger(t-\frac{t}{\dot{\gamma}}\delta\dot{\gamma})+\delta\Omega^\dagger t} \delta f \right\rangle. \end{aligned} \tag{2.27}$$

In the second step we neglected terms of order $\delta\dot{\gamma}^2$. For long times, the dynamics is independent of the bare diffusion coefficient D_0 (which is set to unity) multiplying the equilibrium operator. For these times, it is hence not important whether the equilibrium operator in the exponent is multiplied by t or by $t - \frac{t}{\dot{\gamma}}\delta\dot{\gamma}$ as long as $\frac{t}{\dot{\gamma}}\delta\dot{\gamma} \ll t$ holds. We can write

$$\dot{C}_{\mathrm{f}}^{(t)}(\dot{\gamma}+\delta\dot{\gamma}, t-\frac{t}{\dot{\gamma}}\delta\dot{\gamma}) \overset{D_0 t/d^2\to\infty,\dot{\gamma}t=c}{=} \left\langle \delta f^* \left(\Omega_e^\dagger + \frac{\dot{\gamma}+\delta\dot{\gamma}}{\dot{\gamma}}\delta\Omega^\dagger\right) e^{\Omega_e^\dagger t + \delta\Omega^\dagger t}\delta f \right\rangle. \tag{2.28}$$

The important connection follows: For long times, we can identify the term in Eq. (2.26) with the following fraction,

$$\left\langle \delta f^*\, \delta\Omega^\dagger\, e^{\Omega^\dagger t}\delta f \right\rangle \overset{D_0 t/d^2\to\infty,\dot{\gamma}t=c}{=} \dot{\gamma} \lim_{\delta\dot{\gamma}\to 0} \frac{\dot{C}_{\mathrm{f}}^{(t)}(\dot{\gamma}+\delta\dot{\gamma}, t-\frac{t}{\dot{\gamma}}\delta\dot{\gamma}) - \dot{C}_{\mathrm{f}}^{(t)}(\dot{\gamma}, t)}{\delta\dot{\gamma}}. \tag{2.29}$$

We remember that the transient correlator for long times is a function of $\dot{\gamma}t$, see Sec. 1.6.3 and Ref. [27], to see the following relations at $\dot{\gamma}\to 0$, $\dot{\gamma}t = const.$,

$$\begin{aligned} C_{\mathrm{f}}^{(t)}(t) &= C_{\mathrm{f}}^{+(t)}(\dot{\gamma}t), \\ \dot{C}_{\mathrm{f}}^{(t)}(t) &= \dot{\gamma}\frac{\partial}{\partial\dot{\gamma}t} C_{\mathrm{f}}^{+(t)}(\dot{\gamma}t). \end{aligned}$$

The waiting time derivative then follows with Eq. (2.29) for long times,

$$\left\langle \delta f^*\, \delta\Omega^\dagger\, e^{\Omega^\dagger t}\delta f \right\rangle = \dot{C}_{\mathrm{f}}^{(t)}(t). \tag{2.30}$$

We have thus shown that the approximation (2.16) for the waiting time derivative is very good for long times, i.e., it equals the time derivative of the transient correlator.

2.5.3 Why Our Findings for the Waiting Time Derivative Are Physically Plausible

Let us consider the physical implications of our approximation in Eq. (2.16). Again, we look at the formal expression for the waiting time derivative and the time derivative,

$$\frac{\partial}{\partial t_w} C_{\mathrm{f}}(t, t_w)\Big|_{t_w=0} = \lim_{\delta t\to 0} \frac{C_{\mathrm{f}}(t,\delta t) - C_{\mathrm{f}}(t,0)}{\delta t}, \tag{2.31}$$

and,

$$\frac{\partial}{\partial t} C_{\mathrm{f}}(t,0) = \lim_{\delta t\to 0} \frac{C_{\mathrm{f}}(t+\delta t,0) - C_{\mathrm{f}}(t,0)}{\delta t}. \tag{2.32}$$

At long times in glassy states, these two equations and Eq. (2.16) imply

$$C_{\mathrm{f}}(t,\delta t) = C_{\mathrm{f}}(t+\delta t, 0). \tag{2.33}$$

In glassy states in the limit of small shear rates, the particles wait in their cages (while the transient correlator is on the plateau) for these cages to break for the first time

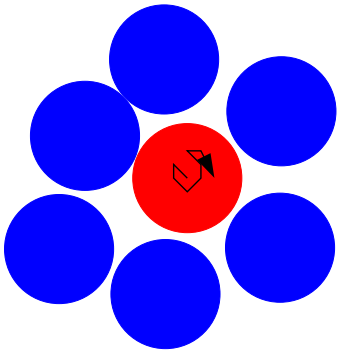

Figure 2.5: The particle is rattling in its cage built by the other particles. After a long time, it has explored the whole cage and the correlator does not decay any more. The decay sets in when the cages break for the first time due to shear and the correlator decays independently of the exact starting point $t = 0$.

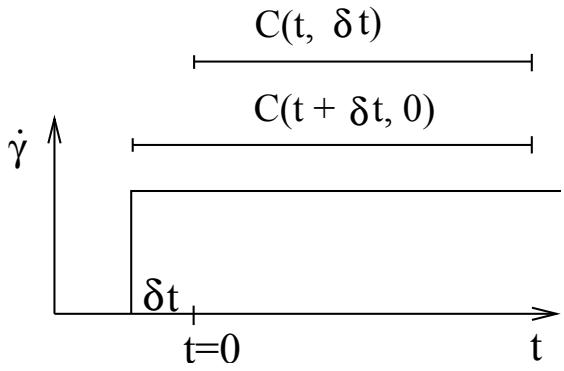

Figure 2.6: The two functions which are equal at long times. At time t, the external shear has been present for a period $t + \delta t$ in both cases.

due to shear. In this situation, the value of the correlator is independent of the exact point when the correlation was started (at $t = 0$ or at $t = -\delta t$), since for all these starting times the particles have exploited their cages for a long time, see Fig. 2.5. The only thing that matters is the time when the cages break up for the first time due to shear. And this first cage break happens at the same time t for the two functions in Eq. (2.33), see Fig. 2.6. This is why they are equal at long times. This physical explanation for Eq. (2.33) supports our approximation in Eq. (2.16). In Sec. 4.6, we will see the consequences for the fluctuation dissipation theorem following from Eq. (2.16).

3 Incoherent Density Fluctuations

From general considerations to very concrete calculations; this chapter is about incoherent density fluctuations, i.e., density fluctuations of a tagged particle. These are studied here for the first time for glassy systems under shear within MCT. If the tagged particle and the bath particles are identical, the dynamics of every bath particle is on average identical to the dynamics of the tagged particle. This leads to much better statistics of incoherent quantities in simulations and experiments compared to coherent ones. This is the reason why in simulations and experiments mostly incoherent quantities are considered which makes their theoretical description a necessary contribution. In Sec. 3.2, we will derive exact equations of motion for the incoherent transient density correlator and then perform approximations to close these equations. This will be in almost complete analogy to the derivation for the coherent transient density correlator shown in Ref. [60]. This technical derivation is mainly interesting for the details-loving reader, while the reader, who is mostly interested in the physical implications and results following from this derivation, might want to skip to Sec. 3.3. There, an expansion of the solution of these equations near the critical plateau, the so called β-analysis, is presented. After this we will derive the equations of motion for the mean squared displacement (MSD) of the tagged particle, an important quantity which has been studied extensively in simulations [14, 65–67] and theoretically for non-Brownian particles [68, 69] or in an expansion in packing fraction and Peclet number [70]. We will show a new type of Taylor dispersion in glassy states compared to the low density case in Eq. (1.9) [23]. We want to briefly discuss other theoretical approaches to the mean squared displacements under shear.

3.1 Previous Theoretical Studies on the Mean Squared Displacements under Shear

Additionally to the low density case, see Eq. (1.9), there have been theoretical studies of the diffusivities of non-Brownian particles, i.e., particles with very small diffusivity D_0. This is e.g. the case for very viscous solvents or very low temperatures. This system is interesting for many reason, e.g. it is not a priori clear that diffusion actually exists, because the motion of the particles is in principle deterministic. Also, the encounter of two particles does not lead to a displacement of the two perpendicular to the shear direction if hydrodynamic interactions are taken into account due to the reversibility of the Stokes flow. See Ref. [68] and the references therein.

In Ref. [68] is is shown that for interacting non-Brownian particles the same relations between the mean squared displacements hold as in the low density limit in Eq. (1.9). This is achieved by splitting the velocities of the particles into a) the drift velocity and

b) the velocity due to interactions. It is then argued that for the probability distribution of a tagged particle, a Fokker-Planck or master equation holds. The resulting solution for the particle distribution is very similar to Eq. (1.8) and the connection between the different directions follows as for low densities [68],

$$\langle zz\rangle = 2D_{zz}t, \tag{3.1a}$$
$$\langle yy\rangle = 2D_{yy}t, \tag{3.1b}$$
$$\langle xx\rangle = 2D_{xx}t + 2D_{xy}\dot\gamma t^2 + \frac{2}{3}D_{yy}\dot\gamma^2 t^3, \tag{3.1c}$$
$$\langle xy\rangle = 2D_{xy}t + D_{yy}\dot\gamma t^2. \tag{3.1d}$$

Eq. (1.9) follows with $D_{\alpha\alpha} = D_0$ and $D_{xy} = \frac{1}{2}\dot\gamma y_0^2$. Note that no short time diffusion exists for non-Brownian particles. In Ref. [68], also expressions for the diffusivity matrix are derived in terms of microscopic quantities which can be evaluated with the help of simulations. We will in our microscopic approach, using the N-particle distribution, show that the relations (3.1) between the different directions also hold for the colloidal system at the glass transition.

3.2 Equation of Motion for the Transient Incoherent Correlator

The transient incoherent density correlator is defined by Eq. (1.17) choosing the variable $\delta f = \varrho_{\mathbf{q}}^s = e^{i\mathbf{q}\cdot\mathbf{r}_s}$ with the particle position $\mathbf{r}_s$. In contrast to the coherent case, the normalization of the correlator is unity since $\delta f^*\delta f = 1$ holds. Why do we derive equations of motion for the transient and not for the stationary correlator which is measured in experiments? In the coherent case this is justified by the generalized Green Kubo relations for the stress, Eq. (1.39) and the fact that the transient correlator can be achieved with the equilibrium structure factor as only input. Here it is just a natural continuation to derive the equation for the transient incoherent correlator, since we will be able to use many insights gained from the coherent case. We recall that if q_x is finite we have to use the advected wavevector,

$$\mathbf{q}(t) = \mathbf{q} - \dot\gamma t q_x \mathbf{e}_y \tag{3.2}$$

in the transient incoherent density correlator,

$$\Phi_{\mathbf{q}}^s(t) = \left\langle e^{-i\mathbf{q}\cdot\mathbf{r}_s} e^{\Omega^\dagger t} e^{i\mathbf{q}(t)\cdot\mathbf{r}_s}\right\rangle = \left\langle \varrho_{\mathbf{q}}^{s*} e^{\Omega^\dagger t} \varrho_{\mathbf{q}(t)}^s\right\rangle. \tag{3.3}$$

The advected wavevector appears in Eq. (3.3) because of translational invariance of the infinite system, this is explained in detail in Refs. [21, 60]. Correlators with wavevectors other than $\mathbf{q}(t)$ on the right hand side vanish. Due to this advection, the density correlator is, strictly speaking, no autocorrelation function for $q_x \neq 0$. It can be rewritten using $e^{-\delta\Omega^\dagger t} e^{i\mathbf{q}\cdot\mathbf{r}_s} = e^{i\mathbf{q}(t)\cdot\mathbf{r}_s}$,

$$\Phi_{\mathbf{q}}^s(t) = \left\langle e^{-i\mathbf{q}\cdot\mathbf{r}_s} e^{\Omega^\dagger t} e^{-\delta\Omega^\dagger t} e^{i\mathbf{q}\cdot\mathbf{r}_s}\right\rangle. \tag{3.4}$$

We see that $\Phi^s_{\mathbf{q}}(t)$ is an autocorrelation function with respect to the time evolution of

$$U(t) = e^{\Omega^\dagger t} e^{-\delta\Omega^\dagger t} = e^{\Omega^\dagger_e t + \delta\Omega^\dagger t} e^{-\delta\Omega^\dagger t}. \tag{3.5}$$

It is worth noting that, if $\Omega^\dagger_e$ and $\delta\Omega^\dagger$ commuted, we would have $\Phi^s_{\mathbf{q}}(t) = \Phi^{s(e)}_q(t)$, the equilibrium correlator. This is, of course, not the case. The following derivation of the equation of motion for $\Phi^s_{\mathbf{q}}(t)$ is analogous to the coherent case [60] and we will therefore be very brief. The time dependence of the evolution operator $U(t)$ can be found by differentiation,

$$\partial_t U(t) = e^{\Omega^\dagger t}(\Omega^\dagger - \delta\Omega^\dagger) e^{-\delta\Omega^\dagger t} = e^{\Omega^\dagger t}\, \Omega^\dagger_e\, e^{-\delta\Omega^\dagger t}. \tag{3.6}$$

We see that the equilibrium operator appears, a fact which is bewildering at first sight (and keeps being so also at second sight). To proceed, it is reasonable to define a well behaved operator as was suggested in Ref. [60],

$$\Omega^\dagger_a(t) = e^{\overline{\delta\Omega^\dagger} t} \Omega^\dagger_e e^{-\delta\Omega^\dagger t}, \tag{3.7}$$

with $\overline{\delta\Omega^\dagger} = \sum_i \mathbf{r}_i \cdot \boldsymbol{\kappa}^T \cdot (\boldsymbol{\partial}_i + \mathbf{F}_i)$. $\overline{\delta\Omega^\dagger}$ is the adjoined of $-\delta\Omega^\dagger$ in the equilibrium average. It follows that $\Omega^\dagger_a(t)$ is Hermitian in the equilibrium average,

$$\left\langle f^* \Omega^\dagger_a(t) g \right\rangle = \left\langle (e^{-\delta\Omega^\dagger t} f^*) \Omega^\dagger_e e^{-\delta\Omega^\dagger t} g \right\rangle = \left\langle (\Omega^\dagger_e e^{-\delta\Omega^\dagger t} f^*) e^{-\delta\Omega^\dagger t} g \right\rangle = \left\langle g \Omega^\dagger_a(t) f^* \right\rangle. \tag{3.8}$$

And with $f = g$ the above equation also shows that the time dependent eigenvalues of $\Omega^\dagger_a(t)$ are real and negative, see Eq. (5.1). Because of

$$\langle \varrho^{s*}_{\mathbf{q}} e^{\overline{\delta\Omega^\dagger} t} = \langle e^{-i\mathbf{q}\cdot\mathbf{r}_s} e^{\overline{\delta\Omega^\dagger} t} = \langle e^{-i\mathbf{q}(t)\cdot\mathbf{r}_s} = \langle \varrho^{s*}_{\mathbf{q}(t)}, \tag{3.9}$$

$\Omega^\dagger_a(t)$ has identical matrix elements as the equilibrium operator for the case of density fluctuations, only the densities are replaced by their time dependent analogs as we will see when regarding the initial decay rate.

The equations of motion are derived in the spirit of the Zwanzig-Mori projection operator formalism [34], where we use the time dependent single particle density projector

$$P^s(t) = \sum_{\mathbf{q}} \varrho^s_{\mathbf{q}(t)} \rangle\langle \varrho^{s*}_{\mathbf{q}(t)} \tag{3.10}$$

with complement $Q^s(t) = 1 - P^s(t)$. We abbreviate $P^s(0) = P^s$. With this, Eq. (3.6) can be rewritten such that the well behaved operator appears

$$\partial_t U(t) = e^{\Omega^\dagger t}\,(P^s(t) + Q^s(t))\Omega^\dagger_e\, e^{-\delta\Omega^\dagger t} = U(t)\,(P^s \Omega^\dagger_a(t) + \Omega^\dagger_r(t)), \tag{3.11}$$

$$\Omega^\dagger_r(t) = e^{\delta\Omega^\dagger t} Q^s(t) \Omega^\dagger_e e^{-\delta\Omega^\dagger t}. \tag{3.12}$$

At $\dot\gamma = 0$, $\Omega^\dagger_r(t)$ is perpendicular to density fluctuations, which is not the case for $\dot\gamma \neq 0$. The part which is not perpendicular can be split off by writing

$$\Omega^\dagger_r(t) = \Omega^\dagger_Q(t) + \Omega^\dagger_\Sigma(t). \tag{3.13}$$

The first part is perpendicular to density fluctuations, $P^s\Omega_Q^\dagger(t) = 0$, while the other one is not. The two parts read

$$\Omega_Q^\dagger(t) = e^{\overline{\delta\Omega^\dagger}t} Q^s(t)\Omega_e^\dagger e^{-\delta\Omega^\dagger t}, \tag{3.14a}$$

$$\Omega_\Sigma^\dagger(t) = e^{\overline{\delta\Omega^\dagger}t}\Sigma(t)\, Q^s(t)\, \Omega_e^\dagger e^{-\delta\Omega^\dagger t}, \tag{3.14b}$$

with the function $\Sigma(t)$ given by [60]

$$\Sigma(t) = \dot\gamma \int_0^t dt' e^{-\overline{\delta\Omega^\dagger}t'} \sigma_{xy} e^{\delta\Omega^\dagger t'}. \tag{3.15}$$

Because of $\Sigma(t)$, the second part of $\Omega_r^\dagger(t)$ couples to density fluctuations. As is done in the equilibrium case, a reduced time evolution operator is employed which satisfies

$$\partial_t\, U_r(t,t') = U_r(t,t')\, \Omega_r^\dagger(t). \tag{3.16}$$

Its formal solution is given in terms of a time ordered exponential, where operators are ordered from left to right as time increases [71],

$$U_r(t,t') = e_-^{\int_{t'}^t ds \Omega_r^\dagger(s)}. \tag{3.17}$$

We still need the connection between reduced and full evolution operators given by

$$U(t) = U_r(t,0) + \int_0^t dt' U(t') P^s \Omega_a^\dagger(t') U_r(t,t'). \tag{3.18}$$

Taking its time derivative leads to the useful operator relation,

$$\partial_t U(t) = U_r(t,0)\Omega_r^\dagger(t) + U(t)P^s\Omega_a^\dagger(t) + \int_0^t dt' U(t') P^s \Omega_a^\dagger(t') U_r(t,t')\Omega_r^\dagger(t). \tag{3.19}$$

The equation of motion for the correlator now follows by sandwiching the expressions above with density fluctuations. As already noted, the operator $\Omega_r^\dagger(t)$ is not perpendicular to density fluctuations and the first term on the right hand side does not vanish as it does at $\dot\gamma = 0$. The equation of motion hence contains an extra term,

$$\partial_t \Phi_{\mathbf{q}}^s(t) + \Gamma_{\mathbf{q}}^s(t)\Phi_{\mathbf{q}}^s(t) + \int_0^t dt' M_{\mathbf{q}}^s(t,t')\, \Phi_{\mathbf{q}}^s(t') = \Delta_{\mathbf{q}}^s(t). \tag{3.20}$$

The extra term $\Delta_{\mathbf{q}}^s(t)$ reads

$$\Delta_{\mathbf{q}}^s(t) = \left\langle e^{-i\mathbf{q}\cdot\mathbf{r}_s} U_r(t,0)\Omega_r^\dagger(t) e^{i\mathbf{q}\cdot\mathbf{r}_s} \right\rangle, \tag{3.21}$$

it vanishes only at time $t = 0$ and grows to lowest order like $\dot\gamma t$. One of the advantages of the present formulation compared to the earlier one in Ref. [21] is that the initial decay

rate is positive; it is equal to the equilibrium initial decay rate for advected wavevectors (we already saw that $\Omega_a^\dagger$ has negative semi-definite spectrum),

$$\Gamma_{\mathbf{q}}^s(t) = \Gamma_{\mathbf{q}(t)}^{s(e)} = -\left\langle e^{-i\mathbf{q}\cdot\mathbf{r}_s}\Omega_a^\dagger\, e^{i\mathbf{q}\cdot\mathbf{r}_s}\right\rangle = -\left\langle e^{-i\mathbf{q}(t)\cdot\mathbf{r}_s}\Omega_e^\dagger\, e^{i\mathbf{q}(t)\cdot\mathbf{r}_s}\right\rangle = q^2(t) \geq 0. \tag{3.22}$$

The memory function $M_{\mathbf{q}}^s(t)$ contains on the left hand side the well behaved operator $\Omega_a^\dagger$,

$$M_{\mathbf{q}}^s(t,t') = -\left\langle \varrho_{\mathbf{q}}^{s*}\Omega_a^\dagger(t')U_r(t,t')\Omega_r^\dagger(t)\varrho_{\mathbf{q}}^s\right\rangle. \tag{3.23}$$

If we knew an approximation for $M_{\mathbf{q}}^s(t,t')$ in terms of the correlator itself, the equation would be closed apart from $\Delta_{\mathbf{q}}^s(t)$. But MCT approximations for Eq. (3.23) are not desirable because they do not take into account that $M_{\mathbf{q}}^s(t,t')$ in Eq. (3.20) is a fast function in terms of $\dot\gamma$-power counting. Also, as is shown in Ref. [21], approximating $M_{\mathbf{q}}^s(t,t')$ in Eq. (3.20), one would have to be very careful to receive an equation which describes slow dynamics. This is not the case for Eq. (3.26) below. The described issue is well known and appears also in quiescent MCT, see e.g. Ref. [72]. We will discuss this again in Sec. 4.5.2. We perform a second projection step following Ref. [21]. To decompose the reduced SO appearing in $U_r(t,t')$, we use the projector

$$\tilde P^s(t) = \varrho_{\mathbf{q}}^s\rangle\frac{1}{\langle\varrho_{\mathbf{q}}^{s*}\Omega_a^\dagger(t)\varrho_{\mathbf{q}}^s\rangle}\langle\varrho_{\mathbf{q}}^{s*}\Omega_a^\dagger(t), \tag{3.24}$$

with complement $\tilde Q^s(t)$. While $\tilde P^s(t)$ is, strictly speaking, not a projector because it is not Hermitian, it is still idempotent, $\tilde P^s(t)\tilde P^s(t) = \tilde P^s(t)$. It is applied in the following way (note the similarity to Eq. (4.34)),

$$\Omega_r^\dagger(t) = \Omega_r^\dagger(t)(\tilde Q^s(t) + \tilde P^s(t)) = \Omega_i^\dagger(t) + \Omega_r^\dagger(t)\varrho_{\mathbf{q}}^s\rangle\frac{1}{\langle\varrho_{\mathbf{q}}^{s*}\Omega_a^\dagger(t)\varrho_{\mathbf{q}}^s\rangle}\langle\varrho_{\mathbf{q}}^{s*}\Omega_a^\dagger(t). \tag{3.25}$$

With this, one can show the connection of $M_{\mathbf{q}}^s(t,t')$ to another memory function, $m_{\mathbf{q}}^s(t,t')$, which is governed by the irreducible operator $\Omega_i^\dagger(t)$ [73, 74]. As is shown in Ref. [60], the equation of motion can, after applying the theory of Volterra integral equations [75], be written as

$$\partial_t\Phi_{\mathbf{q}}^s(t) + \Gamma_{\mathbf{q}}^s(t)\left\{\Phi_{\mathbf{q}}^s(t) + \int_0^t dt' m_{\mathbf{q}}^s(t,t')\partial_{t'}\Phi_{\mathbf{q}}^s(t')\right\} = \tilde\Delta_{\mathbf{q}}^s(t), \tag{3.26}$$

with the new memory function

$$m_{\mathbf{q}}^s(t,t') = \frac{1}{\Gamma_{\mathbf{q}}(t)\Gamma_{\mathbf{q}}(t')}\left\langle \varrho_{\mathbf{q}}^{s\,*}\Omega_a^\dagger(t')U_i(t,t')\Omega_r^\dagger(t)\varrho_{\mathbf{q}}^s\right\rangle. \tag{3.27}$$

It is governed by the irreducible operator,

$$U_i(t,t') = e_-^{\int_{t'}^t ds\,\Omega_i^\dagger(s)}. \tag{3.28}$$

Eq. (3.26) has an extra term compared to Eq. (1.23), which arose from $\Delta^s_{\mathbf{q}}(t)$ in Eq. (3.20),

$$\tilde{\Delta}^s_{\mathbf{q}}(t) = \langle \varrho^{s*}_{\mathbf{q}} U_i(t,0)\Omega^\dagger_r(t)\varrho^s_{\mathbf{q}}\rangle. \tag{3.29}$$

It also vanishes only at $t = 0$ and grows in leading order like $\dot\gamma t$. It does hence not influence the fast decay onto the plateau for $\dot\gamma \to 0$. This exact set of equations for the incoherent transient density correlator is now suitable for approximations in order to get a closed equation for $\Phi^s_{\mathbf{q}}(t)$. The integral in Eq. (3.26) contains the time derivative of $\Phi^s_{\mathbf{q}}(t)$, its product with $m^s_{\mathbf{q}}(t,t')$ has the right $\dot\gamma$-powers after MCT approximations for $m^s_{\mathbf{q}}(t,t')$.

The first simplification concerns the "unpleasant" term $\tilde{\Delta}^s_{\mathbf{q}}(t)$ arising from the stress expression $\Sigma(t)$ in Eq. (3.15). In Ref. [60] it is suggested to set $\Sigma(t) \equiv 0$ in leading approximation, this leads immediately to $\tilde{\Delta}^s_{\mathbf{q}}(t) \equiv 0$. We note the identity

$$e^{\delta\Omega^\dagger t} = e^{\overline{\delta\Omega^\dagger} t}(1 + \Sigma(t)), \tag{3.30}$$

and hence $e^{\delta\Omega^\dagger t} = e^{\overline{\delta\Omega^\dagger} t}$ with $\Sigma(t) \equiv 0$. Approximating $\Sigma(t) \equiv 0$ leads also to a simplification of the memory function $m^s_{\mathbf{q}}(t,t')$ because $\Omega^\dagger_r$ reduces to $\Omega^\dagger_Q(t)$. With this, the time evolution $U_i(t,t')$ becomes

$$U^Q_i(t,t') = e^{\int_{t'}^t ds\, \Omega^\dagger_Q(s)\tilde{Q}^s(s)}_-. \tag{3.31}$$

It is finally in the space perpendicular to density fluctuations, $P^s U^Q_i(t,t') = P^s = U^Q_i(t,t')P^s$. For the memory function follows

$$\begin{aligned} m^s_{\mathbf{q}}(t,t') &= \frac{1}{q^2(t)q^2(t')}\left\langle \varrho^{s*}_{\mathbf{q}(t')}\Omega^\dagger_e e^{-\delta\Omega^\dagger t'} U_i(t,t') e^{\delta\Omega^\dagger t} Q^s(t)\Omega^\dagger_e \varrho^s_{\mathbf{q}(t)}\right\rangle, && (3.32)\\ &\approx \frac{1}{q^2(t)q^2(t')}\left\langle \varrho^{s*}_{\mathbf{q}(t')}\Omega^\dagger_e Q^s(t')\, e^{-\overline{\delta\Omega^\dagger} t'} U^Q_i(t,t') e^{\delta\Omega^\dagger t} Q^s(t)\Omega^\dagger_e \varrho^s_{\mathbf{q}(t)}\right\rangle. && (3.33)\end{aligned}$$

The $Q^s(t')$ on the left hand side can easily be verified; inserting $P^s(t')$ at the same position leads to zero. For the following mode coupling approximations, the pair density projector is used, which is assumed to describe the slow dynamics in the glassy regime. In contrast to the coherent case, the pair projector in the incoherent case consists of the product of coherent and incoherent fluctuations [10]. This has a physical reason; the fluctuation of the tagged particle depends on the collective dynamics, i.e., the dynamics of the surrounding bath particles. Technically this is achieved by the projector,

$$P^s_2(t) = \sum_{\mathbf{p},\mathbf{k},\mathbf{p}',\mathbf{k}'} \frac{\varrho^s_{\mathbf{p}(t)}\varrho_{\mathbf{k}(t)}\rangle\langle\varrho^{s*}_{\mathbf{p}'(t)}\varrho^*_{\mathbf{k}'(t)}}{\langle\varrho^{s*}_{\mathbf{p}'(t)}\varrho^*_{\mathbf{k}'(t)}\varrho^s_{\mathbf{p}(t)}\varrho_{\mathbf{k}(t)}\rangle} \approx \sum_{\mathbf{p},\mathbf{k}} \frac{\varrho^s_{\mathbf{p}(t)}\varrho_{\mathbf{k}(t)}\rangle\langle\varrho^{s*}_{\mathbf{p}(t)}\varrho^*_{\mathbf{k}(t)}}{NS_{k(t)}}. \tag{3.34}$$

Note that in contrast to the coherent pair projector, the two densities can be distinguished here and the wavevectors are not ordered. No counting factor will appear. The memory function (3.33) is written,

$$m^s_{\mathbf{q}}(t,t') \approx \frac{1}{q^2(t)q^2(t')}\left\langle \varrho^{s*}_{\mathbf{q}(t')}\Omega^\dagger_e Q^s(t')P^s_2(t')\, e^{-\overline{\delta\Omega^\dagger} t'} U^Q_i(t,t') e^{\delta\Omega^\dagger t} P^s_2(t)\, Q^s(t)\Omega^\dagger_e \varrho^s_{\mathbf{q}(t)}\right\rangle, \tag{3.35}$$

and in accordance with Ref. [60], the appearing four point correlation function is approximated as the product of correlators with full dynamics,

$$\begin{aligned}&\left\langle \varrho^{s*}_{\mathbf{p}(t')}\varrho^{*}_{\mathbf{k}(t')}e^{-\overline{\delta\Omega^\dagger}t'}U_i^Q(t,t')e^{\delta\Omega^\dagger t}\varrho^{s}_{\mathbf{p}'(t)}\varrho_{\mathbf{k}'(t)}\right\rangle\\ &\approx NS_{k(t')}\Phi^s_{\mathbf{p}(t')}(t-t')\,\Phi_{\mathbf{k}(t')}(t-t')\,\delta_{\mathbf{p},\mathbf{p}'}\delta_{\mathbf{k},\mathbf{k}'}.\end{aligned} \tag{3.36}$$

This factorization of the four point function is the major approximation used also in quiescent MCT [10]. The remaining parts of the vertex are now found easily, since they are identical as in equilibrium using the advected wavevectors instead of the time independent ones. The vertex in equilibrium reads (we have already inserted the restriction of $\mathbf{p}=\mathbf{k}-\mathbf{q}$),

$$V_{\mathbf{qk}}=\frac{\left\langle \varrho^s_{\mathbf{k}-\mathbf{q}}\varrho_{-\mathbf{k}}\,Q^s\,\Omega_e^\dagger\varrho^s_{\mathbf{q}}\right\rangle}{NS_k}=\frac{1}{V}\mathbf{k}\cdot\mathbf{q}\,c^s_k, \tag{3.37}$$

where $c^s_q=\langle\varrho^{s*}_q\varrho_q\rangle/(nS_q)$ is the direct single particle correlation function [29], $n=N/V$ is the density as before. The sum over bath particles does not contain the tagged particle, and we have $c^s_q=(S_q-1)/(nS_q)$ if the tagged particle is identical to the bath particles. Summarizing, we find the following approximate equation of motion for the incoherent transient density correlator,

$$\partial_t\Phi^s_{\mathbf{q}}(t)+\Gamma^s_{\mathbf{q}}(t)\left\{\Phi^s_{\mathbf{q}}(t)+\int_0^t dt' m^s_{\mathbf{q}}(t,t')\partial_{t'}\Phi^s_{\mathbf{q}}(t')\right\}=0, \tag{3.38}$$

with

$$m^s_{\mathbf{q}}(t,t')\approx\frac{1}{N}\sum_{\mathbf{k}}\frac{\mathbf{k}(t)\cdot\mathbf{q}(t)}{q^2(t)}\frac{\mathbf{k}(t')\cdot\mathbf{q}(t')}{q^2(t')}n^2c^s_{k(t)}c^s_{k(t')}S_{k(t')}\,\Phi^s_{\mathbf{k}(t')-\mathbf{q}(t')}(t-t')\Phi_{\mathbf{k}(t')}(t-t').$$

Changing the summation index from $\mathbf{k}$ to $\mathbf{k}'=\mathbf{k}(t')$ and immediately renaming the dummy variable from $\mathbf{k}'$ to $\mathbf{k}$, we get

$$m^s_{\mathbf{q}}(t,t')=\frac{1}{N}\sum_{\mathbf{k}}\frac{\mathbf{k}(t-t')\cdot\mathbf{q}(t)}{q^2(t)}\frac{\mathbf{k}\cdot\mathbf{q}(t')}{q^2(t')}n^2c^s_{k(t-t')}c^s_kS_k\,\Phi^s_{\mathbf{k}-\mathbf{q}(\mathbf{t}')}(t-t')\Phi_{\mathbf{k}}(t-t'). \tag{3.39}$$

This final form depends only explicitely on t'. This dependence comes only from the time dependence of $\mathbf{q}(t)$ as can be seen by writing $m^s_{\mathbf{q}}(t,t')=\bar{m}^s_{\mathbf{q}(t')}(t-t')$ with

$$\bar{m}^s_{\mathbf{q}}(t-t')=\frac{1}{N}\sum_{\mathbf{k}}\frac{\mathbf{k}(t-t')\cdot\mathbf{q}(t-t')}{q^2(t-t')}\frac{\mathbf{k}\cdot\mathbf{q}}{q^2}n^2c^s_{k(t-t')}c^s_kS_k\,\Phi^s_{\mathbf{k}-\mathbf{q}}(t-t')\Phi_{\mathbf{k}}(t-t'). \tag{3.40}$$

Through the pair density projector, the dynamics of the incoherent correlator is coupled to the coherent correlator. Eq. (3.38) can therefore only be solved if the corresponding equation for the coherent dynamics has been solved before. It is clear that a (large enough) tagged particle can only move if the surrounding particles move. There is a certain percolation threshold for the size of the tagged particle, below which it is mobile

even if the bath is arrested [76]. We will in the following only consider the case where the size of the tagged particle is larger than this threshold. Then, at $\dot{\gamma} = 0$, the dynamics of the tagged particle follows the dynamics of the bath particles [10, 77, 78], i.e., the tagged particle is trapped if, and only if, the bath is in the glassy state. In the following section, we will discuss the dynamics near the critical plateau under shear.

The memory function (3.39) depends on t' and $t - t'$. This complicates the following analysis because the convolution theorem cannot be applied. It probably originates from the fact that we investigate the transient regime which is not time translationally invariant. An equation for the stationary correlator should contain a memory function depending on $t - t'$ only.

3.3 β-Analysis

In this section, we will analyze the β-dynamics of the incoherent correlator, i.e., the dynamics near the critical plateau value f_q^{sc} of the un-sheared correlator,

$$\lim_{t\to\infty} \Phi_q^{s(e)}(t) = f_q^s, \qquad \text{glass.} \tag{3.41}$$

f_q^s jumps discontinuously from zero to a finite value at the transition, given the size of the tagged particle is not too close to the percolation threshold [10]. In Sec. 1.6, we introduced the following expansion of the coherent transient density correlator $\Phi_{\mathbf{q}}(t)$ near the plateau,

$$\Phi_{\mathbf{q}}(t) = f_q^c + h_q \mathcal{G}(t) \tag{3.42}$$

with a q-independent β-correlator $\mathcal{G}(t)$ obeying the β-equation,

$$\tilde{\varepsilon} - c^{(\dot{\gamma})}(\dot{\gamma}t)^2 + \lambda \mathcal{G}^2(t) = \frac{d}{dt}\int_0^t dt' \mathcal{G}(t-t')\mathcal{G}(t'). \tag{3.43}$$

According to Ref. [27], the coherent dynamics near the critical plateau is hence isotropic in space even under shear. See Ref. [27] and Sec. 1.6 for the solutions of $\mathcal{G}(t)$. In the following β-analysis for the incoherent transient correlator, we will consider only the case of $\varepsilon \geq 0$, because for $\varepsilon < 0$, the dynamics is independent of shear for $\dot{\gamma} \to 0$ and the equilibrium discussion is recovered [77]. For $0 \leq \varepsilon \ll 1$ and $\dot{\gamma}t \ll 1$, the incoherent correlator is expanded near the critical plateau

$$\Phi_{\mathbf{q}}^s(t) = f_q^{sc} + (1 - f_q^{sc})^2 \mathcal{G}_{\mathbf{q}}^s(t). \tag{3.44}$$

The detailed calculation can be found in appendix A. We find that the correlator near the critical plateau contains an isotropic part given by the coherent β-correlator $\mathcal{G}(t)$ as well as an anisotropic part $\mathcal{G}_{\mathbf{q}}^{(s,aniso)}(t)$,

$$\Phi_{\mathbf{q}}^s(t) = f_q^{sc} + h_q^s \left(\mathcal{G}(t) + \mathcal{G}_{\mathbf{q}}^{(s,aniso)}(t) \right). \tag{3.45}$$

The critical amplitude h_q^s is equal to the one at $\dot\gamma = 0$ [77]. For the anisotropic term, we use the explicit form of the memory function in Eq. (3.39) and find,

$$\mathcal{G}_{\mathbf{q}}^{(s,aniso)}(t) = G(\mathbf{q})\,\dot\gamma t + \mathcal{O}(\dot\gamma t)^2. \tag{3.46}$$

The terms of order $(\dot\gamma t)^2$ must be omitted in the linear equation for $\mathcal{G}_{\mathbf{q}}^s(t)$. The function $G(\mathbf{q})$ reads

$$G(\mathbf{q}) = \frac{(1-f^{sc})^2}{h_q^s}\frac{1}{N}\sum_{\mathbf{k}} n_c^2 c_k^{sc} S_k^c f_k^c f_{|\mathbf{k}-\mathbf{q}|}^{sc}\,\frac{\partial}{\partial\dot\gamma t}\frac{\mathbf{k}(t)\cdot\mathbf{q}(t)}{q^2(t)}\frac{\mathbf{k}\cdot\mathbf{q}}{q^2}c_{k(t)}^{sc}\Big|_{\dot\gamma t=0}. \tag{3.47}$$

It is worth noting that a possible anisotropic contribution in the coherent β-correlator would not change Eq. (3.45) because it would vanish in Eq. (A.7).

We evaluate (3.47) numerically in spherical coordinates for $\mathbf{k}$ using $\Delta k = 0.2$, $k_{max} = 40$ and $\Delta\theta = \Delta\phi = \pi/100$. The directions in $\mathbf{q}$-space are also characterized by spherical coordinates,

$$q_x = q\,\sin(\theta)\cos(\phi), \tag{3.48a}$$
$$q_y = q\,\sin(\theta)\sin(\phi), \tag{3.48b}$$
$$q_z = q\,\cos(\theta). \tag{3.48c}$$

Fig. 3.1 shows the anisotropic part of the β-correlator at wavevector $q = 7$ as function of ϕ. We find a behavior proportional to $\cos(\phi)\sin(\phi)$ for all angles θ and show exemplary two values, $\theta = \pi/2$ corresponding to $q_z = 0$, and $\theta = \pi/4$. In Fig. 3.2, we show the dependence on θ for $\phi = \pi/4$. The anisotropic part is proportional to $\sin^2(\theta)$. Overall we hence find the expected [79] "quadrupole"-dependence proportional to $\sin^2(\theta)\cos(\phi)\sin(\phi) \propto q_x\,q_y$. For $q_xq_y > 0$, the dynamics is slightly slower than on average and for $q_xq_y < 0$ it is slightly faster. In Fig. 3.3, we show the dependence of the anisotropic part on the lengths of q. It decreases slowly with q. The maximum value of the anisotropic part in all the figures is at about $0.25\dot\gamma t$. For the isotropic part, we have $\mathcal{G}(t)/(\dot\gamma t) \approx -2$, see Sec. 1.6.2. The sum of both is hence negative for all directions and the anisotropic part is a correction in the range of 10 to 20 percent.

The anisotropy of the dynamics is not unexpected. Fig. 3.4 shows the low density solution of the Smoluchowski equation under shear, see Eq. (1.8). Shown are the lines in the $z = 0$-plane on which $P(\mathbf{r}, \mathbf{r}_0 = 0, t = 1) = 1/100$ holds, i.e., the equal-probability density lines for the particle which was at the origin at $t = 0$. We have set $\dot\gamma = D_0 = 1$. With shear, the dynamics is faster for some regions (approximately where $xy > 0$) and slower for others (approximately where $xy < 0$) compared to the case of $\dot\gamma = 0$. It is also interesting to note that the distortion of the structure factor under shear is in linear order in shear rate also proportional to q_xq_y [61, 80] for liquid states.

3.4 α-Scaling Equation

For $\varepsilon \geq 0$ and $\dot\gamma \to 0$ with $\dot\gamma t = const.$, the β-correlator discussed in the previous section is a function of $\dot\gamma t$ only, see also Ref. [27] and Sec. 1.6 for the isotropic part $\mathcal{G}(t)$.

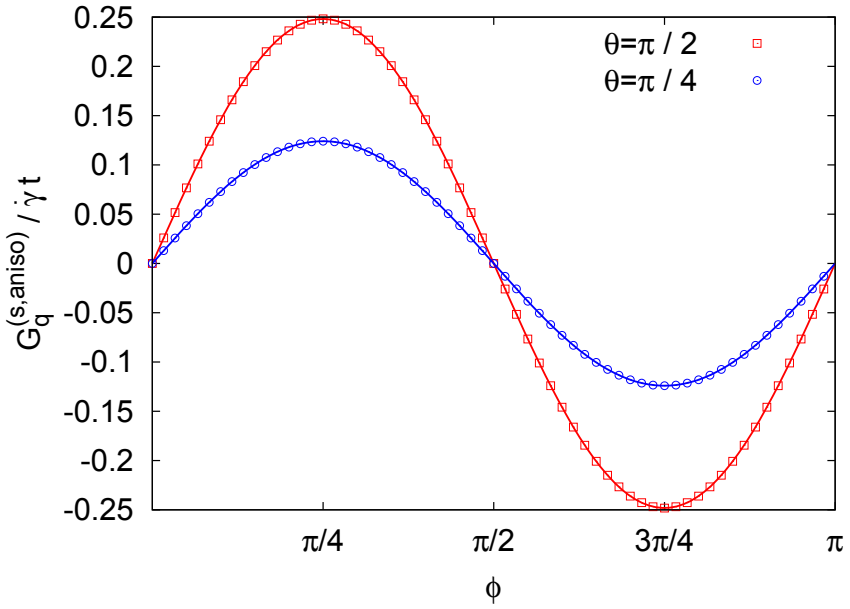

Figure 3.1: The anisotropic part of the β-correlator as function of ϕ at $|\mathbf{q}| = 7$ together with fitted curves proportional to $q_x q_y \propto \sin(\phi)\cos(\phi)$.

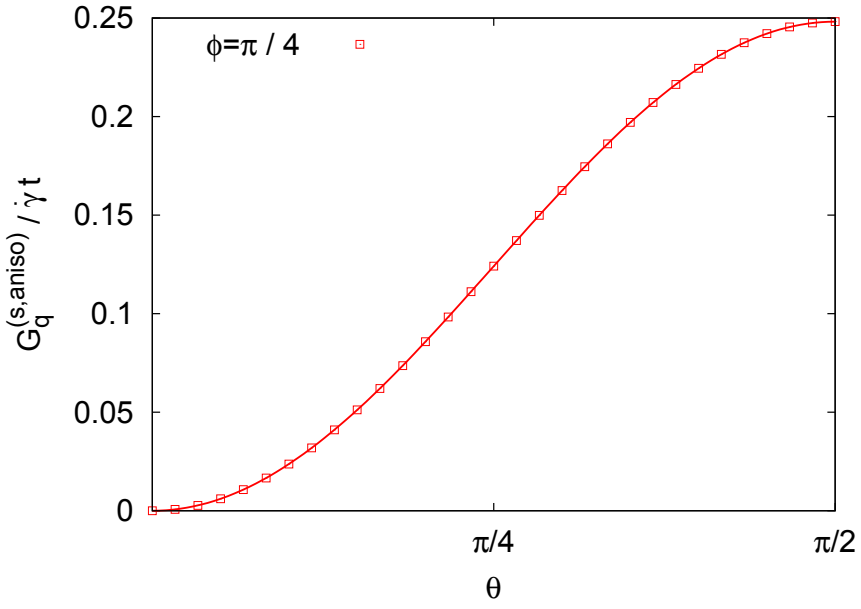

Figure 3.2: The anisotropic part of the β-correlator as function of θ for $|\mathbf{q}| = 7$ and $\phi = \pi/4$. The fitted curve is proportional to $\sin^2(\theta)$.

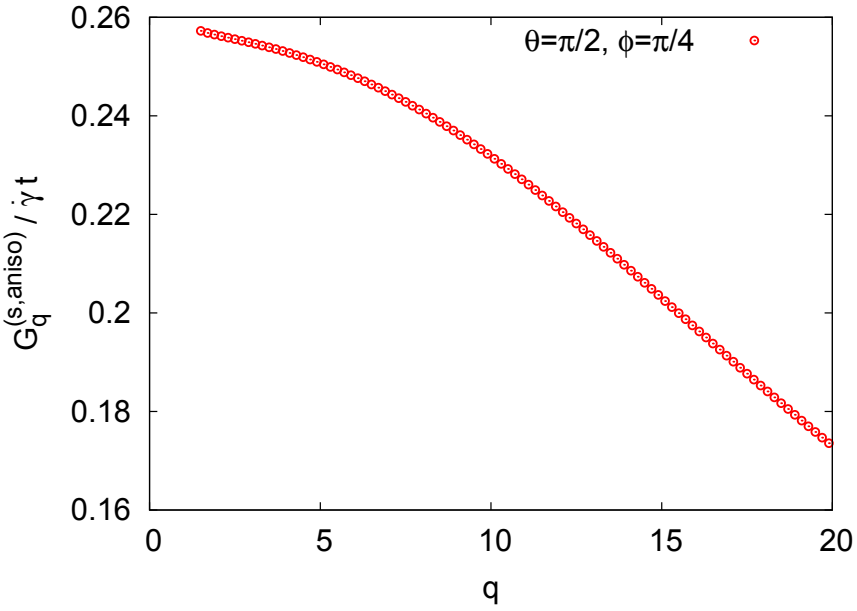

Figure 3.3: Dependence of the anisotropic part of the β-correlator on the lengths q of the wavevector.

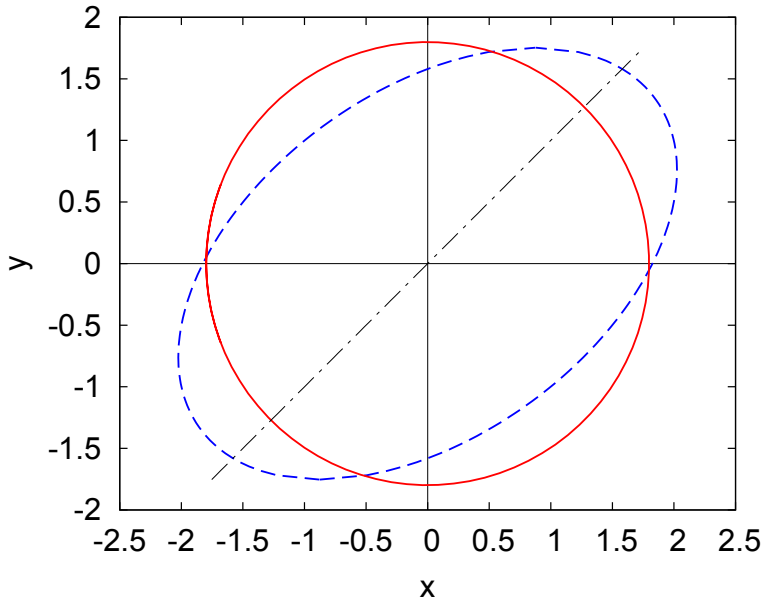

Figure 3.4: Lines with constant single particle probability density $P(\mathbf{r}, \mathbf{r}_0 = 0, t = 1) = 1/100$, see Eq. (1.8). Without shear (solid line), the line forms a circle. With shear (dashed line), the circle is stretched. The dynamics is enhanced for some regions and reduced for others. Dashed dotted line shows $x = y$.

The incoherent density correlator reaches a scaling function $\Phi_{\mathbf{q}}^{s+}(\tilde{t})$ in this limit, with $\tilde{t} = \sqrt{c^{(\dot\gamma)}/(\lambda - \frac{1}{2})}\dot\gamma t$. To derive the equation for $\Phi_{\mathbf{q}}^{s+}(\tilde{t})$, we start with the convolution integral in Eq. (3.38),

$$\int_0^t m_{\mathbf{q}}^s(t,t')\,\partial_{t'}\Phi_{\mathbf{q}}^s(t'). \tag{3.49}$$

In Eq. (3.40), we saw explicitely the dependence[1] of $m_{\mathbf{q}}^s(t,t')$,

$$m_{\mathbf{q}}^s(t,t') = \bar{m}_{\mathbf{q}(\dot\gamma t')}^s(t-t'). \tag{3.50}$$

It depends only on $\dot\gamma t'$ rather than on t'. It does so via the advected wavevector. That means that the dependence on t' already obeys the yield scaling law. Using this, we can rewrite the integral in Eq. (3.49) to

$$\begin{aligned} &-\bar{m}_{\mathbf{q}}^s(t) + \frac{d}{dt}\int_0^t dt'\bar{m}_{\mathbf{q}(\dot\gamma t')}^s(t-t')\Phi_{\mathbf{q}}^s(t') \\ &-\int_0^t dt'\frac{\partial \mathbf{q}(\dot\gamma t')}{\partial t'}\cdot\left(\frac{\partial}{\partial \mathbf{q}(\dot\gamma t')}\bar{m}_{\mathbf{q}(\dot\gamma t')}^s(t-t')\right)\Phi_{\mathbf{q}}^s(t'). \end{aligned} \tag{3.51}$$

We now see that the correlator for long times obeys the scaling equation (with $\dot\gamma t = \sqrt{(\lambda-\frac{1}{2})/c^{(\dot\gamma)}}\,\tilde{t} = \tilde{c}\tilde{t}$),

$$\begin{aligned} \Phi_{\mathbf{q}}^{s+}(\tilde{t}) \;=\; &\bar{m}_{\mathbf{q}}^{s+}(\tilde{t}) - \frac{d}{d\tilde{t}}\int_0^{\tilde{t}} d\tilde{t}'\bar{m}_{\mathbf{q}(\tilde{c}\tilde{t}')}^{s+}(\tilde{t}-\tilde{t}')\Phi_{\mathbf{q}}^{s+}(\tilde{t}') \\ &+\int_0^{\tilde{t}} d\tilde{t}'\frac{\partial \mathbf{q}(\tilde{c}\tilde{t}')}{\partial \tilde{t}'}\cdot\left(\frac{\partial}{\partial \mathbf{q}(\tilde{c}\tilde{t}')}\bar{m}_{\mathbf{q}(\tilde{c}\tilde{t}')}^{s+}(\tilde{t}-\tilde{t}')\right)\Phi_{\mathbf{q}}^{s+}(\tilde{t}'). \end{aligned} \tag{3.52}$$

This equation is difficult to solve because it contains the derivative of the correlator with respect to wavevector, but it shows that the correlator indeed shows yield scaling if the memory function does not depend on $t-t'$ only. The reason is that the advected wavevectors causing the deviation from $t-t'$ naturally show yield scaling. Using Eqs. (3.45) and (1.30), we hence find at $\varepsilon = 0$,

$$\Phi_{\mathbf{q}}^{s+}(\tilde{t}\to 0) = f_q^{sc} - \tilde{h}_{\mathbf{q}}^s\tilde{t}, \tag{3.53}$$

with $\tilde{h}_{\mathbf{q}}^s = h_q^s(1+G(\mathbf{q})\tilde{c})$ with $G(\mathbf{q})$ in Eq. (3.47). It can be straight forwardly shown that (3.53) solves the α-scaling equation Eq. (3.52) for short times. This closes our discussion of the dynamics of the incoherent density correlator.

3.5 Stationary Versus Transient Initial Decay Rate

Before turning to the mean squared displacements, let us briefly discuss a somewhat different topic. In simulations of hard spheres under shear, it is unclear whether the

[1] $\mathbf{q}(\dot\gamma t)$ is equal to $\mathbf{q}(t)$ defined earlier. We apologize for this inconsistency.

initial decay rate of incoherent density fluctuations perpendicular to the shear direction depends on shear rate [66]. This question can be answered by regarding the expressions for the initial decay rate in the stationary state for $q_x = 0$,

$$\Gamma_{\mathbf{q}}^{(s,\dot\gamma)} = -\left\langle e^{-i\mathbf{q}\cdot\mathbf{r}_s}\Omega^\dagger e^{i\mathbf{q}\cdot\mathbf{r}_s}\right\rangle^{(\dot\gamma)} = -\left\langle e^{-i\mathbf{q}\cdot\mathbf{r}_s}\Omega^\dagger e^{i\mathbf{q}\cdot\mathbf{r}_s}\right\rangle - \dot\gamma\int_0^\infty ds\left\langle \sigma_{xy}e^{\Omega^\dagger s}e^{-i\mathbf{q}\cdot\mathbf{r}_s}\Omega^\dagger e^{i\mathbf{q}\cdot\mathbf{r}_s}\right\rangle. \tag{3.54}$$

The first term on the right hand side is equal to q^2. The second one vanishes,

$$\dot\gamma\int_0^\infty ds\left\langle \sigma_{xy}e^{\Omega^\dagger s}e^{-i\mathbf{q}\cdot\mathbf{r}_s}\Omega^\dagger e^{i\mathbf{q}\cdot\mathbf{r}_s}\right\rangle = \dot\gamma\int_0^\infty ds\left\langle \sigma_{xy}e^{\Omega^\dagger s}(-q^2 + i\mathbf{q}\cdot\mathbf{F})\right\rangle = 0. \tag{3.55}$$

The first term in the brackets is a constant and vanishes [60]. The second term contains F_z and F_y. It can be rewritten to

$$\dot\gamma\int_0^\infty ds\left\langle \sigma_{xy}e^{\Omega^\dagger s}F_{z/y}\right\rangle = \left\langle F_{z/y}\right\rangle^{(\dot\gamma)} - \left\langle F_{z/y}\right\rangle = 0. \tag{3.56}$$

It is clear that the average value of the force on the tagged particle perpendicular to the flow must vanish in both averages, and the difference is hence zero as well. We conclude that the initial decay rate in the steady state is equal to the transient initial decay rate. The latter is equal to the one of the un-sheared system for $q_x = 0$ and hence independent of shear rate,

$$\Gamma_{\mathbf{q}}^{(s,\dot\gamma)} = -\left\langle e^{-i\mathbf{q}\cdot\mathbf{r}}\Omega^\dagger e^{i\mathbf{q}\cdot\mathbf{r}}\right\rangle^{(\dot\gamma)} = -\left\langle e^{-i\mathbf{q}\cdot\mathbf{r}}\Omega^\dagger e^{i\mathbf{q}\cdot\mathbf{r}}\right\rangle = q^2. \tag{3.57}$$

3.6 Mean Squared Displacements

In this section, we will derive equations for the mean squared displacement (MSD) of a tagged particle for the different spatial directions and show their asymptotic solutions for long times. We will first rewrite the memory function $m_{\mathbf{q}}^s(t,t')$ into a product of the part which depends only on the difference $t-t'$ and the part which depends explicitely on t and t',

$$m_{\mathbf{q}}^s(t,t') = \sum_{\mathbf{k}}\frac{\mathbf{k}(t-t')\cdot\mathbf{q}(t)}{q^2(t)}\frac{\mathbf{k}\cdot\mathbf{q}(t')}{q^2(t')}F(\mathbf{k},\mathbf{q}(t'),t-t'), \tag{3.58}$$

where the function F depends still explicitely on t' via the wavevector $\mathbf{q}(t')$, see Eq. (3.39). However, this dependence will vanish in the low q limit as used for the calculation of the MSDs. Since the MSD will be anisotropic, as was already seen in the low density case, (1.9), we will discuss the different directions separately.

3.6.1 Neutral Direction

The calculation for the neutral direction is in strong analogy to the equilibrium case [77, 81]. We expand the correlator in q_z to get

$$\Phi_{q\mathbf{e}_z}^s(t) = 1 - \frac{q^2}{2}\delta z^2(t) + \mathcal{O}(q^4), \tag{3.59}$$

where $\delta z^2(t)$ is the transient mean squared displacement of the particle in z-direction, corresponding to the average square of the traveled distance of the particle in simulations or experiments. Its equation of motion is achieved by inserting (3.59) into (3.38) keeping only the terms of order q^2. The equation is then integrated over time to get,

$$-\frac{1}{2}\delta z^2(t) + t - \frac{1}{2}\int_0^t dt' \int_0^{t'} dt'' m_z^0(t'-t'')\partial_{t''}\delta z^2(t'') = 0, \tag{3.60}$$

with the memory function in the low q limit

$$m_z^0(t) = \sum_{\mathbf{k}} k_z k_z \, F(\mathbf{k}, \mathbf{0}, t). \tag{3.61}$$

Since $m_z^0(t)$ has only one time-argument, one can rewrite the above equation using the standard trick of partial integrations and $\delta z^2(t=0) = 0$,

$$\delta z^2(t) + \int_0^t dt' m_z^0(t-t')\delta z^2(t') = 2t. \tag{3.62}$$

Eq. (3.62) now looks similar to the equilibrium case [77]. The long time limit of the solution corresponds to the small-z part of its Laplace transform $\delta z^2(z) = \int_0^\infty e^{-z\,t}\delta z^2(t)$. The convolution theorem can be applied. We find for $t \to \infty$,

$$\lim_{t\to\infty} \delta z^2(t) = \frac{2t}{1 + m_z^0(z=0)}. \tag{3.63}$$

In contrast to the equilibrium case, $m_z^0(z=0)$ is always finite under shear, as we saw in Sec. 3.3, and the MSD is always diffusive at long times. In the glass, we have $\lim_{\dot\gamma\to 0} m_z^0(z=0) \propto |\dot\gamma|^{-1}$ (compare the α-scaling equation Eq. (3.52)) leading to the scaling relation at small shear rates,

$$\lim_{t\to\infty} \delta z^2(t) = 2\beta_z|\dot\gamma|t, \tag{3.64}$$

where the coefficient $\beta_z = (|\dot\gamma| m_z^0(z=0))^{-1}$ is asymptotically independent of shear rate. We see that the long time diffusivity is then independent of the short time diffusivity D_0.

3.6.2 Gradient Direction

The gradient direction is similar to the neutral direction, we only treat it separately here because the MSDs in flow-, i.e. in x-direction will be coupled to the one in y-direction. The correlator is expanded in q_y,

$$\Phi^s_{q\mathbf{e}_y}(t) = 1 - \frac{q^2}{2}\delta y^2(t) + \mathcal{O}(q^4). \tag{3.65}$$

The equation of motion for the MSD in gradient direction reads

$$\delta y^2(t) + \int_0^t dt' m_y^0(t-t')\delta y^2(t') = 2t, \tag{3.66}$$

with the memory function

$$m_y^0(t) = \sum_{\mathbf{k}} k_y(t) k_y \, F(\mathbf{k}, \mathbf{0}, t). \tag{3.67}$$

As expected, the long time limit of $\delta y^2(t)$ is given by

$$\lim_{t\to\infty} \delta y^2(t) = \frac{2t}{1 + m_y^0(z=0)}. \tag{3.68}$$

This leads to a scaling relation similar to Eq. (3.64) for glassy states at low shear rates,

$$\lim_{t\to\infty} \delta y^2(t) = 2\beta_y |\dot\gamma| t. \tag{3.69}$$

We have no reason to expect that the coefficients β_y and β_z are equal. These have been found slightly different in simulations [65, 82].

3.6.3 Flow Direction

The derivation of the MSD in flow direction is more involved. We first have to identify the term that describes the average squared distance of the particle to its position at $t = 0$ measured in experiments or simulations. The connection of the density correlator for $\mathbf{q} = q\mathbf{e}_x$ to measured quantities is a general nontrivial question. Let us recall the *translational invariant* correlator for the x-direction

$$\Phi^s_{q\mathbf{e}_x}(t) = \left\langle e^{-iqx_s} e^{\Omega^\dagger t} e^{iqx_s} e^{-\dot\gamma t i q y_s} \right\rangle. \tag{3.70}$$

In the small density limit, the quantity $\delta x^2(t)$, measured in experiments as the average value of $(x(t) - x(0))^2$ follows from taking the $q \to 0$-limit of $\Phi^s_{q\mathbf{e}_x}(t)$, as we will see below. We hence conclude that this holds also at higher densities and write

$$\Phi^s_{q\mathbf{e}_x}(t) = 1 - \frac{1}{2} q^2 \delta x^2(t) + \mathcal{O}(q^4). \tag{3.71}$$

The equation for $\delta x^2(t)$ is gained by expanding the equation for the correlator $\Phi^s_{\mathbf{q}}(t)$ in q_x and by integrating with respect to t,

$$\begin{aligned} &\delta x^2(t) + \int_0^t dt' \int_0^{t'} dt'' \sum_{\mathbf{k}} \left(k_x - \dot\gamma t' k_y (t' - t'')\right) \frac{k_x - \dot\gamma t'' k_y}{1 + (\dot\gamma t'')^2} F(\mathbf{k}, \mathbf{0}, t' - t'') \partial_{t''} \delta x^2(t'') \\ &= 2 \int_0^t dt' \frac{\Gamma^s_{q\mathbf{e}_x}(t')}{q^2}. \end{aligned} \tag{3.72}$$

As promised, we would like to consider the low density limit before we start analyzing this equation. In this limit, the memory function vanishes, and we have

$$\delta x^2(t) = 2 \int_0^t dt' \frac{\Gamma^s_{q\mathbf{e}_x}(t')}{q^2} = 2t + \frac{2}{3}\dot\gamma^2 t^3, \tag{3.73}$$

i.e., we recover the low density limit of Eq. (1.9) *without* the term proportional to y_0^2. This is due to the fact the we consider translational invariant terms and the calculated expectation values cannot depend on initial conditions.

The memory function in Eq. (3.72) is not a function of the difference of its arguments only and we cannot use the convolution theorem. It is nevertheless still possible to determine the leading long time behavior, in which we are interested here. For this we write

$$\lim_{t\to\infty} \delta x^2(t) = at^3 + bt^2 + ct + \dots. \tag{3.74}$$

The form (3.74) can be justified knowing that the function F in Eq. (3.72) always decays to zero. A term t^4 (or higher powers in t, or fractional powers) does not exist since the initial decay rate does not contain such a term. The long time behavior is hence governed by the initial decay rate, a fact which is interesting because the long time behavior of the correlator $\Phi^s_{\mathbf{q}}(t)$ is independent of the initial decay rate, see the α-scaling equation (3.52). This is due to the fact that the limits of $t \to \infty$ and $q \to 0$ do not commute.

We first determine the coefficient a. For this, the leading long time (large t' and t'') terms in the double integral are needed which are independent of the coefficient b. The equation for b, on the other hand, will contain the coefficient a and can hence only be solved afterwards. The leading term of the first bracket is $-\dot\gamma t' k_y (t' - t'')$, the leading term of the fraction is given by $-k_y/(\dot\gamma t'')$. With this, we get

$$at^3 + \int_0^t dt' \int_0^{t'} dt'' \dot\gamma t' m_y^0(t' - t'') \frac{\partial_{t''} a t''^3}{\dot\gamma t''} = \frac{2\dot\gamma^2}{3} t^3. \tag{3.75}$$

We note that $m_y^0(t)$ appears. This equation can be treated with the following formulae for Laplace transforms [83],

$$\mathcal{L}\left\{\int_0^t dt' f(t')\right\}(z) = \frac{1}{z}\mathcal{L}\left\{f(t)\right\}(z), \tag{3.76a}$$

$$\mathcal{L}\left\{t f(t)\right\}(z) = -\frac{\partial}{\partial z}\mathcal{L}\left\{f(t)\right\}(z). \tag{3.76b}$$

Using this, we find that the two integrals in the expression above contain also one term of order t^2 (because $\partial_z m_y^0(z)$ is finite as $z \to 0$), which is neglected in this order. We find

$$a = \frac{2\dot\gamma^2}{3 + 3m_y^0(z=0)}. \tag{3.77}$$

Let us celebrate: We found the Taylor dispersion for Brownian particles at the glass transition. The intriguing result is that the coefficient for the t^3 term is connected to the long time diffusion coefficient in y-direction in the same way as in the low density limit. We can write

$$\delta x^2(t) = \frac{2}{3}\delta y^2(t)\dot\gamma^2 t^2 + \mathcal{O}(t^2), \tag{3.78}$$

which holds identically in the low density limit, Eq. (1.9), and was also found in Ref. [68] for non-Brownian particles, see Sec. 3.1. We see that this relation comes about because

the long time terms in the memory function in Eq. (3.75) are given by the memory function for the y-direction. This is physically very plausible if we recall the reason for the t^3-term: If the particle diffuses in y-direction, it gets a "boost" in x-direction due to the shear flow. It is hence not surprising that the t^3 term is proportional to $\delta y^2(t)$, but the result that the very same relation holds as in the low density limit is nontrivial and unexpected. Another interesting point is that we find a new type of Taylor dispersion in the glass at small shear rates. It is in contrast to the low density limit independent of the bare diffusivity D_0 (set to unity here) and obeys the yield scaling law,

$$\delta x^2(t) = \frac{2}{3}\beta_y \dot{\gamma}^2 |\dot{\gamma}| t^3 + \mathcal{O}(t^2), \tag{3.79}$$

with the same β_y as in Eq. (3.69). This is in agreement to recent simulations [65, 66].

We should not forget to consider the next order leading term. We will need this term later in order to calculate the xy cross correlation. For the equation for the coefficient b, we have to collect all terms proportional to t^2 at long times, (note that some of the possible contributions vanish in the sum over $\mathbf{k}$ due to symmetries[2]),

$$2b + 2bm_y^0(z=0) - 3a\partial_z m_y^0(z=0) - 3a\frac{m_{xy}^0(z=0)}{\dot{\gamma}} = 0. \tag{3.80}$$

The promised dependence of b on a appears. Also, the diagonal memory function enters,

$$m_{xy}^0(t) = \sum_{\mathbf{k}} k_y(t) k_x \, F(\mathbf{k}, \mathbf{0}, t). \tag{3.81}$$

We find for b,

$$b = \frac{3a}{2} \frac{\left(\partial_z m_y^0(z=0)\right) + \frac{m_{xy}^0(z=0)}{\dot{\gamma}}}{1 + m_y^0(z=0)}. \tag{3.82}$$

We found a term proportional to t^2, which is not present in the low density limit. It comes about because the memory function is not a function of $t - t'$. The actual value of the pre-factor b has to be determined in full microscopic calculations. We also want to recall that we are currently calculating the *transient* MSD. The stationary MSD might not have a term of order t^2 even if the transient has one.

3.6.4 Cross Correlation

In the system under shear, there is a correlation between x and y which is not present without shear, see Eq. (1.9). In order to calculate this, we go to the small q limit for the direction

$$\mathbf{q}(t=0) = \begin{pmatrix} q \\ q \\ 0 \end{pmatrix}. \tag{3.83}$$

[2] Although the memory function including the correlators is not isotropic under shear, it is still symmetric with respect to the origin, $\mathbf{k} = 0$, since the system is symmetric with respect to the origin.

This gives

$$\lim_{q\to 0}\frac{\Phi^s_{q(\mathbf{e}_x+\mathbf{e}_y)}(t)-1}{q^2} \equiv -\frac{1}{2}\delta_{xy}(t). \tag{3.84}$$

Regarding the low density limit[3], we find for the cross correlation measured as the average of $(x(t)-x(0))(y(t)-y(0))$,

$$\langle xy\rangle(t) = \frac{\delta_{xy}(t)-\delta x^2(t)}{2} + \delta y^2(t)\left(\dot\gamma t - \frac{1}{2}\right). \tag{3.85}$$

The equation of motion for δ_{xy} is given by,

$$\int_0^t dt' \int_0^{t'} dt'' \sum_{\mathbf{k}} \left(k_x + (1-\dot\gamma t')k_y(t'-t'')\right)\frac{k_x+(1-\dot\gamma t'')k_y}{1+(1-\dot\gamma t'')^2}F(\mathbf{k},\mathbf{0},t'-t'')\partial_{t''}\delta_{xy}(t'')$$
$$+\delta_{xy} = 2\int_0^t dt' \frac{\Gamma^s_{q\mathbf{e}_x+q\mathbf{e}_y}(t')}{q^2}. \tag{3.86}$$

Again, we can only solve this equation for the long time contributions after making the following ansatz,

$$\lim_{t\to\infty}\delta_{xy}(t) = a't^3 + b't^2 + c't + \dots. \tag{3.87}$$

We note that the leading long time term in Eq. (3.86) is equal to the long time term of δx^2, i.e.,

$$a' = a. \tag{3.88}$$

Additionally to the terms in Eq. (3.80), the equation for b' contains one contribution from the initial decay rate. The additional terms in Eq. (3.86) that come from the memory function exactly cancel each other in this order. We find for b',

$$b' = b - \frac{2\dot\gamma}{1+m^0_y(z=0)}. \tag{3.89}$$

It is important that $a'=a$, leading to the cancellation of the t^3-terms in Eq. (3.85). The leading order of $\langle xy\rangle(t)$ is hence proportional to t^2 as in the case without interactions,

$$\lim_{t\to\infty}\langle xy\rangle(t) = -\frac{\dot\gamma}{1+m^0_y(z=0)}t^2 + \dot\gamma t\delta y^2(t) + \mathcal{O}(t) = \frac{\dot\gamma}{1+m^0_y(z=0)}t^2 + \mathcal{O}(t). \tag{3.90}$$

The last step followed with the result for the long time diffusion in y-direction in Eq. (3.68). We see that $\delta y^2(t)$ and $\langle xy\rangle(t)$ are related to each other as in the low density limit, another interesting finding. For glassy states at low shear rates, we again find a scaling relation,

$$\lim_{t\to\infty}\langle xy\rangle(t) = \beta_y|\dot\gamma|\dot\gamma t^2 + \mathcal{O}(t), \tag{3.91}$$

with β_y as in Eq. (3.69). We note that the sign of $\langle xy\rangle$ depends on the sign of $\dot\gamma$, which is expected since inverting the direction of shearing corresponds to inverting either x or y.

[3] One has to use an anisotropic diffusivity D_0 in order to find that $\delta y^2(t)$ enters this relation instead of e.g. $\delta z^2(t)$. The two are identical in the low density limit with isotropic D_0.

3.7 Schematic Models

In order to illustrate the results we gained in the previous sections of this chapter, we introduce a schematic model for the incoherent transient density correlator $\Phi^s_{\mathbf{q}}(t)$, where the $\mathbf{q}$ dependence is dropped. We will therefore advance the so called Sjögren model [84] for the incoherent transient density correlator without shear and afterwards introduce schematic equations for the MSDs.

3.7.1 $(\dot\gamma)$-Sjögren Model

The equation of motion for $\Phi^s(t)$ in the $(\dot\gamma)$-Sjögren model reads

$$\dot\Phi^s(t) + \Gamma\left\{\Phi^s(t) + \int_0^t dt' m^s(\dot\gamma, t-t')\dot\Phi^s(t')\right\} = 0. \tag{3.92}$$

The memory function is approximated in analogy to (3.39) and (1.41),

$$m^s(\dot\gamma, t) = \frac{1}{1+(\dot\gamma t/\gamma_c^s)^2} v_s \Phi^s(t)\Phi(t). \tag{3.93}$$

The original Sjögren model is given with $m^s(0,t)$. The additional advection of the vertex in (3.39) is modeled by the shear dependent pre-factor. The coupling of the tagged particle to the surrounding particles is represented by the parameter v_s. One can show that the non-ergodicity parameter f^s of $\Phi^s(t)$ is connected to the parameter of the coherent correlator by

$$f^s = 1 - \frac{1}{v_s f}. \tag{3.94}$$

For $v_s < 1/f$, the incoherent correlator is decoupled from the coherent one, corresponding to the percolation threshold discussed above. The tagged particle is then small enough to move through the glassy matrix of host particles. For the standard values v_1^c and v_2^c used in the $F_{12}^{(\dot\gamma)}$-model, this threshold value for v_s is roughly $v_s = 3.4$ at $\varepsilon = 0$. We will use[4] $v_s = 5$. The parameter γ_c^s plays a role analogous to γ_c in Eq. (1.41), i.e., it tunes the strain $\dot\gamma t$, at which the cages break. Again, see Refs. [53, 55, 56] for the numerical algorithm to solve Eq. (3.92), which is similar to the one for the $F_{12}^{(\dot\gamma)}$-model. Fig. 3.5 shows Φ^s together with Φ for a glassy state and $\gamma_c^s = 1$. We see that the final decay of the incoherent correlator is faster than the decay of the coherent correlator due to the additional advection in the incoherent vertex.

3.7.2 Mean Squared Displacements

For the MSDs, we use the simplest possible equations that contain our findings of Sec. 3.6. They will be isotropic in the plane perpendicular to the flow and $\mathbf{e}_{\tilde z}$ shall denote any

[4] This value is rather small compared to studies of the original Sjögren model [63], but the author found the final shear induced relaxation to get slower with increasing values of v_s making smaller values of $\dot\gamma_c^s$ necessary to observe the linear part in the MSD in Sec. 3.7.2.

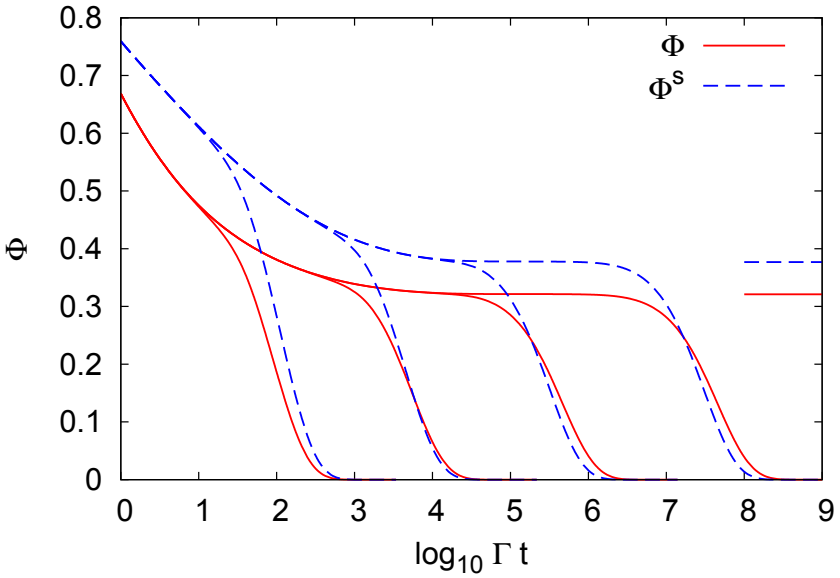

Figure 3.5: Transient coherent and incoherent correlators from the $F_{12}^{(\dot\gamma)}$-model and the $(\dot\gamma)$-Sjögren model for a glassy state ($\varepsilon = 10^{-3}$) at shear rates of $\dot\gamma/\Gamma = 10^{-8}$, 10^{-6}, 10^{-4}, 10^{-2} from right to left. Lines on the right hand side mark the non-ergodicity parameters.

direction in the yz-plane. The schematic equation reads (compare Eq. (3.62)),

$$\delta\bar{z}^2(t) + \int_0^t m^s(t-t')\delta\bar{z}^2(t) = 2t, \tag{3.95}$$

where the memory function $m^s(t-t')$ is given in Eq. (3.93). In the microscopic equation (3.62) the limit of $q \to 0$ of the memory function appears. This limit cannot be performed in the schematic model and there is no reason to introduce a difference between the memory function at $q \to 0$ and at finite q. From Eq. (3.95), the diffusive long time limit of the MSD in $\bar{z}$-direction follows directly,

$$\lim_{t\to\infty} \delta\bar{z}^2(t) = \frac{2t}{1 + m^s(z=0)}. \tag{3.96}$$

For the x-direction, we use a schematic version of Eq. (3.72), which can be simplified because $m^s(t,t') = m^s(t-t')$,

$$\delta x^2(t) + \int_0^t m^s(t-t')\delta x^2(t) = 2t + \frac{2}{3}\dot\gamma^2 t^3. \tag{3.97}$$

The long time limit follows,

$$\lim_{t\to\infty} \delta x^2(t) = \frac{2t + \frac{2}{3}\dot\gamma^2 t^3}{1 + m^s(z=0)}, \tag{3.98}$$

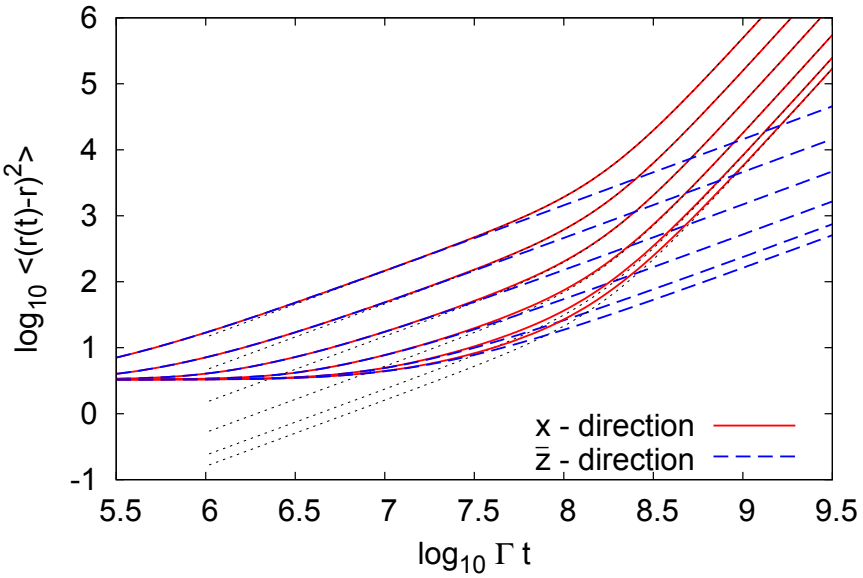

Figure 3.6: The MSD in flow direction and perpendicular for $\dot{\gamma}/\Gamma = 10^{-8}$ and $\varepsilon = 10^{-3}$. ${\gamma_c^s}^{-2} = 10^n$ with $n = 0, \ldots, 5$ from right to left. The dotted curves show the long time behavior according to Eq. (3.98).

i.e., $b = 0$ in Eq. (3.74), in contrast to the microscopic calculation. We already stressed in Sec. 3.6.3 that $b \neq 0$ appears due to the two arguments t and t' of the memory function. See again Refs. [53, 55] for the numerical algorithm to solve Eqs. (3.95) and (3.97). While in all our calculations concerning coherent quantities, the parameter γ_c can be scaled out, the parameter γ_c^s cannot be scaled out concerning the MSDs. This is due to the fact that a new timescale, namely $\dot{\gamma}^{-1}$, enters via the initial decay rate in x-direction in Eq. (3.97). Fig 3.6 shows the MSDs for different values of γ_c^s at $\dot{\gamma}/\Gamma = 10^{-8}$ and $\varepsilon = 10^{-3}$. For $\gamma_c^s = 1$, the dynamics of the system is slow compared to the initial decay rate, and the term proportional to t in Eq. (3.98) cannot be observed. For smaller values of γ_c^s, the linear term becomes more and more pronounced. In the following, we will use the value of $\gamma_c^s = 1/10$, as was done in Ref. [13] for the coherent case. In Fig. (3.7) we show the MSDs for different shear rates for a glassy state. The different shear rates look qualitatively similar, we observe the diffusive behavior for the $\bar{z}$-direction and the Taylor behavior for the x-direction. In Fig. 3.8, the curves are shown as function of strain $\dot{\gamma}t$, where the yield scaling of Eq. (3.69) and (3.79) is observed, i.e., for $\dot{\gamma} \to 0$, the curves fall on top of each other. The liquid case is of interest also, as shown in Fig. 3.9. At small shear rates, the MSD perpendicular to the shear direction becomes indistinguishable from the $\dot{\gamma} = 0$ case. But the Taylor dispersion is still present, i.e., the MSD in x-direction still shows a term t^3 at long times. Only the pre-factor shows no yield scaling any more, i.e, $m^s(z = 0)$ in Eq. (3.98) becomes independent of shear rate.

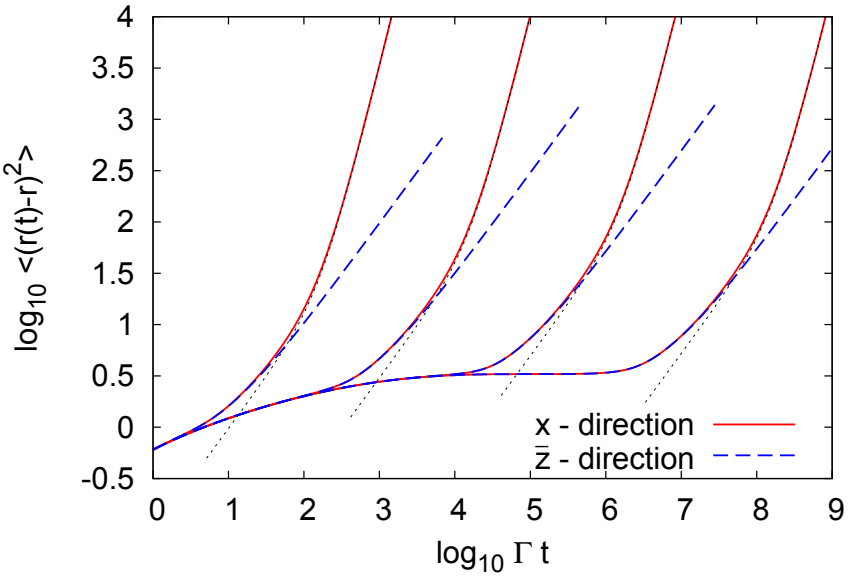

Figure 3.7: The MSD in flow direction and perpendicular for $\varepsilon = 10^{-3}$ and $\gamma_c^s = 1/10$. Shear rates are $\dot{\gamma}/\Gamma = 10^{-8,-6,-4,-2}$ from right to left. The dotted curves show the long time behavior according to Eq. (3.98).

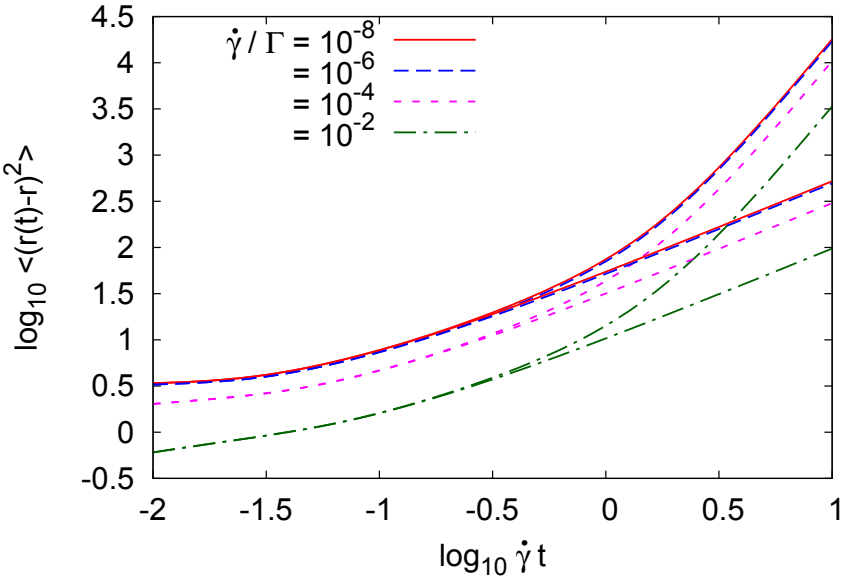

Figure 3.8: The MSD in flow direction and perpendicular for $\varepsilon = 10^{-3}$ and $\gamma_c^s = 1/10$ as function of strain $\dot{\gamma}t$. For $\dot{\gamma} \to 0$, the long time part of the curves fall on top of each other.

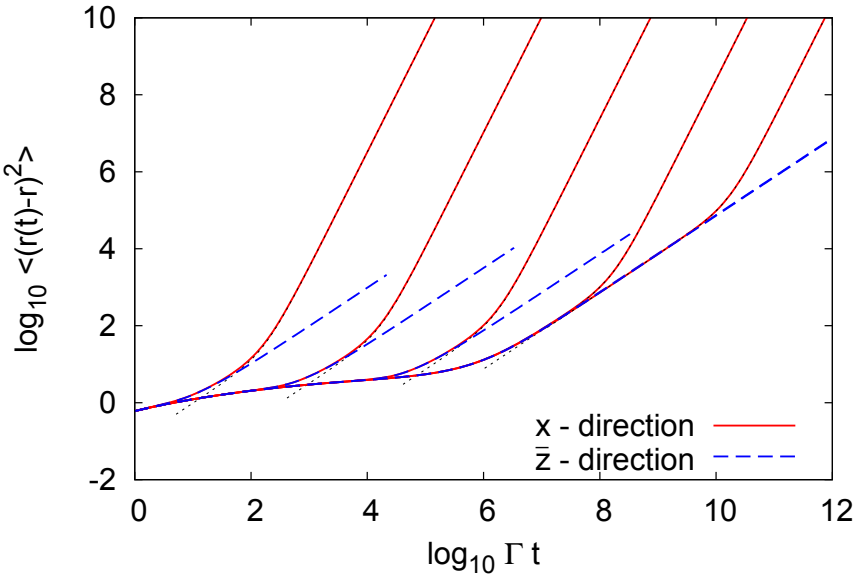

Figure 3.9: The MSD in flow direction and perpendicular for $\varepsilon = -10^{-3}$ (fluid). Shear rates are $\dot{\gamma}/\Gamma = 10^{-10,-8,-6,-4,-2}$ from right to left. The dotted curves show the long time behavior according to Eq. (3.98).

We note that the MSD in x-direction is an example for a quantity which can distinguish the shear from the no shear case even in the fluid at low shear rates.

3.8 Stationary Mean Squared Displacements

Let us recall that we so far calculated the transient mean squared displacements, i.e., $\dot{\gamma} = 0$ for $t < 0$ and $\dot{\gamma} \neq 0$ for $t \geq 0$. Before we discuss the difference between these and the stationary ones, let us emphasize their commonality: A very long time after switch-on of the rheometer the time derivative of the transient MSD must reach the time derivative of the corresponding stationary MSD. This is true because at these very long times the transient correlator describes the stationary state and the long time diffusivity must be the one of the steady state. All the results for the respective leading order ($\propto t$ perpendicular and $\propto t^3$ parallel to the flow) we achieved in the previous section are valid for the stationary MSDs as well, with the same pre-factors. Our ITT approach of first deriving the transient quantities and then deriving the stationary ones from them, proves to be a simplification and advantage here: For the long time diffusivity, the second step is not necessary, it follows directly from the equation for the transient MSD.

Nevertheless, at intermediate times, there is a difference, as measured in Ref. [14]. In the following, the notation $\delta^{(\dot{\gamma})}z^2(t)$ and $\delta^{(e)}z^2(t)$ for stationary and equilibrium MSDs will be used to distinguish them from the transient ones. The stationary MSD can easily

be derived via Eq. (2.19) for the respective correlator. At $t = 0$ the MSDs are trivially zero, i.e., the first term in (2.19) vanishes. For the directions perpendicular to the flow (again denoted $\bar{z}$), we find

$$\delta^{(\dot{\gamma})}\bar{z}^2(t) \approx \delta\bar{z}^2(t) - 2\frac{\tilde{\sigma}}{\dot{\gamma}} \lim_{q\to 0} \frac{\dot{\Phi}^s_{q\mathbf{e}_{\bar{z}}}(t) - \dot{\Phi}^{s(e)}_{q\mathbf{e}_{\bar{z}}}(t)\frac{\Phi^s_{q\mathbf{e}_{\bar{z}}}(t)}{\Phi^{s(e)}_{q\mathbf{e}_{\bar{z}}}(t)}}{q^2}. \tag{3.99}$$

The limit $q \to 0$ is easily performed since the derivatives are of order q^2 and the $q = 0$ value of the fraction $\Phi^s_{q\mathbf{e}_{\bar{z}}}(t)/\Phi^{(s,e)}_{q\mathbf{e}_{\bar{z}}}(t)$ is equal to unity,

$$\delta^{(\dot{\gamma})}\bar{z}^2(t) \approx \delta\bar{z}^2(t) + \frac{\tilde{\sigma}}{\dot{\gamma}}\partial_t \left(\delta\bar{z}^2(t) - \delta^{(e)}\bar{z}^2(t)\right). \tag{3.100}$$

From Eq. (3.100) we have that the stationary MSD is larger than the transient one if $\delta z^2(t)$ is larger than $\delta^{(e)}z^2(t)$, which is expected and observed in experiments and simulations. It cannot be shown rigorously.

Using the schematic model in Eq. (3.95) and the normalized stress $\tilde{\sigma}$ from Eq. (2.7), we can visualize the two different MSDs. We want to emphasize that we use $\gamma^s_c = 1$, because otherwise the modulus, as approximated in Eq. (3.100), would relax too slowly compared to the memory function $m^s(t)$, giving a too large $\tilde{\sigma}$. Another option would be to use $\gamma^s_c = 1/10$ and $\gamma_c = 1/10$ in Eq. (1.40), i.e., we need $\gamma^s_c = \gamma_c$ here. In Fig. 3.10 we show the result for a glassy state and different shear rates. The discussed relation is observed. Fig. 3.10 is in excellent qualitative agreement to the simulations and experiments reported in Ref. [14]. The transient MSD follows the quiescent one until $\dot{\gamma}t/\gamma^s_c \approx 0.1$ and joins the steady one at $\dot{\gamma}t/\gamma^s_c \approx 1$, which is also in good agreement with the simulations and experiments. A last comment; in the simulations and, less pronounced, also in the experiments in Ref. [14], the transient MSD is super-diffusive for intermediate times. This behavior is connected to the overshoot of the transient shear stress. Such a behavior can only result from Eq. (3.95) if $m^s(t)$ is negative for intermediate times and needs further theoretical studies. The stress overshoot is not contained in the schematic model by construction.

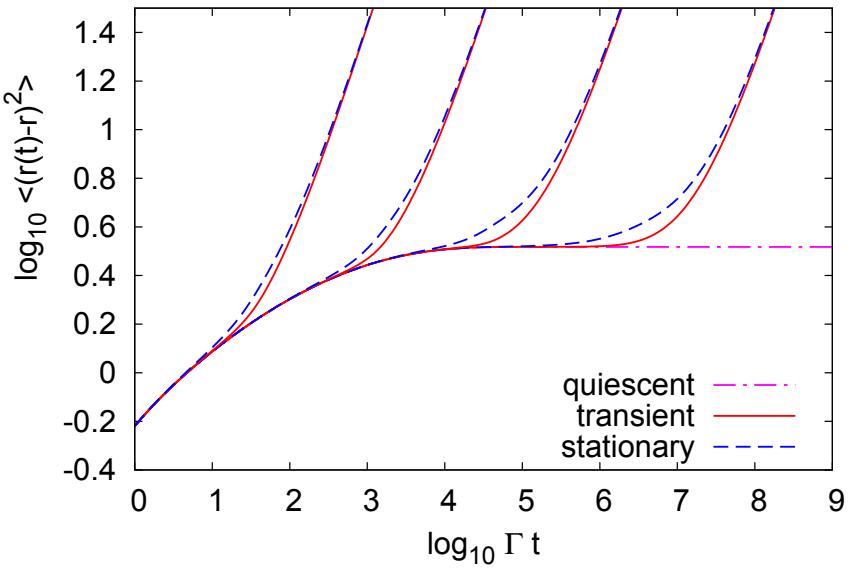

Figure 3.10: Quiescent, transient and stationary MSDs perpendicular to the flow direction in the schematic model for $\varepsilon = 10^{-3}$ (glass) and $\gamma_c^s = 1$. Shear rates are $\dot{\gamma}/\Gamma = 10^{-8,-6,-4,-2}$ from right to left.

4 Fluctuation Dissipation Relations under Steady Shear

In this chapter, we study the fluctuation dissipation theorem (FDT) [22, 85] under shear. This was the focus of study of the author during the last three years and was motivated by the findings in the simulations in Ref. [1] and the interpretation of these findings in terms of an effective temperature. After the introduction, Secs. 4.1–4.4, this chapter will be split into two parts. First, we will in Sec. 4.5 show a treatment of the new terms in the FDT within the Zwanzig-Mori projection operator formalism. In Sec. 4.6 we will show the connection of one of the new terms to the waiting time derivative discussed in Chap. 2, which will lead to interesting and special predictions. In both approaches we find the same qualitative features of the FDT under shear, namely the response function is smaller at long times as estimated by the equilibrium FDT and the ratio between response and fluctuation functions is nearly constant in time. The reader primarily interested in the final results and opinion of the author may want to skip Sec. 4.5. The reader who wants to see that the results presented in Sec. 4.6 are backed by a detailed analysis within MCT is referred to Sec. 4.5.

4.1 Fluctuation Dissipation Theorem (FDT) and – Ratio (FDR)

In thermal equilibrium, the response of a system to a small external force follows directly from thermal fluctuations of the unperturbed system. This connection is the essence of the fluctuation dissipation theorem (FDT) which lies at the heart of linear response theory. In our framework, the FDT *in equilibrium* connects the correlator $C_{\mathrm{fg}}^{(e)}(t)$ with the response function, the susceptibility $\chi_{\mathrm{fg}}^{(e)}(t)$ (defined below), and reads with restored units

$$\chi_{\mathrm{fg}}^{(e)}(t) = \frac{-1}{k_B T}\frac{\partial}{\partial t} C_{\mathrm{fg}}^{(e)}(t). \tag{4.1}$$

Eq. (4.1) will be proven when deriving the microscopic form of the susceptibility for Smoluchowski dynamics in Sec. 4.3. It states that the relaxation of a small fluctuation is independent of the origin of this fluctuation: Whether induced by a small external force or developed spontaneously by thermal fluctuations, the relaxation cannot distinguish these cases.

The most famous example for the FDT is given by the Einstein relation for the diffusivity of a free Brownian particle. One can consider two experiments, see Fig. 4.1: First, we watch the particle perform the random walk and measure the average mean squared

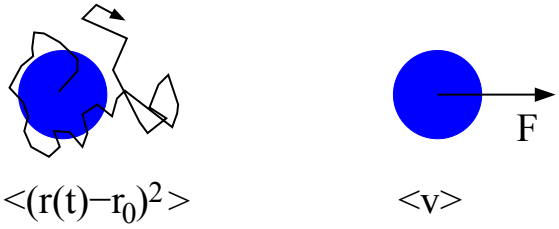

Figure 4.1: The Einstein relation as an example for the FDT: The mean squared displacement (left) of the particle and its mobility $\langle|\mathbf{v}|\rangle/|\mathbf{F}|$ (right).

displacement. Second, we drag the particle through the otherwise quiescent fluid with a test force and measure the average velocity of the particle. These two experiments measure very different properties of the system, i.e., the diffusivity of the particle in the first case and its mobility in the fluid in the latter case. Still, knowing the outcome of one of the experiments, one can predict the outcome of the other. The two experiments are connected by the FDT, which in this example is represented by the Einstein relation between diffusivity D_0 and mobility μ_0 of the particle [86],

$$D_0 = k_B T \, \mu_0. \tag{4.2}$$

This example shows the power of the FDT. It is of importance for various applications in the field of material sciences since for example transport coefficients can be related to equilibrium quantities, i.e., the fluctuations of the corresponding variables [49, 87, 88]. So was it first formulated by Nyquist in 1928 [89] as the connection between thermal fluctuations of the charges in a conductor (mean square voltage) and the conductivity. The FDT holds also for quantum mechanical systems.

In non-equilibrium systems, this connection is not valid in general and much work is devoted to understanding the relation between fluctuation and response functions. This relation is often characterized by the fluctuation dissipation ratio (FDR) $X_{\mathrm{fg}}(t)$. In this thesis we shall seek the relation between stationary susceptibility and correlation function,

$$\chi_{\mathrm{fg}}(t) = -\frac{X_{\mathrm{fg}}(t)}{k_B T} \frac{\partial}{\partial t} C_{\mathrm{fg}}(t) \; . \tag{4.3}$$

Close to equilibrium, we recover the FDT in Eq. (4.1) with $X^{(e)}_{\mathrm{fg}}(t) \equiv 1$. In non-equilibrium, $X_{\mathrm{fg}}(t)$ deviates from unity. We will see that this is related to the existence of non-vanishing probability currents (see Eq. (1.5) in the introduction); FDRs are hence considered a possibility to quantify the currents and to signal non-equilibrium [90].

4.2 Previous Studies on the FDT in Non-Equilibrium

Note that in all the studies summarized below, the susceptibility is denoted R instead of χ. We will in this section keep the units used in the cited articles.

4.2.1 The General Formula for the Susceptibility in Non-Equilibrium

The general linear response susceptibility for non-equilibrium states with Fokker-Planck dynamics [22] has been derived by Agarwal in 1972 [91]. It is Eq. (4.28) for our Smoluchowski dynamics, which will be the starting point of our analysis. The susceptibility is given in terms of microscopic quantities, which cannot be identified with a measurable quantity in general in contrast to the equilibrium case.

4.2.2 FDT Violation for a Single Driven Particle

For a single driven Brownian particle in a periodic potential, the FDT violation for the velocity correlation has been studied in Ref. [92]. The susceptibility for fluctuations of the velocity $\dot{x}$ of the particle is defined as

$$R_{\dot{x}}(t-\tau) = \left.\frac{\delta\langle\dot{x}(t)\rangle_p}{\delta f_p(\tau)}\right|_{f_p=0}, \tag{4.4}$$

where $\langle\dots\rangle_p$ denotes the average under the probe force f_p on the particle. They find

$$TR_{\dot{x}}(t-\tau) = \langle\dot{x}(t)\dot{x}(\tau)\rangle - \langle\dot{x}(t)v_s(x(\tau))\rangle, \tag{4.5}$$

where $\langle\dots\rangle$ is the average in the unperturbed driven system. The last term in Eq. (4.5) is the term violating the equilibrium FDT. $v_s(x)$ is the local mean velocity at position x given by the probability current corresponding to $\Psi_s^{-1}\mathbf{j}_i^s$ in Eq. (1.5). It is found that the equilibrium FDT is restored if the velocity fluctuations are measured with respect to $v_s(x)$, i.e. for $v(t) = \dot{x}(t) - v_s(x(t))$,

$$TR_v(t-\tau) = \langle v(t)v(\tau)\rangle. \tag{4.6}$$

The local mean velocity depends on the position of the particle in the potential. We will come back to this in Chap. 5. These derivations have successfully been compared to the experimental realization of the system [93]. The authors achieved to measure the diffusivity, the mobility and the theoretical expressions for the violating term separately to show that the derived expressions hold.

4.2.3 FDT Violation in Spin Glasses – Effective Temperature

We want to briefly summarize the violation of the equilibrium FDT as derived in spin-glass calculations following Ref. [94]. A so called p-spin model is considered with Hamiltonian containing the interactions,

$$H = \sum_{j_1<\dots<j_p} J_{j_i\dots j_p}\, s_i \dots s_{j_p}. \tag{4.7}$$

J is the coupling between the continuous variables s_i. The Langevin equations for the spins s_i read,

$$\frac{\partial s_i(t)}{\partial t} = -\mu(t)s_i(t) - \frac{\delta H}{\delta s_i(t)} + f_i^{\text{drive}}(t) + \eta_i(t). \tag{4.8}$$

They contain the damping $\mu(t)$, the external drive (corresponding to the shear) $f_i^{\text{drive}}(t)$ and a Gaussian noise term $\eta_i(t)$. The equations are coupled via the Hamiltonian. In elaborate approximation steps, which are known to hold for "mean field like" systems, the above equation is then written as two coupled equations for the correlation $C(t,t') = \sum_i \langle s_i(t) s_i(t') \rangle$ and the response $R(t,t') = \sum_i \langle \delta s_i(t) / \delta \eta_i(t') \rangle$.

Without external drive, the system shows a transition from equilibrium above T_c to an aging system below T_c. With external drive, time translational invariance and ergodicity are recovered. For small external driving, the solutions for R and C are then split into a short time and a long time contribution. While the short time contributions are connected by the equilibrium FDT, the slow parts are found to be related as

$$R_s(\tau) = -\frac{1}{T_{\text{eff}}} \frac{dC_s(\tau)}{d\tau}. \tag{4.9}$$

The equilibrium form of the FDT is restored with pre-factor $1/T_{\text{eff}}$ instead of $1/T$. The value of T_{eff} is found to agree with the one of the corresponding calculation for the aging system. We note that in the initial equations of motion, the susceptibility is coupled to the correlation function, i.e., as far as the author can judge, one can only solve for both functions simultaneously. This introduces the susceptibility in a natural way in contrast to the mode coupling theory for colloidal systems, where the correlation function is derived without knowing the susceptibility. It remains questionable, whether the mean field closure leaves enough freedom for relations between R and C different from the simple one in Eq. (4.9). While the prediction in Eq. (4.9) deserves appreciation, we will shortly summarize why the study of the FDT for sheared colloidal suspensions is still necessary.

The presented approach (MCT-ITT) for dense colloidal suspensions under shear is very specific to the system under consideration, the sheared fluid. It starts from microscopic expressions containing the actual particle positions as functions of space and time, and the external shear is implemented with its geometric specialties in contrast to Eq. (4.8). The derived observables are directly related to quantities measured in experiments and simulations. As a consequence, specific properties of different observables can be derived, MCT-ITT predicts e.g. a yield stress which is not contained in the spin glass approach. The non-equilibrium FDT can hence also be studied for different observables, measured in simulations, and possible differences for different variables can be detected, as will be shown. Also, the general exact expression for the susceptibility connects it to the probability current, thereby giving deeper insight into the nature of the FDT violation.

4.2.4 Universal FDRs $X = \frac{1}{2}$ in Spin Models

Interesting universal FDRs were found in different spin models under coarsening [95–99] and under shear [100], where, at the critical temperature, a universal value of $X = \frac{1}{2}$ (with corrections [101]) in the long time limit was found. Since we will also find a value of the long time FDR close to $\frac{1}{2}$, we want to exemplary consider the derivation in Ref. [95] more closely. Considered is the ferromagnetic Ising chain with Glauber dynamics [102].

The Hamiltonian for the spins $\sigma_n = \pm 1$ reads

$$H = -J \sum_n \sigma_n \sigma_{n+1}. \tag{4.10}$$

The Glauber dynamics consists of picking at every time step $\delta t = 1/N$ a site i at random and updating its spin according to the stochastic rule

$$\sigma_n(t) \to \begin{cases} +1 & \text{with probability } \frac{1+\tanh(h_n(t)/k_B T)}{2}, \\ -1 & \text{with probability } \frac{1-\tanh(h_n(t)/k_B T)}{2}. \end{cases} \tag{4.11}$$

The update probability for the spin depends on the two neighboring sites,

$$h_n(t) = J(\sigma_{n-1}(t) + \sigma_{n+1}(t)). \tag{4.12}$$

For high temperatures, the updated spin is random, whereas for low temperatures, it strongly follows its neighbors. Starting from a random initial condition and quenching the system to a low temperature, the system relaxes to its paramagnetic equilibrium. The relaxation time τ_{eq} diverges exponentially as approaching $T = 0$, the critical temperature of the system. At $T = 0$, the updated spin will take the value of its neighbors if these are equal and will be updated randomly if these are different. Domains of positive and negative spins grow forever. Generally, one observes an aging regime for $\tau \sim t_w \ll \tau_{eq}$ with $t = \tau + t_w$ the correlation time and t_w the waiting time, both measured after the quench. The two-time autocorrelation function is introduced as

$$C(t, t_w) = \langle \sigma_n(t) \sigma_n(t_w) \rangle. \tag{4.13}$$

Due to translational invariance, it does not depend on n. The susceptibility R is given as the change of the average of spin n with external field $H_n(t)$ entering the local field in Eq. (4.12),

$$h_n(t) = J(\sigma_{n-1}(t) + \sigma_{n+1}(t)) + H_n(t). \tag{4.14}$$

R follows as

$$R(t, t_w) = T \left. \frac{\delta \langle \sigma_n(t) \rangle}{\delta H_n(t_w)} \right|_{H=0}. \tag{4.15}$$

The fluctuation dissipation ratio is defined as

$$X(t, s) = \frac{R(t, t_w)}{\partial C(t, t_w)/\partial t_w}. \tag{4.16}$$

Interestingly, one uses the derivative with respect to waiting time. For time translationally invariant states, one has $C(t, t_w) = C(t - t_w)$ and the derivative with respect to waiting time is equal to minus the time derivative. Eq. (4.3) follows. In the regime where all times are large, $\tau \sim t_w \sim \tau_{eq} \gg 1$, one finds the FDR in closed form ($\tau_{eq} = 2/\mu^2$),

$$X(t_w + \tau, t_w) = \frac{e^{-\mu^2 t_w} + \mu \sqrt{\pi t_w}\, \mathrm{erf}(\mu \sqrt{t_w})}{[2(t_w + \tau)/(2t_w + \tau)] e^{-\mu^2 t_w} + \mu \sqrt{\pi t_w} \mathrm{erf}(\mu \sqrt{t_w})}. \tag{4.17}$$

There are many time regimes with different values of the FDR between unity and $\frac{1}{2}$. In the aging regime $1 \ll t_w \ll \tau_{eq}$, the FDR for long times $\tau \gg t_w$ approaches the limiting value of

$$X_\infty = \frac{1}{2}. \tag{4.18}$$

At $T = 0$ this value holds for arbitrarily large waiting times t_w. Unfortunately, it is not apparent from the derivation why the FDR takes this special value.

4.2.5 Simulation Results for the FDR under Shear and Further Works

As presented in Chap. 1, colloidal dispersions exhibit slow cooperative dynamics at high concentrations and can arrest into metastable soft solids (glasses). Recall that when putting these glassy states under shear, the final decay of the correlation from the plateau to zero is governed solely by shear, however small the shear rate. In these states, a very unexpected 'restoration' of the equilibrium FDT was found in computer simulations by Berthier and Barrat [1, 103, 104], which initiated the presented studies: During the final shear governed decay, the FDR measured in the vorticity direction, i.e., the z-direction in our coordinate system, is different from unity, but constant in time. This ratio was also found to be independent of observable, which lead to the notion of an effective temperature $X_\mathrm{f} = T/T_\mathrm{eff}$ describing the non-equilibrium state. The findings are summarized by

$$\chi_\mathrm{f}(t) = \begin{cases} \frac{-1}{k_B T} \frac{\partial}{\partial t} C_\mathrm{f}(t) & \text{short times,} \\ \frac{-1}{k_B T_\mathrm{eff}} \frac{\partial}{\partial t} C_\mathrm{f}(t) & \text{long times.} \end{cases} \tag{4.19}$$

The corresponding spin glass calculations have been discussed in Sec. 4.2.3. T_eff was found to be larger than the real temperature, which translates into an FDR smaller than unity. Further simulations with shear also saw $T_\mathrm{eff} > T$ [105–108], but the variable dependence was not studied in as much detail as in Ref. [1], and partially other definitions of T_eff were used. As mentioned in Sec. 4.2.3, it is argued in Refs. [1, 94, 109] that T_eff in Eq. (4.19) agrees with the effective temperature connected with the FDT violation in the corresponding aging system [110, 111]. This has not yet been demonstrated for different temperatures. The fluctuation dissipation relation of aging systems using MCT was investigated in Ref. [112]. Recently T_eff was also connected to barrier crossing rates [113] replacing the real temperature in Kramers escape problem [22]. A theoretical approach for the effective temperature under shear in the so called "shear-transformation-zone" (STZ) model is proposed in Ref. [114]. Different techniques (with different findings) to measure FDRs in aging colloidal glasses were used in Refs. [115–117]. No experimental realization of an FDT study of colloidal suspensions under shear is known to the author. An overview over the research situation (in 2003) can be found in Ref. [90].

4.3 Linear Response and Susceptibility

As pointed out in the example of the Einstein relation, the susceptibility describes the response of the system to an external perturbation. We will consider susceptibilities

in the stationary state, i.e., the external steady shear flow was turned on a very long time ago. The force necessary to shear the system is finite, see Sec. 1.6.4, i.e., the term 'linear response' does not correspond to the shear, but to the small test force $h_e(t)$ acting on the particles. It tests their linear response. Because the system is always ergodic due to shearing, the linear response will always exist in contrast to un-sheared glasses [118, 119], where a finite force is needed to mobilize the particles. Formally, the susceptibility $\chi_{\text{fg}}(t)$ describes the linear response of the stationary expectation value of g to the external perturbation $h_e(t)$ shifting the internal energy U to $U - f^* h_e(t)$. In the following we will use dimensionless units again,

$$\langle g \rangle^{(\dot\gamma, h_e)}(t) - \langle g \rangle^{(\dot\gamma)} = \int_{-\infty}^{t} dt' \chi_{\text{fg}}(t - t') h_e(t') + \mathcal{O}(h_e^2) \,. \tag{4.20}$$

Note that the definition above is equivalent to the definitions used in the articles summarized in Sec. 4.2, we can also write

$$\chi_{\text{fg}}(t - t') = \left. \frac{\delta \langle g \rangle^{(\dot\gamma, h_e)}(t)}{\delta h_e(t')} \right|_{h_e = 0} . \tag{4.21}$$

To derive the microscopic form of the susceptibility, we consider the change of the stationary distribution function Ψ_s under the external perturbation. The SO changes to $\Omega - \Delta\Omega(\Gamma, t)$ with [21] (recall $\Gamma = \{\mathbf{r}_i\}$)

$$\Delta\Omega(\Gamma, t) = \sum_i \boldsymbol{\partial}_i \cdot \left(\frac{\partial}{\partial \mathbf{r}_i} f^*(\Gamma) \right) h_e(t). \tag{4.22}$$

The linear change of Ψ_s due to the external force is then

$$\Psi(t) = \Psi_s + \Delta\Psi(t) + \mathcal{O}(h_e^2). \tag{4.23}$$

With this, we can linearize the Smoluchowski equation,

$$\frac{\partial}{\partial t}(\Psi_s + \Delta\Psi(t)) = (\Omega - \Delta\Omega(t))(\Psi_s + \Delta\Psi(t)) + \mathcal{O}(h_e^2). \tag{4.24}$$

Using $\frac{\partial}{\partial t}\Psi_s = \Omega\Psi_s = 0$, we have

$$\frac{\partial}{\partial t}\Delta\Psi(t) = \Omega\Delta\Psi(t) - \Delta\Omega(t)\Psi_s + \mathcal{O}(h_e^2). \tag{4.25}$$

Eq. (4.25) can be viewed as a homogeneous equation for $\Delta\Psi(t)$ with inhomogeneity $\Delta\Omega(t)\Psi_s$. The solution for $\Psi(t)$ is given by [91]

$$\Psi(t) = \Psi_s - \int_{-\infty}^{t} dt' e^{\Omega(t-t')} \Delta\Omega(t')\Psi_s + \mathcal{O}(h_e^2). \tag{4.26}$$

Calculating the difference of the expectation values,

$$\langle g \rangle^{(\dot\gamma, h_e)}(t) - \langle g \rangle^{(\dot\gamma)} = \int d\Gamma \Psi(t) g - \int d\Gamma \Psi_s g, \tag{4.27}$$

we arrive at the final expression for the susceptibility after partial integrations,

$$\chi_{\rm fg}(t) = \left\langle \sum_i \frac{\partial f^*}{\partial \mathbf{r}_i} \cdot \boldsymbol{\partial}_i e^{\Omega^\dagger t} g \right\rangle^{(\dot\gamma)} . \tag{4.28}$$

If one replaces Ψ_s by Ψ_e and $\Omega^\dagger$ by $\Omega_e^\dagger$ in Eq. (4.28), the equilibrium FDT in Eq. (4.1) follows by partial integrations,

$$\chi^{(e)}_{\rm fg}(t) = \left\langle \sum_i \frac{\partial f^*}{\partial \mathbf{r}_i} \cdot \boldsymbol{\partial}_i e^{\Omega_e^\dagger t} g \right\rangle = -\left\langle f^* \Omega_e^\dagger e^{\Omega_e^\dagger t} g \right\rangle = -\frac{\partial}{\partial t} C^{(e)}_{\rm fg}(t). \tag{4.29}$$

4.4 Violation of Equilibrium FDT – Exact Starting Point

In the considered non-equilibrium system, where detailed balance is broken and a nonzero stationary probability current $\mathbf{j}_i^s = \hat{\boldsymbol{j}}_i \Psi_s = [-\boldsymbol{\partial}_i + \mathbf{F}_i + \boldsymbol{\kappa} \cdot \mathbf{r}_i]\Psi_s$ exists, the equilibrium FDT (4.1) is extended as we see now. The above expression, Eq. (4.28), can be rewritten (with adjoint current operator $\hat{\boldsymbol{j}}_i^\dagger$) to

$$\Delta\chi_{\rm fg}(t) = \chi_{\rm fg}(t) + \dot C_{\rm fg}(t) = -\left\langle \sum_i \hat{\boldsymbol{j}}_i^\dagger \cdot \frac{\partial f^*}{\partial \mathbf{r}_i} e^{\Omega^\dagger t} g \right\rangle^{(\dot\gamma)} . \tag{4.30}$$

Note that the new term in the FDT, $\Delta\chi_{\rm fg}(t)$, in the following called *violating term*, is directly proportional to the stationary probability current. A deviation of the fluctuation dissipation ratio (FDR), Eq. (4.3), from unity, the value close to equilibrium, arises. While the extended FDT in Eq. (4.30) has been known since the work of Agarwal [91], we will analyze it for driven metastable (glassy) states and show that the additive $\Delta\chi_{\rm fg}(t)$ correction [92, 93, 120] leads to the nontrivial multiplicative correction, i.e., a constant FDR at long times, which was found in the simulations. Specifically, we will look at autocorrelations, $g = f$ of functions without explicit advection, $f = f(\{y_i, z_i\})$, where the flow-term in the current operator $\hat{\boldsymbol{j}}_i^\dagger$ in (4.30) vanishes. For variables depending on x_i, the equilibrium FDT is already violated at low densities as seen from the Einstein relation: The mean squared displacement grows cubically in time, see Eq. (1.9), while the mobility of the particle is constant and equal to μ_0 for $y_0 = 0$.

Stationary averages are as always calculated via the ITT approach (1.13). ITT simplifies the following analysis because averages can now be evaluated in equilibrium, while otherwise non-equilibrium forces would be required [121]. E.g. due to $\boldsymbol{\partial}_i \Psi_e = \mathbf{F}_i \Psi_e$, the expression (4.30) vanishes in the equilibrium average and reduces to

$$\Delta\chi_{\rm f}(t) = -\dot\gamma \int_0^\infty ds \left\langle \sigma_{xy}\, e^{\Omega^\dagger s} \sum_i (\boldsymbol{\partial}_i + \mathbf{F}_i) \cdot \frac{\partial f^*}{\partial \mathbf{r}_i}\, e^{\Omega^\dagger t}\, f \right\rangle . \tag{4.31}$$

Eq. (4.31) is still exact and we will follow two approaches to approximate it. First, we will analyze it for the case of density fluctuations using Zwanzig-Mori projection

formalisms and MCT approximations in Sec. 4.5. In Sec. 4.6, we present the connection of the dominating contribution of $\Delta\chi_{\mathrm{f}}(t)$ to the waiting time derivative in Sec. 2.2 as presented in Ref. [64]. Both approaches lead to qualitatively similar findings, namely the time independent FDR at long times smaller than unity. They strongly support each other since there is not a single contradicting detail, only the exact numbers are different, the signs of the respective terms are equal. Additionally, the latter approach predicts a long time FDR in glasses of $X_{\mathrm{f}}(t \to \infty) \leq \frac{1}{2}$. As already mentioned in the outline of this chapter, the reader interested only in the final results of this thesis can safely skip Sec. 4.5.

4.5 Mode Coupling Approach

4.5.1 Zwanzig-Mori Formalism – FDT Holds at $t = 0$

We consider the violating term for coherent density fluctuations, $\delta f = f = \varrho_{\mathbf{q}} = \sum_i e^{i\mathbf{q}\cdot\mathbf{r}_i}$ with $q_x = 0$. Normalized equilibrium, transient and stationary correlators, as defined in Sec. 1.5, are denoted $\Phi_q^{(e)}(t)$, $\Phi_{\mathbf{q}}(t)$ and $C_{\mathbf{q}}(t)$. Stationary averages are normalized with the distorted static structure factor $S_{\mathbf{q}}^{(\dot\gamma)} = \langle \varrho_{\mathbf{q}}^* \varrho_{\mathbf{q}} \rangle^{(\dot\gamma)}/N$, the initial value of the stationary correlator in Eq. (2.5) [61]. The FDT-analysis for incoherent density fluctuations, which will be strongly analogous, follows in Sec. 4.5.6. It would, in principle, be possible to analyze both cases at once, but we do not want to unnecessarily complicate the notation. Also, the cases now appear in chronological order, as they were studied by the author. The term of consideration, Eq. (4.31), reads in this case

$$\Delta\chi_{\mathbf{q}}(t) = \frac{-\dot\gamma}{N S_{\mathbf{q}}^{(\dot\gamma)}} \int_0^\infty ds \left\langle \sigma_{xy} e^{\Omega^\dagger s} \sum_i (\boldsymbol{\partial}_i + \mathbf{F}_i) \cdot \frac{\partial \varrho_{\mathbf{q}}^*}{\partial \mathbf{r}_i} e^{\Omega^\dagger t} \varrho_{\mathbf{q}} \right\rangle .$$

Since we are left with an equilibrium average, it is useful to express $\Delta\chi_{\mathbf{q}}(t)$ in terms of $\Phi_{\mathbf{q}}(t) = \langle \varrho_{\mathbf{q}}^* e^{\Omega^\dagger t} \varrho_{\mathbf{q}} \rangle / (N S_q)$. We use an identity obtained in the Zwanzig-Mori projection operator formalism [59] (see Eq. (11) in Ref. [58] and compare Eq. (2.2)) to find the exact relation

$$\begin{aligned} \Delta\chi_{\mathbf{q}}(t) &= \int_0^t dt'\, N_{\mathbf{q}}(t-t')\, \Phi_{\mathbf{q}}(t'), \\ N_{\mathbf{q}}(t) &= \frac{-\dot\gamma}{N S_{\mathbf{q}}^{(\dot\gamma)}} \int_0^\infty ds \left\langle \sigma_{xy} e^{\Omega^\dagger s} \sum_i (\boldsymbol{\partial}_i + \mathbf{F}_i) \cdot \frac{\partial \varrho_{\mathbf{q}}^*}{\partial \mathbf{r}_i}\, Q e^{Q\Omega^\dagger Q t} Q\, \Omega^\dagger \varrho_{\mathbf{q}} \right\rangle, \end{aligned} \tag{4.32}$$

with $Q = 1 - P$ projecting on a subspace perpendicular to density fluctuations, P is defined in (1.22). Eq. (4.32) also contains a second term, $\Delta\chi_{\mathbf{q}}(t=0)\Phi_{\mathbf{q}}(t)$, the static coupling at $t = 0$. It vanishes in (4.32), i.e., $\Delta\chi_{\mathbf{q}}(0) = 0$, as can be shown; $\Delta\chi_{\mathbf{q}}$ is real [60], and we can write $\Delta\chi_{\mathbf{q}}(0) = \frac{1}{2}(\Delta\chi_{\mathbf{q}}(0) + \Delta\chi_{\mathbf{q}}^*(0))$. The integration over s can then be performed,

$$\Delta\chi_{\mathbf{q}}(0) = \frac{1}{2}\frac{-\dot\gamma}{N S_q^{(\dot\gamma)}} \int_0^\infty ds \left\langle \sigma_{xy} e^{\Omega^\dagger s} \Omega^\dagger \varrho_{\mathbf{q}}^* \varrho_{\mathbf{q}} \right\rangle = \frac{1}{2}\frac{-\dot\gamma}{N S_q^{(\dot\gamma)}} \left[\left\langle \sigma_{xy} e^{\Omega^\dagger s} \varrho_{\mathbf{q}}^* \varrho_{\mathbf{q}} \right\rangle \right]_{s=0}^{s=\infty} = 0. \tag{4.33}$$

The primitive vanishes at $s = \infty$, because the real parts of the eigenvalues of $\Omega^\dagger$ are negative. The one at $s = 0$ vanishes due to symmetry. It has thus been shown that the equilibrium FDT is exactly valid at $t = 0$.

4.5.2 Second Projection Step

It is necessary to perform a second projection step following Cichocki and Hess [74], before using MCT approximations for the memory function $N_\mathbf{q}$. Such a second projection step is also performed to achieve the equation of motion for the correlator, see Chap. 3. Regarding Eq. (4.32), one sees that $N_\mathbf{q}(t)$ is very similar to $\Delta\chi_\mathbf{q}(t)$ itself, up to one operator $\Omega^\dagger$ and the projectors Q. Due to this $\Omega^\dagger$, one can expect that $N_\mathbf{q}(t)$ behaves similar as a time derivative of $\Delta\chi_\mathbf{q}(t)$. MCT approximations applied to $N_\mathbf{q}(t)$ would not yield such a behavior. It is achieved only after the following second step. The adjoined of the Smoluchowski operator is formally decomposed as

$$\Omega^\dagger = \Omega^i + \Omega^\dagger \varrho_\mathbf{q} \rangle \langle \varrho_\mathbf{q}^* \Omega^\dagger \varrho_\mathbf{q} \rangle^{-1} \langle \varrho_\mathbf{q}^* \Omega^\dagger. \tag{4.34}$$

The function $N_\mathbf{q}(t)$ is then connected to a new function $n_\mathbf{q}(t)$ governed by Ω^i. The following identity can be proven by differentiation,

$$N_\mathbf{q}(t)/\Gamma_q = n_\mathbf{q}(t) - \int_0^t dt'\, N_\mathbf{q}(t')\, m_\mathbf{q}(t-t'), \tag{4.35}$$

$$n_\mathbf{q}(t) = \frac{-\dot\gamma}{N S_\mathbf{q}^{(\dot\gamma)} \Gamma_q} \int_0^\infty ds \left\langle \sigma_{xy} e^{\Omega^\dagger s} \sum_i (\boldsymbol{\partial}_i + \mathbf{F}_i) \cdot \frac{\partial \varrho_\mathbf{q}^*}{\partial \mathbf{r}_i}\, Q e^{Q\Omega^i Q t} Q\, \Omega^\dagger \varrho_\mathbf{q} \right\rangle, \tag{4.36}$$

$$m_\mathbf{q}(t) = \frac{S_q}{N q^4} \left\langle \varrho_\mathbf{q}^* \Omega^\dagger Q e^{Q\Omega^i Q t} Q\, \Omega^\dagger \varrho_\mathbf{q} \right\rangle. \tag{4.37}$$

The initial decay rate $\Gamma_q = q^2/S_q$ is time independent because of $q_x = 0$, compare Eq. (1.24). $m_\mathbf{q}$ is identified as the memory function, which appears in the equation of motion of the transient correlator. It is related to the transient correlator for $q_x = 0$ exactly by [21]

$$\dot\Phi_\mathbf{q}(t) + \frac{q^2}{S_q} \left\{ \Phi_\mathbf{q}(t) + \int_0^t dt' m_\mathbf{q}(t-t') \dot\Phi_\mathbf{q}(t') \right\} = 0. \tag{4.38}$$

We will later be interested in the Laplace transform, $m_\mathbf{q}(z) = \int_0^\infty e^{-zt} m_\mathbf{q}(t)$, which at $z = 0$ is in the limit of slow dynamics given with Eq. (4.38) by [77],

$$m_\mathbf{q}(z=0) = \Phi_\mathbf{q}(z=0). \tag{4.39}$$

The benefit of the second projection step can now be illuminated by regarding $N_\mathbf{q}(z)$, which is given via Eq. (4.35) by

$$N_\mathbf{q}(z) = \frac{n_\mathbf{q}(z)}{1/\Gamma_q + m_\mathbf{q}(z)}. \tag{4.40}$$

The divergent behavior of $m_{\mathbf{q}}(z=0)$ as $\dot\gamma \to 0$ in the glass will support $N_{\mathbf{q}}$ with an additional power of $\dot\gamma$ compared to $n_{\mathbf{q}}$. For a slow glassy function, such an additional power of $\dot\gamma$ signals a time derivative. The properties of $m_{\mathbf{q}}(z)$ are well known [27]. It decays on a timescale $(\tau^{-1}+\dot\gamma)^{-1}$, where τ is the timescale of the structural relaxation. In the glass, it is formally infinity leading to the yield scaling, see Secs. 1.6.3 and 3.4. We have

$$m_{\mathbf{q}}(z\to 0) \sim \begin{cases} \frac{1}{1/\tau+z+|\dot\gamma|} & \text{liquid,} \\ \frac{1}{z+|\dot\gamma|} & \text{glass.} \end{cases} \tag{4.41}$$

As will be shown below by MCT approximations, $n_{\mathbf{q}}(z)$ has the following properties,

$$n_{\mathbf{q}}(z\to 0) \sim \begin{cases} \frac{\dot\gamma^2\tau}{1/\tau+z+|\dot\gamma|} & \text{liquid,} \\ \frac{|\dot\gamma|}{z+|\dot\gamma|} & \text{glass.} \end{cases} \tag{4.42}$$

These lead via Eq. (4.40) to the following behavior for $N_{\mathbf{q}}(z=0)$ in the limit of $\dot\gamma \to 0$,

$$\lim_{\dot\gamma\to 0} N_{\mathbf{q}}(z=0) = \begin{cases} \mathcal{O}(\dot\gamma^2) & \text{liquid,} \\ \mathcal{O}(|\dot\gamma|) & \text{glass.} \end{cases} \tag{4.43}$$

The time integrated violating term $\Delta\chi_{\mathbf{q}}$ finally follows at small shear rates,

$$\lim_{\dot\gamma\to 0} \Delta\chi_{\mathbf{q}}(z=0) = \begin{cases} \mathcal{O}(\dot\gamma^2) & \text{liquid,} \\ \mathcal{O}(1) & \text{glass.} \end{cases} \tag{4.44}$$

Eq. (4.44) is in accordance with simulations and with the physically expected property of $\chi_{\mathbf{q}}$ to be always finite at $z=0$. The response should not diverge. The powers in $\dot\gamma$ above are the benefit of the second projection step.

In both the liquid and the glass, the violating term $\Delta\chi_{\mathbf{q}}$ is symmetric in $\dot\gamma$, reflecting the fact that fluctuations in z- and y-direction are independent of the direction of shearing. While $\Delta\chi_{\mathbf{q}}$ is analytic in $\dot\gamma$ in the fluid, it is nonanalytic in the glass.

4.5.3 Markov Approximation – Long Time FDR

Using a special projection step, we have shown in the previous section that the function $N_{\mathbf{q}}(z=0)$ is of order $|\dot\gamma|$ in the glass, i.e., we have reason to assume that $N_{\mathbf{q}}(t)$ decays fast in time compared to $\Phi_{\mathbf{q}}(t)$ which diverges at $z=0$ like $|\dot\gamma|^{-1}$. With this assumption, Eq. (4.32) can be written using the δ-function, $N_{\mathbf{q}}(t) \approx N_{\mathbf{q}}(z=0)\,\delta(t)$. For the susceptibility follows

$$\chi_{\mathbf{q}}(t) \approx -\frac{\partial}{\partial t} C_{\mathbf{q}}(t) + N_{\mathbf{q}}(z=0)\Phi_{\mathbf{q}}(t). \tag{4.45}$$

According to Eq. (4.45), the equilibrium FDT is violated if $N_{\mathbf{q}}(z=0)$ is nonzero. For short times, $\dot\gamma t \ll 1$, we have $|N_{\mathbf{q}}(z=0)| \ll |\dot C_{\mathbf{q}}(t)|$ and the equilibrium FDT holds. $N_{\mathbf{q}}(z=0)$ is of order $|\dot\gamma|$, see (4.43), $\dot C_{\mathbf{q}}(t)$ is of order Γ_q. For long times, $\dot\gamma t \approx 1$, $\dot C_{\mathbf{q}}(t)$

is also of order $|\dot\gamma|$, the two terms are comparable in size and the equilibrium FDT is violated. The long time FDR is additionally independent of time, if $C_{\mathbf{q}}(t)$ and $\Phi_{\mathbf{q}}(t)$ decay exponentially for long times with the same timescale. Approximating the two correlators to be equal and relaxing exponentially in glassy states,

$$\lim_{t\to\infty} C_{\mathbf{q}}(t) \approx \Phi_{\mathbf{q}}(t) \approx f_q e^{-a_{\mathbf{q}}|\dot\gamma|t}, \tag{4.46}$$

we find the FD relation in the glass,

$$\chi_{\mathbf{q}}(t) = \begin{cases} -\frac{\partial}{\partial t} C_{\mathbf{q}}(t) & \dot\gamma t \ll 1, \\ -\left(1 + \frac{N_{\mathbf{q}}(z=0)}{|\dot\gamma| a_{\mathbf{q}}}\right) \frac{\partial}{\partial t} C_{\mathbf{q}}(t) & \dot\gamma t = \mathcal{O}(1). \end{cases} \tag{4.47}$$

The long time FDR

$$X_{\mathbf{q}}(t\to\infty) = 1 + \frac{N_{\mathbf{q}}(z=0)}{|\dot\gamma| a_{\mathbf{q}}} \tag{4.48}$$

is time independent and also independent of shear rate for $\dot\gamma \to 0$. It is hence non-analytic in the glass as pointed out before. As we will see later, $N_{\mathbf{q}}(z=0)$ is negative in MCT approximations and the FDR is smaller than unity. All these findings are in agreement with the simulation results in Ref. [1].

In Sec. 4.5.5, we present a schematic model which allows to calculate the convolution in Eq. (4.32) and compare the results to the Markov approximation in Eq. (4.45). We will see that Eq. (4.45) is quite accurate but there are slight differences to the full convolution.

4.5.4 FDT Violation Quantitative – Numbers for the FDR

We will now perform MCT approximations for the memory functions $n_{\mathbf{q}}(t)$ and $m_{\mathbf{q}}(t)$. While the approximation for the latter is possible on 'standard routes' [60], the function $n_{\mathbf{q}}(t)$ in (4.36) is more involved. It contains two evolution operators, one for the correlation time t and one for the transient time s, which entered through the ITT approach. It furthermore contains derivatives with respect to s, as is shown by rewriting (4.36) via the following identity, which holds for general functions $f(\{y_i, z_i\})$ and $g(\{\mathbf{r}_i\})$. It is important to note that without identifying these s-derivatives, the correct $\dot\gamma$-dependence of $\Delta\chi_{\mathbf{q}}(t)$ would not be achieved[1],

$$\sum_i (\boldsymbol{\partial}_i + \mathbf{F}_i) \cdot \frac{\partial f^*}{\partial \mathbf{r_i}}\, g = \frac{1}{2}\left[\Omega^\dagger f^* g - f^* \Omega^\dagger g + (\Omega^\dagger f^*) g\right]. \tag{4.49}$$

[1] Remembering our arguments in Sec. 4.5.2, the reader realizes that finding the correct $\dot\gamma$-dependence was one of the major tasks in this approach.

This leads to three contributions for $n_{\mathbf{q}}(t)$,

$$\begin{aligned}
n_{\mathbf{q}}(t) &= n_{\mathbf{q}}^{(1)}(t) + n_{\mathbf{q}}^{(2)}(t) + n_{\mathbf{q}}^{(3)}(t), \\
n_{\mathbf{q}}^{(1)}(t) &= \frac{-\dot\gamma}{2NS_{\mathbf{q}}^{(\dot\gamma)}\Gamma_{\mathbf{q}}} \int_0^\infty ds \left\langle \sigma_{xy} e^{\Omega^\dagger s} \Omega^\dagger \varrho_{\mathbf{q}}^* U(t) \Omega^\dagger \varrho_{\mathbf{q}} \right\rangle, \\
&= \frac{\dot\gamma}{2NS_{\mathbf{q}}^{(\dot\gamma)}\Gamma_{\mathbf{q}}} \left\langle \sigma_{xy} \varrho_{\mathbf{q}}^* U(t) \Omega^\dagger \varrho_{\mathbf{q}} \right\rangle, \qquad (4.50a) \\
n_{\mathbf{q}}^{(2)}(t) &= \frac{\dot\gamma}{2NS_{\mathbf{q}}^{(\dot\gamma)}\Gamma_{\mathbf{q}}} \int_0^\infty ds \left\langle \sigma_{xy} e^{\Omega^\dagger s} \varrho_{\mathbf{q}}^* \Omega^\dagger U(t) \Omega^\dagger \varrho_{\mathbf{q}} \right\rangle, \qquad (4.50b) \\
n_{\mathbf{q}}^{(3)}(t) &= \frac{-\dot\gamma}{2NS_{\mathbf{q}}^{(\dot\gamma)}\Gamma_{\mathbf{q}}} \int_0^\infty ds \left\langle \sigma_{xy} e^{\Omega^\dagger s} (\Omega^\dagger \varrho_{\mathbf{q}}^*) U(t) \Omega^\dagger \varrho_{\mathbf{q}} \right\rangle, \qquad (4.50c) \\
U(t) &= Q e^{Q\Omega^i Q t} Q.
\end{aligned}$$

A large benefit from Eq. (4.49) is that the s-integration in $n_{\mathbf{q}}^{(1)}$ could be done directly. $n_{\mathbf{q}}^{(1)}$ will turn out to be the dominating term and will be connected to the waiting time derivative from Chap. 2 in Sec. 4.6. We can now approximate the formally exact expressions for $n_{\mathbf{q}}$ in (4.50) and $m_{\mathbf{q}}$ (4.37) by projection onto densities. Again, this physical approximation amounts to assuming that these are the only slow variables, sufficient to describe the relaxation of the local structure in the glassy regime. The special form of the functions $n_{\mathbf{q}}^{(2,3)}$ makes it necessary to use also the triple density projector. The detailed derivation of the expressions below can be found in appendix B. We show that the functions $n_{\mathbf{q}}^{(2)}$ and $n_{\mathbf{q}}^{(3)}$ have a term in common with different sign, which cancels, see Eq. (B.12). $\bar n_{\mathbf{q}}^{(2)}$ and $\bar n_{\mathbf{q}}^{(3)}$ denote the functions without these terms. We want to stress again that in the following expressions for $\bar n_{\mathbf{q}}^{(2)}$ and $\bar n_{\mathbf{q}}^{(3)}$, derivatives with respect to s show up due to the SOs in the exact expressions,

$$\begin{aligned}
n_{\mathbf{q}}^{(1)}(t) &= \frac{\dot\gamma S_q^2}{4nq^2 S_{\mathbf{q}}^{(\dot\gamma)}} \int \frac{d^3k}{(2\pi)^3} V_{\mathbf{qk}(-t)}^{(1)} V_{\mathbf{qk}}^{(2)} \Phi_{\mathbf{k}(-t)}(t) \Phi_{\mathbf{k}(-t)-\mathbf{q}}(t), \qquad (4.51a) \\
\bar n_{\mathbf{q}}^{(2)}(t) &= \frac{\dot\gamma S_q^2}{4nq^2 S_{\mathbf{q}}^{(\dot\gamma)}} \int_0^\infty ds \int \frac{d^3k}{(2\pi)^3} V_{\mathbf{qk}(-s)}^{(1)} V_{\mathbf{qk}(t)}^{(2)} \Phi_{\mathbf{q}}(s) \\
&\quad \left(\left[\frac{\partial}{\partial s} - \mathbf{k}'(-s) \cdot \frac{\partial}{\partial \mathbf{k}} \right] \Phi_{\mathbf{k}(-s)}(s) \Phi_{\mathbf{k}(-s)-\mathbf{q}}(s) \right) \Phi_{\mathbf{k}}(t) \Phi_{\mathbf{k}-\mathbf{q}}(t), \qquad (4.51b) \\
\bar n_{\mathbf{q}}^{(3)}(t) &= \frac{-\dot\gamma S_q^2}{4nq^2 S_{\mathbf{q}}^{(\dot\gamma)}} \int_0^\infty ds \int \frac{d^3k}{(2\pi)^3} V_{\mathbf{qk}(-s)}^{(1)} V_{\mathbf{qk}(t)}^{(2)} \left(\frac{\partial}{\partial s} \Phi_{\mathbf{q}}(s) \right) \\
&\quad \Phi_{\mathbf{k}(-s)}(s) \Phi_{\mathbf{k}(-s)-\mathbf{q}}(s) \Phi_{\mathbf{k}}(t) \Phi_{\mathbf{k}-\mathbf{q}}(t), \qquad (4.51c) \\
V_{\mathbf{qk}}^{(1)} &= k_x(k_y - q_y) \frac{S'_{q-k}}{q-k} S_k + k_x k_y \frac{S'_k}{k} S_{q-k}, \\
V_{\mathbf{qk}}^{(2)} &= \mathbf{q} \cdot ((\mathbf{k}-\mathbf{q}) n c_{k-q} + \mathbf{k} n c_k).
\end{aligned}$$

With $q - k = |\mathbf{q} - \mathbf{k}|$ and $\mathbf{k}(t) = \mathbf{k} - \mathbf{k} \cdot \boldsymbol{\kappa}\, t$ as before. c_k is the equilibrium direct

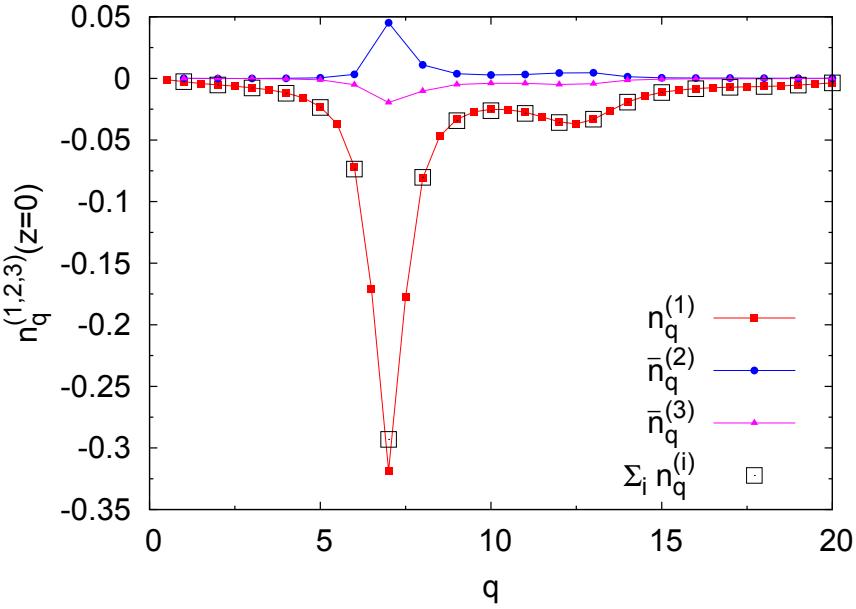

Figure 4.2: The three memory functions for $\mathbf{q} = q\mathbf{e}_z$. Shown are the time-integrated functions, $n_{\mathbf{q}}(z=0) = \int_0^\infty dt' n_{\mathbf{q}}(t')$.

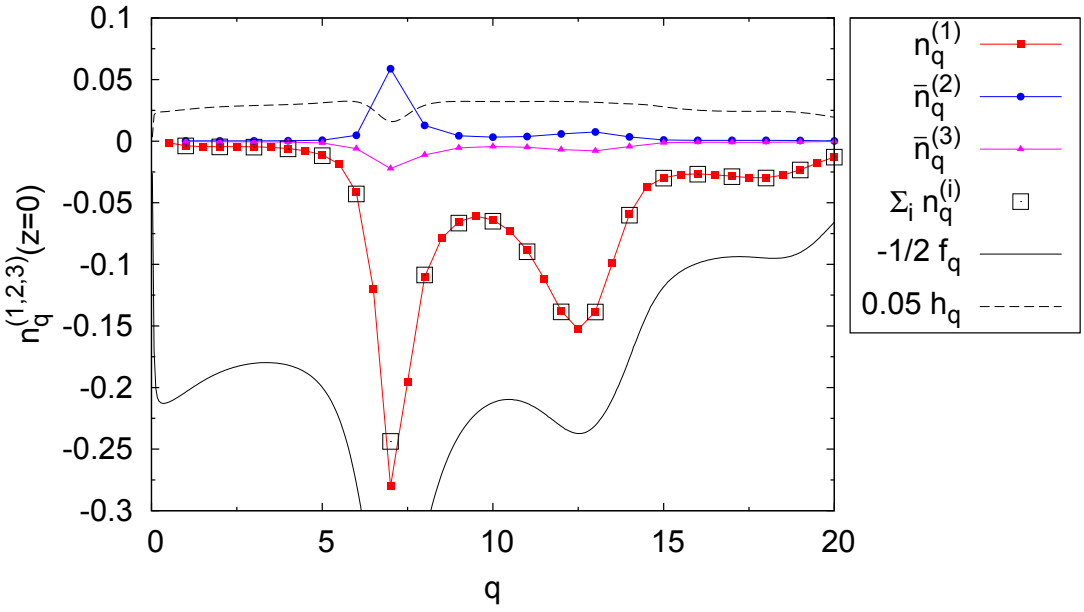

Figure 4.3: The three memory functions for $\mathbf{q} = q\mathbf{e}_y$. Shown are the time-integrated functions, $n_{\mathbf{q}}(z=0) = \int_0^\infty dt' n_{\mathbf{q}}(t')$. According to our arguments in Sec. 4.6.1, $n_{\mathbf{q}}^{(1)}(z=0)$ should coincide with $-1/2 f_q$. This would lead to $X_{\mathbf{q}} = \frac{1}{2}$ in Fig. 4.4. For the dashed line see the discussion in Sec. 4.6.2.

correlation function connected to the structure factor via the Ornstein-Zernicke equation $S_k = 1/(1 - nc_k)$ [29]. The memory function $m_{\mathbf{q}}$ is to lowest order in $\dot\gamma$ approximated by

$$m_{\mathbf{q}}(t) = \frac{S_q}{2nq^4}\int_0^\infty dt \int \frac{d^3k}{(2\pi)^3} S_{k(-t)-q} S_{k(-t)} V^{(2)}_{\mathbf{qk}} V^{(2)}_{\mathbf{qk}(-t)} \Phi_{\mathbf{k}(-t)}(t)\Phi_{\mathbf{k}(-t)-\mathbf{q}}(t). \quad (4.52)$$

From the expressions in (4.51) one can now see the earlier proposed properties, Eq. (4.42). The function $n_{\mathbf{q}}$ can schematically be written

$$n_{\mathbf{q}}(t) = a\,\dot\gamma\dot\gamma\, t f(t) + b\int_0^\infty ds\,\dot\gamma\dot\gamma s\, g(s)\, h(t). \quad (4.53)$$

The first term in (4.53) corresponds to $n^{(1)}_{\mathbf{q}}$, the second term to $n^{(2,3)}_{\mathbf{q}}$. $f(t), g(t), h(t)$ are functions of t/τ in the liquid and $\dot\gamma t$ in the glass. Eq. (4.42) follows. The fact that the terms in (4.53) start linearly with t and s respectively comes because $V^{(2)}$ in Eq. (4.51) is symmetric in k_x, $V^{(2)} = V^{(2)}(k_x^2)$, and because $V^{(1)}$ at time $t = 0$ (or $s = 0$) is anti-symmetric in k_x, $V^{(1)}(-k_x) = -V^{(1)}(k_x)$, and the property $n^{(1)}_{\mathbf{q}}(t \to 0) \sim \dot\gamma^2 t$ follows after integration over d^3k. The linear increase with time follows for example from $k_y(t) = k_y - \dot\gamma t k_x$. We see that $n^{(1)}_{\mathbf{q}}$ has a very different form compared to $n^{(2,3)}_{\mathbf{q}}$, but the Laplace transforms at $z = 0$ are similar.

For the numerical evaluation of Eqs. (4.51) and (4.52), the transient correlator $\Phi_{\mathbf{q}}(t)$ and the static structure factors S_q and $S^{(\dot\gamma)}_{\mathbf{q}}$ are needed. As a purely technical simplification, we use the isotropic approximation [27], which reads for long times in glassy states

$$\Phi_{\mathbf{q}}(t) \approx \Phi_q(t) = f_q\, e^{-c\frac{h_q}{f_q}|\dot\gamma|t}, \quad (4.54)$$

with the non ergodicity parameter f_q and the amplitude h_q. Eq. (4.54) is in accordance with the expansion near the critical plateau, see Sec. 1.6.2. The parameter c is related to the parameters in the β-equation, $c = \sqrt{c^{(\dot\gamma)}/(\lambda - 1/2)}$, we use $c = 3$ [27]. For the static equilibrium structure factor, we use the Percus-Yevick closure [29], and approximate $S_q = S^{(\dot\gamma)}_{\mathbf{q}}$, which holds astonishingly well at small shear rates [1], although the structure is nonanalytic [61]. In the limit of small shear rates, the contribution of the short time decay of the correlators to the above expressions vanishes. The above expressions were evaluated using spherical coordinates with grid $k_{max} = 50$, $\Delta k = 0.05$ and $\Delta\theta = \Delta\phi = \pi/40$ or smaller. The time grid in both t and s was $\dot\gamma t = 2^{i/4}/10^{10}$, starting from $i = 90$ corresponding to $\dot\gamma t \approx 6\ 10^{-4}$.

Figs. 4.2 and 4.3 show the Laplace transforms of the memory functions, $n^{(1,2,3)}_{\mathbf{q}}(z = 0)$, for the z- and the y-direction respectively, at the critical packing fraction. It can be seen that the sum of all three functions is negative, this will lead to an FDR smaller than unity. Also, the sum is very nearly equal to $n^{(1)}_{\mathbf{q}}$, since $n^{(2,3)}_{\mathbf{q}}$ are smaller and in addition to this partially cancel each other. We do not show the function $m_{\mathbf{q}}$, which is with Eqs. (4.54) and (4.39) given by

$$m_{\mathbf{q}}(z = 0) = \frac{f_q^2}{ch_q|\dot\gamma|}. \quad (4.55)$$

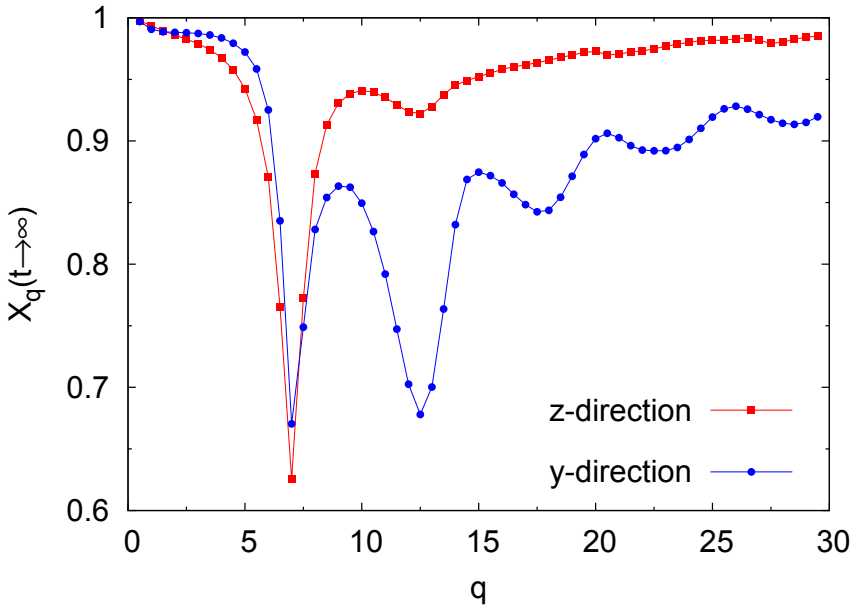

Figure 4.4: Long time FDR as function of wavevector q for density fluctuations in z- and y-direction in the limit of small shear rates. The packing fraction is the critical one, $\phi = \phi_c$.

We verified this by comparison to the result of Eq. (4.52). Now we can compute the value of the long time FDR in Eq. (4.48), which is given with (4.54) and (4.40),

$$X_{\mathbf{q}}(\varepsilon \geq 0, \dot{\gamma} \to 0) = \lim_{\dot{\gamma}\to 0} 1 + \frac{f_q n_{\mathbf{q}}(z=0)}{|\dot{\gamma}|\, c\, h_q m_{\mathbf{q}}(z=0)}. \tag{4.56}$$

This is shown in Fig. 4.4 for the parameters given above and $n_{\mathbf{q}}(z=0) \approx n^{(1)}_{\mathbf{q}}(z=0)$. The FDR ranges between zero and unity for all wavevectors in accordance with Ref. [1]. Its dependence on wavevector is stronger than found in Ref. [1], where a q-independent FDR was proposed. Given the complexity of the involved functions, the results are still satisfying. In Sec. 4.6, we will show that the findings of Chap. 2 lead to a q-independent FDR in first approximation and to q-dependent corrections.

4.5.5 FDT Violation Qualitative – Schematic Model $F_{12}^{(FDR)}$

In this section, we simplify our equations for the susceptibility by dropping the $\mathbf{q}$-dependence. This will not yield quantitative results as in Sec. 4.5.4, but we can learn about the qualitative shape of the involved functions, because we can explicitely take into account the convolution in Eq. (4.45) and test the validity of the Markov approximation. We will again approximate stationary and transient correlators to be equal and given by the $F_{12}^{(\dot{\gamma})}$-model in (1.40). For $m_{\mathbf{q}}(t)$ in (4.37), $m(t)$ in (1.40) is taken, see Eq. (4.38). We only need a schematic version of $n_{\mathbf{q}}(t)$ which was already sketched in (4.53). We use

$n_{\mathbf{q}}(t) \approx n_{\mathbf{q}}^{(1)}(t)$, i.e., $b = 0$ in Eq. (4.53). The actual form of $n_{\mathbf{q}}^{(1)}(t)$ is chosen following $m(t)$, i.e., it grows linear with $\dot{\gamma}t$ and has a pre-factor which gets smaller for growing time, modeling the advection in the vertex. We state all the functions again for clarity,

$$\chi(t) = -\frac{\partial}{\partial t}\Phi(t) + \int_0^t dt' N(t-t')\,\Phi(t'), \tag{4.57a}$$

$$N(t)/\Gamma = n(t) - \int_0^t dt'\, N(t')\, m(t-t'), \tag{4.57b}$$

$$0 = \dot{\Phi}(t) + \Gamma\left\{\Phi(t) + \int_0^t dt'\, m(t-t')\dot{\Phi}(t')\right\}, \tag{4.57c}$$

$$m(t) = \frac{1}{1+(\dot{\gamma}\,t)^2}\left[v_1^c\,\Phi(t) + (v_2^c+\epsilon)\,\Phi^2(t)\right], \tag{4.57d}$$

$$n(t) = v_3\frac{-\dot{\gamma}\dot{\gamma}t}{1+v_4\,(\dot{\gamma}\,t)^2}\left[v_1^c\,\Phi(t) + (v_2^c+\epsilon)\,\Phi^2(t)\right]. \tag{4.57e}$$

Eq. (4.57b) for $N(t)$ has the form of Eq. (3.95), i.e., it can be solved with the algorithm used for the MSDs. The numerical treatment of the convolution in (4.57a) is then straight forward since the "moments" of N and Φ are already known. The shape of the resulting susceptibility depends on the parameters v_3 and v_4, which are positive according to our quantitative analysis. If we choose $v_3 = 7$ and $v_4 = 10$ (and the standard values for v_1^c and v_2^c, see Eq. (1.40)), the long time FDR is nearly time independent. In Fig. 4.5, we show the susceptibility as well as Φ for a glassy state and different shear rates. In the parametric plot (inset), one sees straight lines for long times, indicating time independent FDRs. Also shown are the results for the Markov approximation in Eq. (4.45), i.e.,

$$\chi(t) = -\frac{\partial}{\partial t}\Phi(t) + N(z=0)\,\Phi(t). \tag{4.58}$$

We see that the convolution in (4.57b) is quite well followed by the Markov approximation, there are deviations at intermediate times where the FDT violation initiates. The shape of the susceptibilities is in good agreement to the simulation results [1].

In Fig. 4.6, we show the long time FDR as a function of shear rate evaluated by fitting the long time slope in the parametric plot. The long time FDR is analytic in shear rate in the fluid, but shows the nonanalytic behavior in the glass. As was discussed in the previous sections, this dependence on $\dot{\gamma}$ is nontrivial and was achieved through the ITT approach and by establishing the probability current in Eq. (4.30) as quickly decaying quantity. The latter was achieved by the identification of the different terms with derivatives with respect to the transient time s. A more detailed discussion of the FDR will follow in Sec. 4.6.

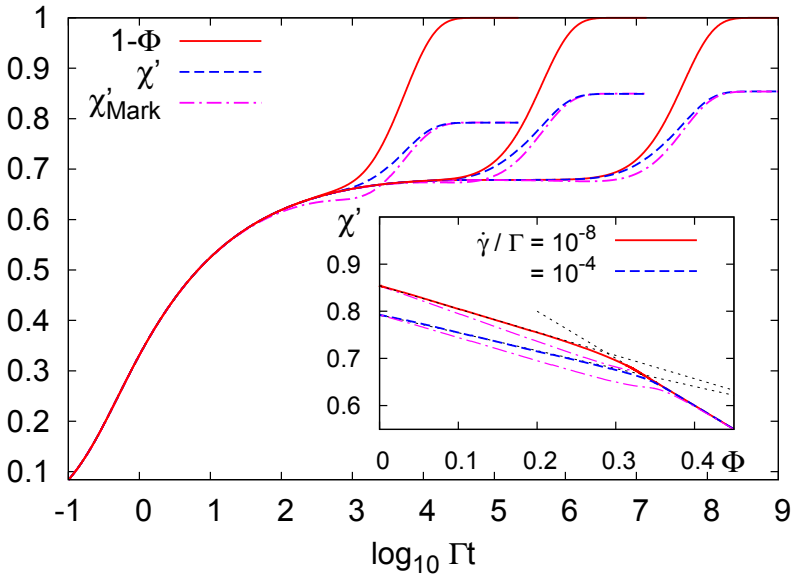

Figure 4.5: The transient correlator $\Phi(t)$ and the susceptibility $\chi(t)$ from the schematic model $F_{12}^{(FDR)}$ for a glassy state ($\varepsilon = 10^{-3}$) and shear rates $\dot{\gamma}/\Gamma = 10^{-8,-6,-4}$. Shown are integrated quantities, $1 - \Phi(t)$ and $\chi'(t) = \int_0^t dt' \chi(t')$. Inset: Parametric plot for the same susceptibilities together with long time fitted time independent FDRs. The curve for the third shear rate would lie just between these two. Dashed dotted lines mark the result from the Markov approximation.

4.5.6 FDR for Incoherent Fluctuations

How does the FDR look like for incoherent fluctuations which where most intensively studied in Ref. [1]? For this, we have $\delta f = \varrho_{\mathbf{q}}^s = e^{i\mathbf{q}\cdot\mathbf{r}_s}$, with $q_x = 0$ as before. We then can write the violating term as in Eq. (4.32) to

$$\Delta\chi_{\mathbf{q}}^s(t) \quad = \quad \int_0^t dt' \, N_{\mathbf{q}}^s(t-t') \, \Phi_{\mathbf{q}}^s(t'). \tag{4.59}$$

The formal approach is identical to the coherent case, i.e., the memory function $N_{\mathbf{q}}^s(t)$ is expressed in terms of another function $n_{\mathbf{q}}^s(t)$. Doing this, the relations (4.40 – 4.44) hold with evident changes in notation. Also the schematic model holds similarly[2]. What still misses is the quantitative analysis of the function $n_{\mathbf{q}}^s(t)$ which will give us the numbers

[2] In principle one would have to use the ($\dot{\gamma}$)-Sjögren model for the correlators, but the resulting plots would be equivalent to the ones achieved in the F_{12}^{FDR}-model.

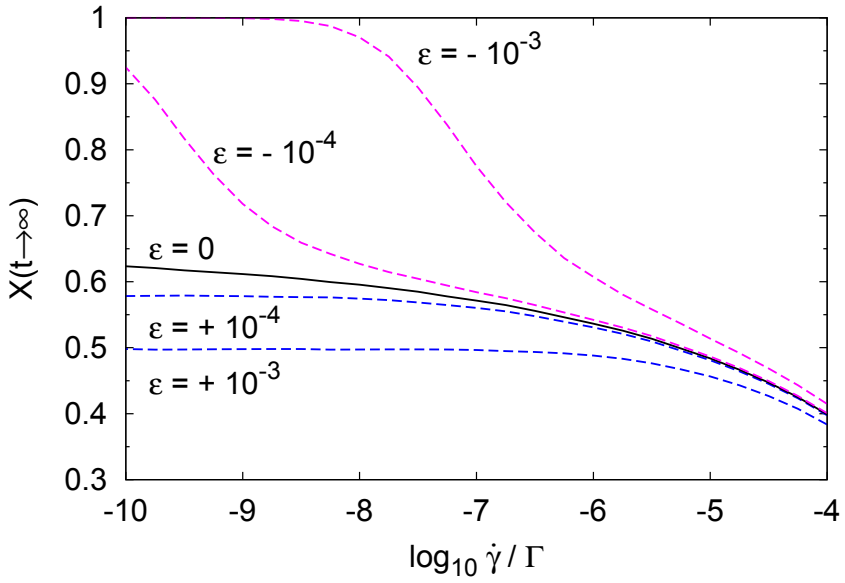

Figure 4.6: Long time FDR as function of shear rate in the schematic model $F_{12}^{(FDR)}$ for glassy ($\varepsilon \geq 0$) and liquid ($\varepsilon < 0$) states.

for the long time FDR. $n_{\mathbf{q}}^s(t)$ is also split up into three terms according to Eq. (4.49)

$$\begin{aligned}
n_{\mathbf{q}}^s(t) &= n_{\mathbf{q}}^{(s,1)}(t) + n_{\mathbf{q}}^{(s,2)}(t) + n_{\mathbf{q}}^{(s,3)}(t), \\
n_{\mathbf{q}}^{(s,1)}(t) &= \frac{-\dot\gamma}{2\Gamma_q^s} \int_0^\infty ds \left\langle \sigma_{xy} e^{\Omega^\dagger s} \Omega^\dagger \varrho_{\mathbf{q}}^{s*} U^{(s)}(t) \Omega^\dagger \varrho_{\mathbf{q}}^s \right\rangle, \\
&= \frac{\dot\gamma}{2\Gamma_q^s} \left\langle \sigma_{xy} \varrho_{\mathbf{q}}^{s*} U^s(t) \Omega^\dagger \varrho_{\mathbf{q}}^s \right\rangle, \qquad (4.60a) \\
n_{\mathbf{q}}^{(s,2)}(t) &= \frac{\dot\gamma}{2\Gamma_q^s} \int_0^\infty ds \left\langle \sigma_{xy} e^{\Omega^\dagger s} \varrho_{\mathbf{q}}^{s*} \Omega^\dagger U^s(t) \Omega^\dagger \varrho_{\mathbf{q}}^s \right\rangle, \qquad (4.60b) \\
n_{\mathbf{q}}^{(s,3)}(t) &= \frac{-\dot\gamma}{2\Gamma_q^s} \int_0^\infty ds \left\langle \sigma_{xy} e^{\Omega^\dagger s} (\Omega^\dagger \varrho_{\mathbf{q}}^{s*}) U^s(t) \Omega^\dagger \varrho_{\mathbf{q}}^s \right\rangle, \qquad (4.60c) \\
U^s(t) &= Q^s e^{Q^s \Omega^{(i,s)} Q^s t} Q^s.
\end{aligned}$$

The irreducible operator $\Omega^{(i,s)}$ is related to $\Omega^\dagger$ as in Eq. (4.34) with $\varrho_{\mathbf{q}}$ replaced by $\varrho_{\mathbf{q}}^s$, and $\Gamma_q^s = q^2$. We approximate these terms in the same way as was done in the coherent case in Sec. 4.5.4, see Appendix C. Figs. 4.7 and 4.8 show the Laplace transforms of the three memory functions at $z = 0$ for $\mathbf{q} = q\,\mathbf{e}_z$ and $\mathbf{q} = q\,\mathbf{e}_y$ at the critical density in the limit of $\dot\gamma \to 0$. The results are consistent with the coherent case, i.e., the respective functions have the same sign and the sum of the three functions is negative and almost equal to the first one alone. This does not hold for $q \lesssim 7$ for both directions, but

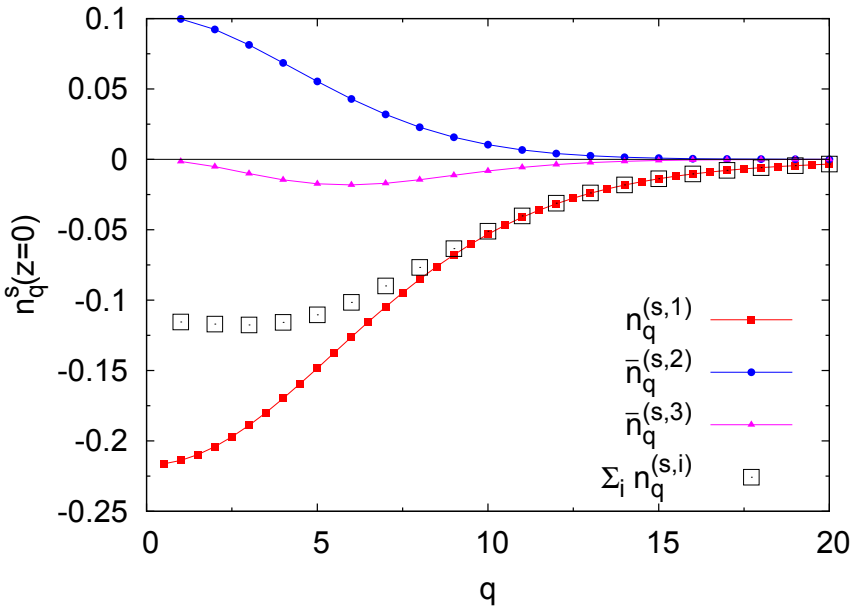

Figure 4.7: The three contributions to the memory function $n^s_{\mathbf{q}}$ for the z-direction. Shown are the time-integrated functions, $n^s_{\mathbf{q}}(z=0) = \int_0^\infty dt' n^s_{\mathbf{q}}(t')$.

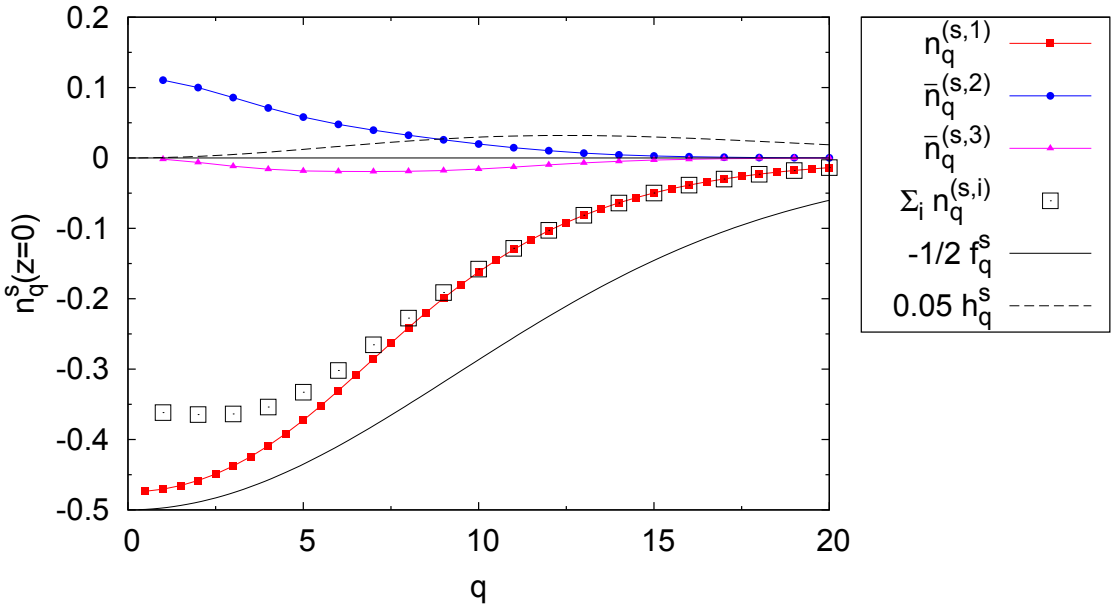

Figure 4.8: The three contributions to the memory function $n^s_{\mathbf{q}}$ for the y-direction. Shown are the time-integrated functions, $n^s_{\mathbf{q}}(z=0) = \int_0^\infty dt' n^s_{\mathbf{q}}(t')$. According to our arguments in Sec. 4.6.1, $n^{(s,1)}_{\mathbf{q}}(z=0)$ should coincide with $-1/2 f^s_q$. This would lead to $X_{\mathbf{q}} = \frac{1}{2}$ in Fig. 4.9. For the dashed line, see the discussion in Sec. 4.6.2.

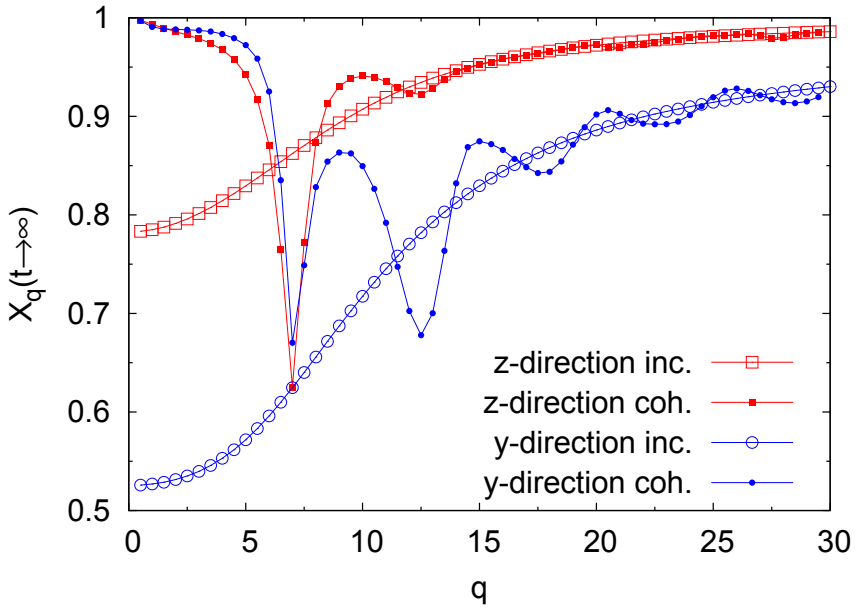

Figure 4.9: Long time FDR $X_{\mathbf{q}}$ for the z- and the y-direction as function of q. The results for the coherent case are shown for comparison.

the difference between $n^s_{\mathbf{q}}(z=0)$ and $n^{(s,1)}_{\mathbf{q}}(z=0)$ is larger for the z-direction. It is interesting to note that the functions $n^{(s,2)}_{\mathbf{q}}$ and $n^{(s,3)}_{\mathbf{q}}$ are almost isotropic, while $n^{(s,1)}_{\mathbf{q}}$ is smaller in z- compared to the y-direction. In the following section, we will neglect the sum of $n^{(s,2)}_{\mathbf{q}}$ and $n^{(s,3)}_{\mathbf{q}}$. What are the consequences of the observation that the sum is not negligible for small q? Fortunately, we will see in Eq. (4.79) that the FDR $X_{\mathbf{q}}(t\to\infty)$ does not depend on $n^{(s,2)}_{\mathbf{q}}$, although it is part of the violating term. We will also see that the long time FDR approaches $\frac{1}{2}$ if $n^{(s,3)}_{\mathbf{q}}(z=0)$ goes to zero since it is directly proportional to the term in Eq. (4.81).

Fig. 4.9 shows the long time FDR $X_{\mathbf{q}}$ calculated via Eq. (4.56). We observe that the dependence on q is much smoother than in the coherent case. For large values of q, the coherent and the incoherent values collapse. While this is expected, it is still worth noting that our approximations give this, because the respective vertices for coherent and incoherent case are quite different.

4.6 $X = \frac{1}{2}$ Approach

In this section, we follow the approach to the FDR under shear for general functions f, which was presented in Ref. [64]. f is not explicitely advected, $f = f(\{y_i, z_i\})$. We start again at the exact expression (4.31) for the violating term, which can be split up according to Eq. (4.49),

$$\begin{aligned}\Delta\chi_{\mathrm{f}} &= \frac{-\dot\gamma}{2}\int_0^\infty ds \left\langle \sigma_{xy} e^{\Omega^\dagger s} \sum_i (\boldsymbol{\partial}_i + \mathbf{F}_i)\cdot \frac{\partial f^*}{\partial \mathbf{r}_i} e^{\Omega^\dagger t} f \right\rangle \\ &= \frac{-\dot\gamma}{2}\int_0^\infty ds \left\langle \sigma_{xy} e^{\Omega^\dagger s} [\Omega^\dagger f^* - f^*\Omega^\dagger + (\Omega^\dagger f^*)] e^{\Omega^\dagger t} f \right\rangle . \end{aligned} \tag{4.61}$$

4.6.1 The First Term as the Waiting Time Derivative

The first term in (4.61) can be integrated over s and reads (without the factor $\frac{1}{2}$)

$$\dot\gamma \left\langle \sigma_{xy} \delta f^* e^{\Omega^\dagger t} \delta f \right\rangle = \left\langle \delta f^* \delta\Omega^\dagger e^{\Omega^\dagger t} \delta f \right\rangle = \frac{\partial}{\partial t_w} C_{\mathrm{f}}(t, t_w)\Big|_{t_w=0} , \tag{4.62}$$

where we use again $\delta f = f - \langle f\rangle$, the constant $\langle f\rangle$ cancels in (4.61). Eq. (4.62) states the intriguing connection of the term to the two-time correlator as discussed in Chap. 2. In Sec. 2.2, we found the following approximation for the waiting time derivative,

$$\left\langle \delta f^* \delta\Omega^\dagger e^{\Omega^\dagger t} \delta f \right\rangle = \frac{\partial}{\partial t_w} C_{\mathrm{f}}(t, t_w)\Big|_{t_w=0} \approx \dot C_{\mathrm{f}}^{(t)}(t) - \dot C_{\mathrm{f}}^{(e)}(t) \frac{C_{\mathrm{f}}^{(t)}(t)}{C_{\mathrm{f}}^{(e)}(t)}, \tag{4.63}$$

and we saw that it can be interpreted as the long time derivative $\dot C_{\mathrm{f}}^{(t,l)}(t)$ of the transient correlator. The author regards (4.63) as very accurate for small shear rates, see the arguments given in Sec. 2.5.

Let us briefly compare this result to our findings in Sec. 4.5. We found (after the Markov approximation) the term (4.63) for density fluctuations to be equal to

$$\frac{1}{2}\left\langle \delta f^* \delta\Omega^\dagger e^{\Omega^\dagger t} \delta f \right\rangle\Big|_{f=\varrho_{\mathbf{q}}} = \frac{n_{\mathbf{q}}^{(1)}(z=0)}{m_{\mathbf{q}}(z=0)} \Phi_{\mathbf{q}}(t). \tag{4.64}$$

This holds as well for the incoherent case. With Eq. (4.54) for $\Phi_{\mathbf{q}}(t)$, the term above is equal to $\dot\Phi_{\mathbf{q}}(t)$ for long times if $n_{\mathbf{q}}^{(1)}(z=0) = -\frac{1}{2} f_q$ holds. This is additionally shown in Figs. 4.2 and 4.8 of the previous section[3]. $n_{\mathbf{q}}^{(1)}(z=0)$ and $-\frac{1}{2}f_q$ do not agree, but they have same size and sign and similar shape. We conclude that both approaches give very similar results, the current one with Eq. (4.63) being more precise.

[3] We show it only in the curves for the y-direction, it should hold for the z-direction as well.

4.6.2 The Other Terms

The second term in Eq. (4.61) has a physical interpretation as well: It is the time derivative of the difference between stationary and transient correlator, see Eq. (1.18). With our approximation for the two-time correlator in Eq. (2.19), we have, neglecting the renormalization at $t = 0$,

$$\frac{\dot\gamma}{2}\int_0^\infty \left\langle \sigma_{xy} e^{\Omega^\dagger s} f^* \Omega^\dagger e^{\Omega^\dagger t} f \right\rangle \approx \frac{\tilde\sigma}{\dot\gamma}\frac{\partial}{\partial t}\left(\dot C_{\mathrm{f}}^{(t)}(t) - \dot C_{\mathrm{f}}^{(e)}(t)\frac{C_{\mathrm{f}}^{(t)}(t)}{C_{\mathrm{f}}^{(e)}(t)}\right). \tag{4.65}$$

How does this compare to the findings in Sec. 4.5? We found for this term for long times,[4]

$$\frac{\dot\gamma}{2}\int_0^\infty ds \left\langle \sigma_{xy} e^{\Omega^\dagger s} f^* \Omega^\dagger e^{\Omega^\dagger t} f \right\rangle\Big|_{f=\varrho_{\mathbf{q}}} = \frac{n_{\mathbf{q}}^{(2)}(z=0)}{m_{\mathbf{q}}(z=0)}\Phi_{\mathbf{q}}(t). \tag{4.66}$$

In order to have both approximations equal, we need $n_{\mathbf{q}}^{(2)}(z=0) = \frac{1}{2}\tilde\sigma c h_q$. This curve with $\tilde\sigma c = 0.1$ is additionally shown in Figs. 4.2 and 4.8 in the previous section. The terms have the same sign and a comparable size, which must be appreciated given the complexity of the microscopic form of $n_{\mathbf{q}}^{(2)}(z=0)$. The q-dependence is different. The comparison to simulations in the future might give clarity about the q-dependence of the difference between transient and stationary correlators.

Let us turn to the last term in Eq. (4.61). It has no physical interpretation and has to remain the only piece missing in our FDT puzzle. Nevertheless, we have the approximation given in Sec. 4.5, where we found that it nearly cancels with the second term. Note that the terms exactly cancel each other at $t = 0$. We will see that neglecting the sum of these two terms will lead to excellent agreement with the simulation results in Ref. [1].

4.6.3 FD Relation under Shear

Neglecting the subdominant terms in Eq. (4.61), we write

$$\Delta\chi_{\mathrm{f}}(t) \approx \frac{1}{2}\frac{\partial}{\partial t_w} C_{\mathrm{f}}(t,t_w)\Big|_{t_w=0} \approx \frac{1}{2}\left(\dot C_{\mathrm{f}}^{(t)}(t) - \dot C_{\mathrm{f}}^{(e)}(t)\frac{C_{\mathrm{f}}^{(t)}(t)}{C_{\mathrm{f}}^{(e)}(t)}\right) = \frac{1}{2}\dot C_{\mathrm{f}}^{(t,l)}. \tag{4.67}$$

Eq. (4.67) states the connection of two very different physical mechanisms: The violation of the equilibrium FDT and the waiting time dependence of the two-time correlator. It can be tested in simulations, were both quantities are accessible independently. The connection of the violating term to time derivatives captures the additional dissipation provided by the coupling to the stationary probability current in Eq. (4.30). The last expression stresses that the extra term in the FDT can indeed be connected to a time

[4] Eq. (4.66) holds only exactly for the incoherent case. In the coherent case, it neglects contributions from $t = 0$-couplings.

derivative of a correlation function, but no such simple relation occurs as in equilibrium. We can hence finally write our FD relation

$$\chi_{\mathrm{f}}(t) \approx -\dot{C}_{\mathrm{f}}(t) + \frac{1}{2}\left(\dot{C}_{\mathrm{f}}^{(t)}(t) - \dot{C}_{\mathrm{f}}^{(e)}(t)\frac{C_{\mathrm{f}}^{(t)}(t)}{C_{\mathrm{f}}^{(e)}(t)}\right), \tag{4.68a}$$

$$= -\dot{C}_{\mathrm{f}}(t) + \frac{1}{2}\dot{C}_{\mathrm{f}}^{(t,l)}. \tag{4.68b}$$

As discussed in Chap. 2, the long time derivative in (4.68) is zero for short times $\dot{\gamma}t \ll 1$ and the equilibrium FDT holds. For long times in glassy states, i.e., for $\dot{\gamma} \to 0$, and $t \to \infty$ with $\dot{\gamma}t = \text{const.}$, the long time derivative equals the time derivative of the transient correlator. A non-trivial FDR follows. Summarized we find in the glass

$$\lim_{\dot{\gamma}\to 0}\chi_{\mathrm{f}}(t) = \begin{cases} -\dot{C}_{\mathrm{f}}(t) & \dot{\gamma}t \ll 1, \\ -\dot{C}_{\mathrm{f}}(t) + \frac{1}{2}\dot{C}_{\mathrm{f}}^{(t)}(t) & \dot{\gamma}t = \mathcal{O}(1). \end{cases} \tag{4.69}$$

Eq. (4.68) states the relation between the susceptibility and correlation functions for the non-equilibrium system under shear. It is nontrivial because it gives qualitatively different results for short times compared to long times. We would like to emphasize that it has no adjustable parameters.

4.6.4 Universal $X = \frac{1}{2}$ Law

It is interesting to note that approximating stationary and transient correlator to be equal [27], $C_{\mathrm{f}}^{(t)}(t) \approx C_{\mathrm{f}}(t)$, we find the universal $X = \frac{1}{2}$-law for long times,

$$\lim_{\dot{\gamma}\to 0}\chi_{\mathrm{f}}(t \to \infty) = -\frac{1}{2}\dot{C}_{\mathrm{f}}(t). \tag{4.70}$$

The FDR, in this case, takes the universal value $\lim_{\dot{\gamma}\to 0} X_{\mathrm{f}}(t \to \infty) = \hat{X}^{(\mathrm{univ})}(\dot{\gamma}t) = \frac{1}{2}$, independent of f. This is in good agreement with the findings in Ref. [1], and corresponds to an effective temperature of $T_{\mathrm{eff}}/T = 2$ for all observables. The initially additive correction in Eq. (4.30) hence turns then into a multiplicative one, which does not depend on rescaled time during the complete final relaxation process. The deviation from the value $\frac{1}{2}$ of the long time FDR will come from the difference between stationary and transient correlators, which was discussed in Chap. 2.

As summarized in Sec. 4.2, there are many spin models that yield the same value at the critical temperature. In Chap. 6, we will further discuss this special value of the FDR.

4.6.5 Plotting the Final Susceptibilities

Now we are ready to discuss the FDRs in detail. Therefore, we again employ the schematic $F_{12}^{(\dot{\gamma})}$-model in (1.40) to calculate normalized transient ($\Phi(t)$) and quiescent density correlators. The stationary correlator C is calculated in a second step via

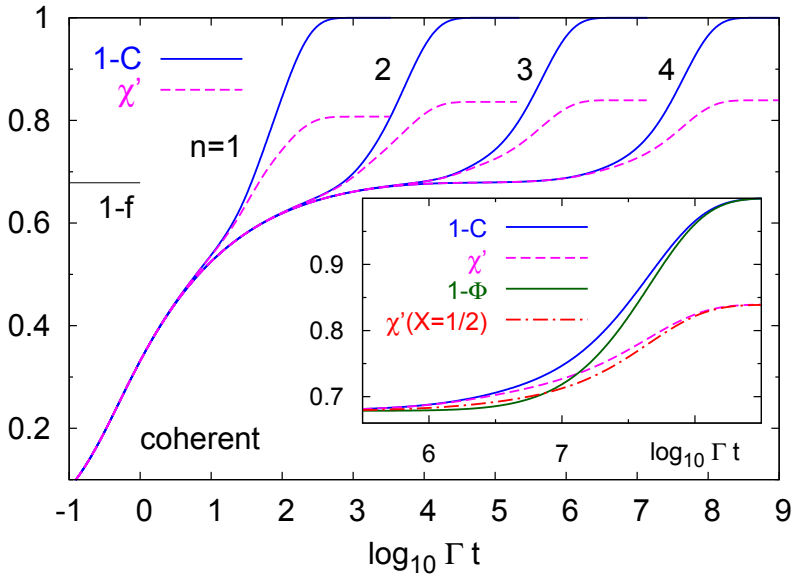

Figure 4.10: $C(t)$ from the $F_{12}^{(\dot\gamma)}$-model with Eq. (2.19) and $\chi(t)$ via Eq. (4.68) for a glassy state ($\varepsilon = 10^{-3}$) and $\dot\gamma/\Gamma = 10^{-2n}$ with $n = 1...4$. Shown are integrated correlation, $1 - C(t)$ and response $\chi'(t) = \int_0^t \chi(t')dt'$. Inset shows additionally the transient correlator Φ for comparison and the $\hat X^{(\mathrm{univ})} = \frac{1}{2}$ susceptibility for $\dot\gamma/\Gamma = 10^{-8}$.

Eqs. (2.19) and (2.7)[5]. Fig. 4.10 shows the resulting χ together with C for a glassy state at different shear rates. For short times, the equilibrium FDT is valid, while for long times the susceptibility is smaller than expected from the equilibrium FDT. This deviation is qualitatively similar for the different shear rates. For the smallest shear rate, we also plot χ calculated by Eq. (4.68) with $\dot C_{\mathrm{f}}^{(t)}$ replaced by $\dot C_{\mathrm{f}}$, from which the universal $\hat X^{(\mathrm{univ})}(\dot\gamma t) = \frac{1}{2}$ follows. In the parametric plot (Fig. 4.11), this leads to two perfect lines with slopes -1 and $-\frac{1}{2}$ connected by a sharp kink at the non ergodicity parameter f. For the other (realistic) curves, this kink is smoothed out, but the long time part is still well described by a straight line, i.e., the FDR is still almost constant during the final relaxation process. We predict a non-trivial time-independent FDR $\hat X_{\mathrm{f}}(\dot\gamma t)$ =const. if $C_{\mathrm{f}}^{(t)}$ (and with Eq. (2.19) also C_{f}) decays exponentially for long times, because $\Delta\chi_{\mathrm{f}}$ then decays exponentially with the same exponent. The line cuts the FDT line *below* f for $\dot\gamma \to 0$. All these findings are in excellent agreement with the data in Ref. [1]. The FDR itself is of interest also, as function of time (inset of Fig. 4.11). A rather sharp transition from 1 to $\frac{1}{2}$ is observed when $\Phi \approx C$ is approximated, which already takes place at $\dot\gamma t \approx 10^{-3}$, a time when the FDT violation is still invisible in Fig. 4.10. For the realistic curves, this transition happens two decades later. Strikingly, the huge difference is not apparent in the parametric plot.

Fig. 4.12 shows $C(t)$ and $\chi(t)$ for a fluid state. For large shear rates, these curves are

[5] We neglect the renormalization at $t = 0$ in Eq. (2.19), which is exact for incoherent fluctuations.

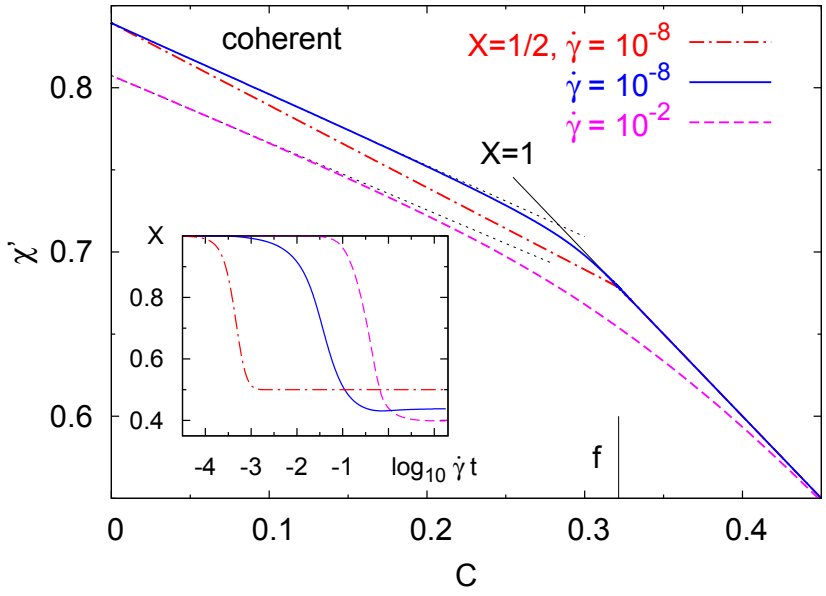

Figure 4.11: Parametric plot of correlation $C(t)$ versus response $\chi'(t) = \int_0^t \chi(t')dt'$ from Fig. 4.10 ($\varepsilon = 10^{-3}$) together with constant non-trivial FDR (straight lines) at long times. The vertical solid line marks the plateau f. Inset shows the FDR $X(t)$ as function of strain for the same susceptibilities.

similar to the glassy case, while for $\dot\gamma \to 0$, the equilibrium FDT holds for all times. In the parametric plot (inset of Fig. 4.12) one sees that the long time FDR is still approximately constant in time for the case $\dot\gamma \approx \tau^{-1}$, where the long time dynamics is influenced, but not dominated, by shear, because shear relaxation and structural relaxation compete.

4.6.6 FDR as Function of Shear Rate

Fig. 4.13 shows the long time FDR as a function of shear rate for different densities above and below the glass transition, determined via fits to the parametric plot in the interval $[0 : 0.1]$. In the glass $X(t \to \infty)$ is nonanalytic while it goes to unity in the fluid as $\dot\gamma \to 0$ (compare Fig. 4.12), where we verified that the FDT-violation starts quadratic in $\dot\gamma$, as is to be expected due to symmetries. For all densities, the FDR decreases with increasing shear rate. For constant shear rate, it decreases with the density. This is also in agreement with the simulations.

4.6.7 FDR as Function of Wavevector

Due to the difference of transient and stationary correlator, the long time FDR from Eq. (4.68) in general depends on the variable f. This can be quantified by approximating the long time transient correlator as (compare Eq. (4.54))

$$C_{\mathrm{f}}^{(t)}(t \to \infty) \approx f_{\mathrm{f}}\, e^{-a_{\mathrm{f}}|\dot\gamma|t}, \tag{4.71}$$

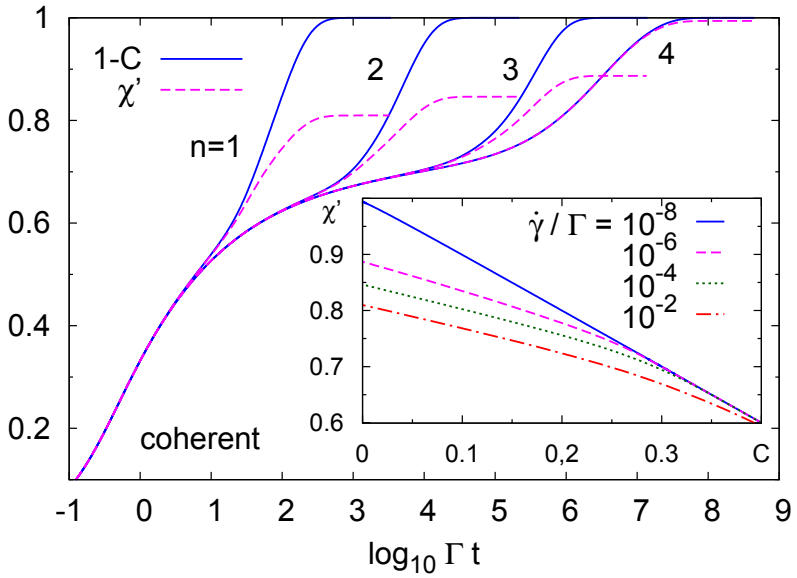

Figure 4.12: $C(t)$ and $\chi(t)$ via Eq. (4.68) for a fluid state ($\varepsilon = -10^{-3}$) and $\dot{\gamma}/\Gamma = 10^{-2n}$ with $n = 1...4$. Shown are integrated correlation, $1 - C(t)$ and response $\chi'(t) = \int_0^t \chi(t')dt'$. Inset shows the parametric plot for the different shear rates.

With Eqs. (4.68) and (2.19), the long time FDR follows,

$$X_\mathrm{f}(t \to \infty) = \frac{\frac{1}{2} - a_\mathrm{f}\tilde{\sigma}}{1 - a_\mathrm{f}\tilde{\sigma}}. \tag{4.72}$$

Fig. 4.14 shows the long time FDR for coherent and incoherent density fluctuations at the critical density. We used the isotropic long time approximations (4.54) and (C.7) respectively and $c\tilde{\sigma} = 0.1$ from Eq. (2.7). The incoherent case was most extensively studied in Ref. [1]. The FDR in Fig. 4.14 is isotropic in the plane perpendicular to the shear direction but not independent of wave vector q, contradicting the idea of an effective temperature as proposed in Refs. [1, 94] and others. In Fig. 13 of Ref. [1], the trend given in Fig. 4.14 might be visible, i.e., the FDR seems to decrease slightly with increasing wavevector.

For $\tilde{\sigma}\, a_\mathrm{f} \geq \frac{1}{2}$, the long time FDR in Eq. (4.72) is negative, a condition eventually reached for density fluctuations. The curves in Fig. 4.14 will eventually cross zero. According to our considerations in Chap. 6 and the available simulation data, a negative FDR is unphysical. Where does it come from? Inserting Eq. (4.71) into Eq. (2.19) we see that for $\tilde{\sigma}\, a_\mathrm{f} = \frac{1}{2}$, we have

$$C_\mathrm{f}(t \to \infty) = \frac{1}{2} C_\mathrm{f}^{(t)}(t \to \infty). \tag{4.73}$$

At the zero of X_f, the stationary correlator is half the value of the transient correlator

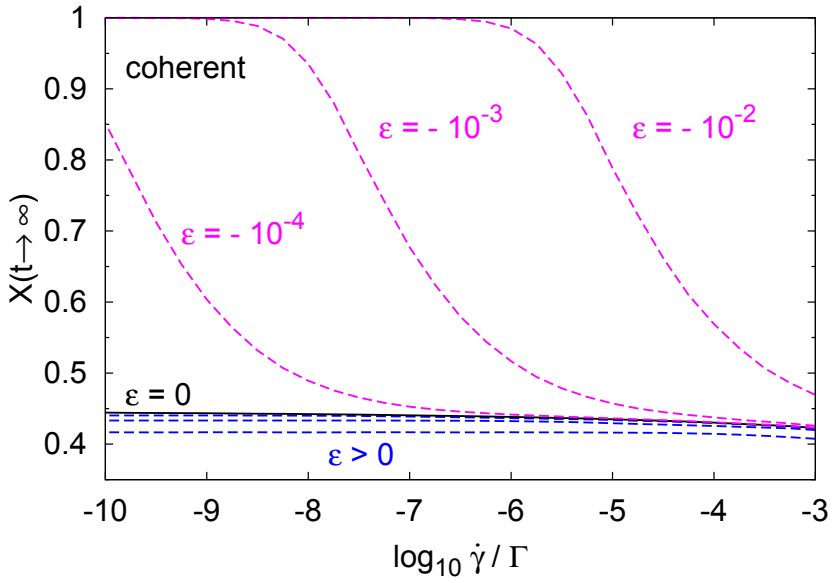

Figure 4.13: Long time FDR as function of shear rate for glassy ($\varepsilon = 10^{-n}$) and liquid ($\varepsilon = -10^{-n}$) states with $n = 2, 3, 4$. $X(t \to \infty)$ is determined from fits to the parametric plot as shown in Figs. 4.10 and 4.12.

for long times. There are three possibilities: Either the stationary correlator is never as small as half the value of the transient one. This would mean our approximation for the two-time correlator in Eq. (2.19) is not good for large $\tilde{\sigma} a_{\mathrm{f}}$. Or the two neglected terms in $\Delta\chi_{\mathrm{f}}(t)$ (i.e., their sum) are important at large $\tilde{\sigma} a_{\mathrm{f}}$. Or, finally, the FDR can indeed be negative.

4.6.8 Direct Comparison to Simulation Data

Despite the dependence of the long time FDR on wavevector, Eq. (4.68) is not in contradiction to the data in Ref. [1], as can be seen by direct comparison to their Fig. 11. For this, we need the quiescent as well as the transient correlator as input. $C_q^{(e)}$ has been measured in Ref. [122], suggesting that it can be approximated by a straight line beginning on the plateau of $C_{\mathbf{q}}(t)$. In Fig. 4.15 we show the resulting susceptibilities. There is no adjustable parameter, when $C_{\mathbf{q}}^{(t)} \approx C_{\mathbf{q}}$ is taken. For the other curve, we calculated $C_{\mathbf{q}}^{(t)}(t)$ from Eq. (2.19) using $\tilde{\sigma} = 0.01$ (in LJ units) as fit parameter. The agreement is striking. In the inset we show the original $C_{\mathbf{q}}$ from Ref. [1] together with our construction of $C_q^{(e)}$ and the calculated $C_{\mathbf{q}}^{(t)}$, which appears very reasonable compared with recent simulation data on $C_{\mathrm{f}}(t, t_w)$ [14].

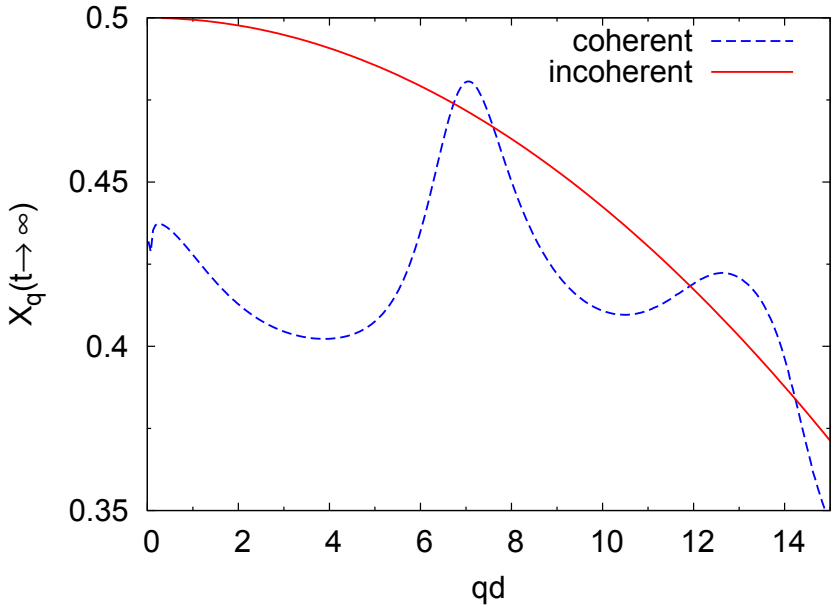

Figure 4.14: Long time FDR as function of wavevector q for coherent and incoherent density fluctuations at the critical density ($\varepsilon = 0$).

4.6.9 Universal FDR in the β-Regime

Let us assume the transient correlator near the critical plateau reads for variable f with the β-correlator from Eq. (1.29),

$$C_{\rm f}^{(t)}(t) = f_{\rm f}^c + h_{\rm f}\mathcal{G}(t). \tag{4.74}$$

Using Eq. (2.19) for the stationary correlator, we find (neglecting the renormalization at $t = 0$),

$$C_{\rm f}(t) = f_{\rm f}^c + h_{\rm f}\left[\mathcal{G}(t) + \frac{\tilde{\sigma}}{\dot{\gamma}}\left(\dot{\mathcal{G}}(t) - \dot{\mathcal{G}}^{(e)}(t)\right)\right], \tag{4.75}$$

where $\mathcal{G}^{(e)}(t)$ is the β-correlator of the un-sheared system. For the susceptibility follows with Eq. (4.68),

$$\chi_{\rm f}(t) = -h_{\rm f}\left[\frac{1}{2}\left(\dot{\mathcal{G}}(t) + \dot{\mathcal{G}}^{(e)}(t)\right) + \frac{\tilde{\sigma}}{\dot{\gamma}}\left(\ddot{\mathcal{G}}(t) - \ddot{\mathcal{G}}^{(e)}(t)\right)\right]. \tag{4.76}$$

The FDR in this regime is universal, i.e., independent of f, but time-dependent,

$$X_{\rm f}(t) = \frac{\left[\frac{1}{2}\left(\dot{\mathcal{G}}(t) + \dot{\mathcal{G}}^{(e)}(t)\right) + \frac{\tilde{\sigma}}{\dot{\gamma}}\left(\ddot{\mathcal{G}}(t) - \ddot{\mathcal{G}}^{(e)}(t)\right)\right]}{\left[\dot{\mathcal{G}}(t) + \frac{\tilde{\sigma}}{\dot{\gamma}}\left(\ddot{\mathcal{G}}(t) - \ddot{\mathcal{G}}^{(e)}(t)\right)\right]}. \tag{4.77}$$

This is an interesting and testable prediction.

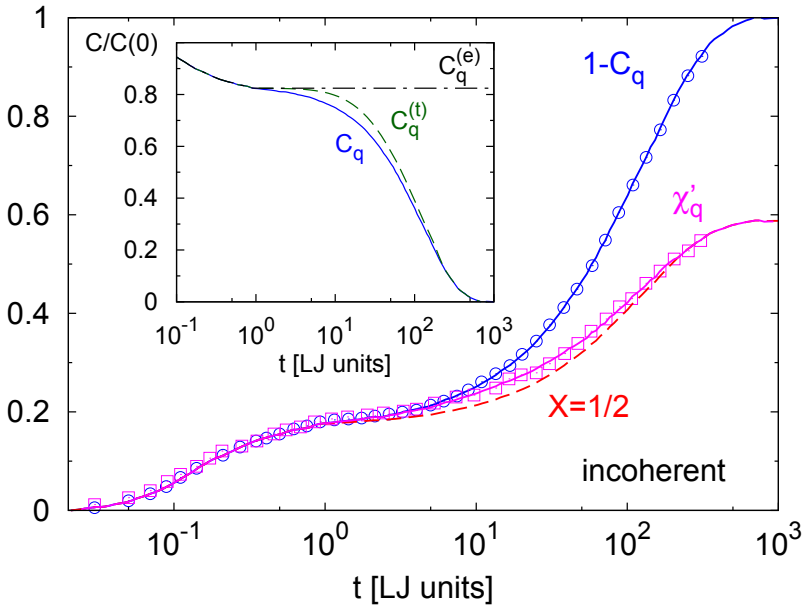

Figure 4.15: Comparison to simulation data for incoherent density fluctuations in the neutral direction (wave vector $\mathbf{q} = 7.47\mathbf{e}_z$) at temperature $T = 0.3$ ($T_c = 0.435$) and $\dot\gamma = 10^{-3}$. Circles and squares are the data (including units) from Fig. 11 in Ref. [1], lines are $1 - C_\mathbf{q}$ from Fig. 8 in Ref. [1], and the response $\chi'_\mathbf{q}(t) = \int_0^t \chi_\mathbf{q}(t')dt'$ calculated via Eq. (4.68). The dashed line shows $\chi'_\mathbf{q}$ with approximation $C_\mathbf{q}^{(t)} \approx C_\mathbf{q}$. Inset shows the different correlators, see main text.

4.6.10 What Makes us Believe That $X_\mathrm{f}(t\to\infty) \leq \frac{1}{2}$ in the Glass?

In Fig. 4.13, we see that the FDR for long times in glassy states is smaller than $\frac{1}{2}$. Does this prediction hold when we take into account the two terms in (4.61), which we neglected? To answer this, we rewrite our FD relation (4.30) in an exact way,

$$\chi_\mathrm{f}(t) = -\frac{1}{2}\left\langle f^* \Omega^\dagger e^{\Omega^\dagger t} f \right\rangle^{(\dot\gamma)} - \frac{1}{2}\left\langle (\Omega^\dagger f^*) e^{\Omega^\dagger t} f \right\rangle^{(\dot\gamma)} . \tag{4.78}$$

The author likes this form because it explicitely shows that the FDT violation occurs because $\Omega^\dagger$ is not Hermitian in the stationary average. If it was, the two terms above would be equal and the equilibrium FDT would hold. Eq. (4.78) can be rewritten using the ITT approach (1.13) for the second term (a constant $\langle f\rangle$ cancels in (4.78))

$$\chi_\mathrm{f}(t) = -\frac{1}{2}\dot C_\mathrm{f}(t) - \frac{1}{2}\left\langle (\Omega^\dagger f^*) e^{\Omega^\dagger t}\delta f \right\rangle - \frac{1}{2}\dot\gamma \int_0^\infty ds \left\langle \sigma_{xy} e^{\Omega^\dagger s} (\Omega^\dagger f^*) e^{\Omega^\dagger t}\delta f \right\rangle . \tag{4.79}$$

With (2.15), we have that the second term in (4.79), the short time derivative, is zero at long times,

$$\chi_\mathrm{f}(t\to\infty) = -\frac{1}{2}\dot C_\mathrm{f}(t) - \frac{1}{2}\dot\gamma \int_0^\infty ds \left\langle \sigma_{xy} e^{\Omega^\dagger s} (\Omega^\dagger f^*) e^{\Omega^\dagger t}\delta f \right\rangle . \tag{4.80}$$

term-#	1	2	3
microscopic	$\frac{1}{2}\left\langle f^* \delta\Omega^\dagger e^{\Omega^\dagger t} f \right\rangle$	$\frac{1}{2}\left\langle f^* \Omega^\dagger e^{\Omega^\dagger t} f \right\rangle^\delta$	$-\frac{1}{2}\left\langle (\Omega^\dagger f^*) e^{\Omega^\dagger t} f \right\rangle^\delta$
physical	$\frac{1}{2}\frac{\partial}{\partial t_w} C_\mathrm{f}(t, t_w)\Big\|_{t_w=0}$	$\frac{1}{2}\frac{\partial}{\partial t}\left[C_\mathrm{f}(t) - C_\mathrm{f}^{(t)}(t)\right]$	–
Sec. 4.6 $\approx$	$\frac{1}{2}\frac{\partial}{\partial t} C_\mathrm{f}^{(t)}(t) < 0$	$\frac{1}{2}\frac{\tilde{\sigma}}{\dot{\gamma}}\frac{\partial}{\partial t}\frac{\partial}{\partial t} C_\mathrm{f}^{(t)}(t) > 0$	–
Sec. 4.5 $\approx$	$\propto -\dot{\gamma}\Phi_{\mathbf{q}}(t) < 0$	$\propto \dot{\gamma}\Phi_{\mathbf{q}}(t) > 0$	$\propto -\dot{\gamma}\Phi_{\mathbf{q}}(t) < 0$
Eq. (4.80) with simulations			< 0

Table 4.1: The three contributions to the violating term $\Delta\chi_\mathrm{f}$. The table summarizes the knowledge gained about these terms and their approximations in the different approaches at long times in glassy states. $\langle \ldots \rangle^\delta$ denotes the average with $\Psi_s - \Psi_e$. From the negative sign of the third term and Eq. (4.80) follows $X_\mathrm{f}(t \to \infty) < \frac{1}{2}$.

The last term in Eq. (4.80) is the third violating term in Eq. (4.61). Interestingly, the second violating term in Eq. (4.61) is missing here. It is part of $\Delta\chi_\mathrm{f}$, but the susceptibility does not depend on it. This is because it is connected to $\dot{C}_\mathrm{f} - \dot{C}_\mathrm{f}^{(t)}$, see Sec. 4.6.2. It is clear now that in order to get values of the FDR smaller than $\frac{1}{2}$, we must have at long times

$$-\frac{1}{2}\dot{\gamma}\int_0^\infty ds \left\langle \sigma_{xy} e^{\Omega^\dagger s}(\Omega^\dagger f^*) e^{\Omega^\dagger t}\delta f \right\rangle < 0, \qquad \dot{\gamma}t = \mathcal{O}(1). \tag{4.81}$$

We have reasons to believe that $X_\mathrm{f}(t \to \infty) < \frac{1}{2}$ occurs at least at higher densities, see the discussion of the FDR in Chap. 6 and Ref. [1]. It is very unlikely that (4.81) changes its sign as a function of density, as long as it is not too far away from the glass transition. We can hence assume that the inequality in (4.81) holds for all densities. If it does, it follows from Eq. (4.80) for glassy states,

$$X_\mathrm{f}(t \to \infty) \leq \frac{1}{2}. \tag{4.82}$$

Note that our approximations for density fluctuations in Sec. 4.5 agree with Eq. (4.81). Tab. 4.1 summarizes the knowledge gained about the three different terms.

4.6.11 Equilibrium FDT for Eigenfunctions

There are functions f for which the equilibrium FDT holds, i.e, which are in some sense perpendicular to the current in Eq. (4.30). These are the eigenfunctions $f = \phi_n$ of the SO, $\Omega^\dagger\phi_n = \lambda_n\phi_n$. It can be seen from Eq. (4.78) which holds for arbitrary $f = f(\{x_i, y_i, z_i\})$. Using that also $\Omega^\dagger\phi_n^* = \lambda_n\phi_n^*$, we see that the susceptibility obeys the equilibrium FDT. $f = \phi_n$ is a special case since $C_\mathrm{f}(t) = C_\mathrm{f}^{(t)}(t)$[6] up to the normalization at $t = 0$ and both follow a single exponential. The finding that the equilibrium FDT holds for $f = \phi_n$ is an interesting prediction from our equations. It can shed new light

[6] Because of this, it is clear that the waiting time derivative, the dominating violating term, vanishes.

on the discussion concerning effective temperatures, because eigenfunctions do clearly not obey the generalized FDT in Eq. (4.19). The only problem with eigenfunctions of $\Omega^\dagger$ (except for the trivial one with $\lambda_n = 0$) is that they share an unfortunate property with the Yeti: Nobody has ever seen one.

4.6.12 FDT for the MSDs – Einstein Relation under Shear

Let us finally consider the mobility of a tagged particle. In equilibrium, it is connected to the diffusivity by the Einstein relation, see Eq. (4.2) for the single particle case. For higher densities, the mobility is time dependent. At short times, it equals the mobility of the isolated particle[7] (neglecting hydrodynamic interactions), while at long times, it takes a value smaller than the one of the isolated particle [20, 123]. In glassy states without shear it is zero for long times [77, 118]. The time dependent mobility $\mu(t)$ is given by the $q \to 0$ value of the incoherent susceptibility,

$$\mu(t) = \lim_{q\to 0} \frac{\chi^s_q(t)}{q^2}. \tag{4.83}$$

In equilibrium, $\mu(t)$ equals the time derivative of the MSD with pre-factor $\frac{1}{2}$ for the one dimensional case. Under shear, we use our approximation for the susceptibility in Eq. (4.68) to derive the mobility. It involves the expression in Eq. (3.99) and reads (Recall the notation for transient, stationary and equilibrium MSD, $\delta\bar{z}^2$, $\delta^{(\dot\gamma)}\bar{z}^2$ and $\delta^{(e)}\bar{z}^2$ from Chap. 3. The $\bar{z}$-direction is any direction perpendicular to the shear.),

$$\mu_{\bar{z}}(t) = \lim_{q\to 0} \frac{\chi^s_{q\mathbf{e}_{\bar{z}}}(t)}{q^2} \approx \frac{1}{2}\partial_t \delta^{(\dot\gamma)}\bar{z}^2(t) - \frac{1}{4}\partial_t\left(\delta\bar{z}^2(t) - \delta^{(e)}\bar{z}^2(t)\right). \tag{4.84}$$

Note that in Eq. (4.68) (and hence in (4.84)) the two subdominant terms in $\Delta\chi_{\mathrm{f}}$ are neglected. Fig. 4.16 shows the stationary MSD (see Sec. 3.8) together with the time integrated mobility for a glassy state at different shear rates. The mobility is finite under shear. The FDT violation is qualitatively equal as for the correlators, i.e., at short times, the equilibrium FDT holds while at long times, it is violated. The response, i.e., the mobility is smaller than estimated from the equilibrium FDT. At long times, the FDR X_{MSD} is constant in time, as is seen in the parametric plot in Fig. 4.17. We also show the mobility from Eq. (4.84) with transient replaced by stationary MSD, from which the ideal $X = \frac{1}{2}$-law follows. It leads to a sharp kink in the parametric plot. The mobility at long times is constant,

$$\lim_{t\to\infty} \mu_{\bar{z}}(t) = \mu^\infty_{\bar{z}} = \frac{1}{2} X^\infty_{\mathrm{MSD}} \partial_t \delta^{(\dot\gamma)}\bar{z}^2. \tag{4.85}$$

This equation can be rewritten to arrive at the Einstein relation for the long time diffusivity $D^\infty_{\bar{z}}$ in the glass under shear (we restore the units only for this equation),

$$D^\infty_{\bar{z}} = k_B T \frac{\mu^\infty_{\bar{z}}}{X^\infty_{\mathrm{MSD}}}. \tag{4.86}$$

[7] This holds also for the steady state under shear for directions perpendicular to the shear flow, see Sec. 3.5. At $t = 0$, the equilibrium FDT is valid.

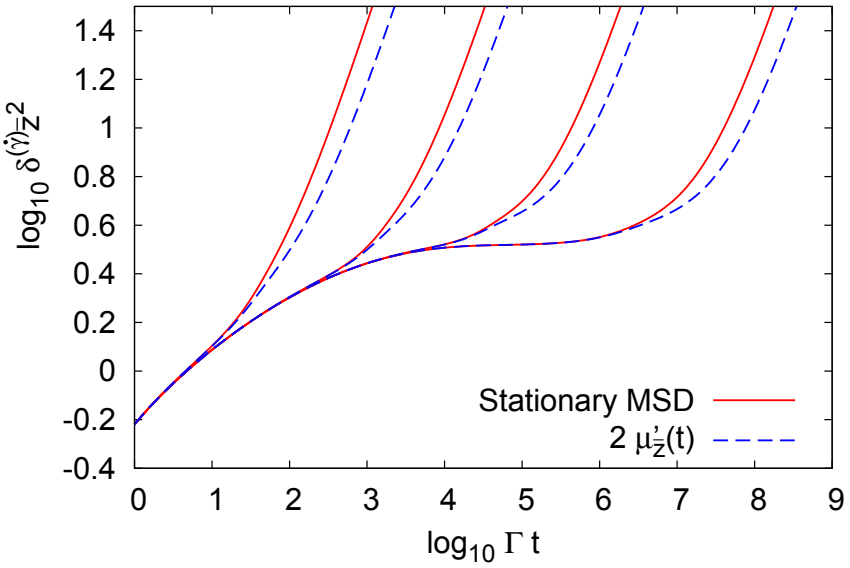

Figure 4.16: Stationary MSDs and twice the integrated mobility $\mu'_{\bar{z}}(t) = \int_0^t dt' \mu_{\bar{z}}(t')$ perpendicular to the flow direction for a glassy state ($\varepsilon = 10^{-3}$). Shear rates are $\dot{\gamma}/\Gamma = 10^{-8,-6,-4,-2}$ from right to left.

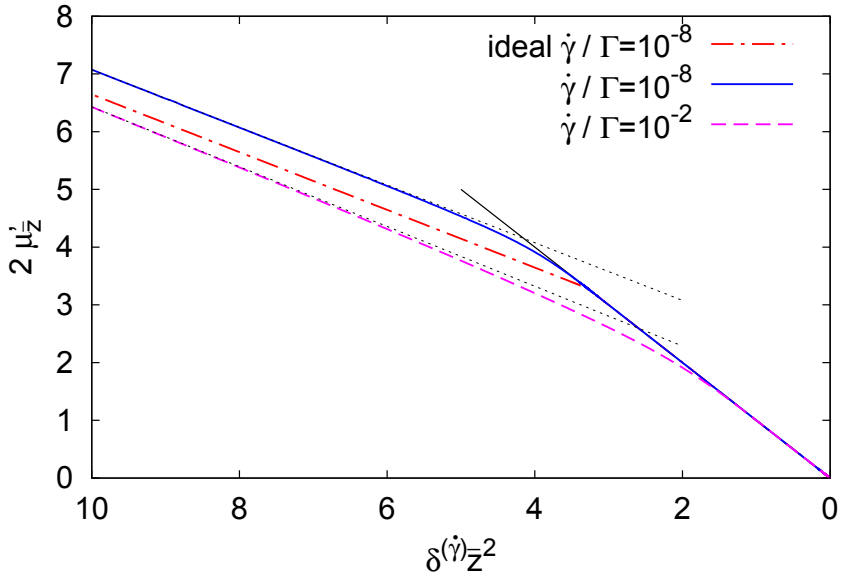

Figure 4.17: Parametric plot of integrated mobility versus the stationary MSD for a glassy state ($\varepsilon = 10^{-3}$).

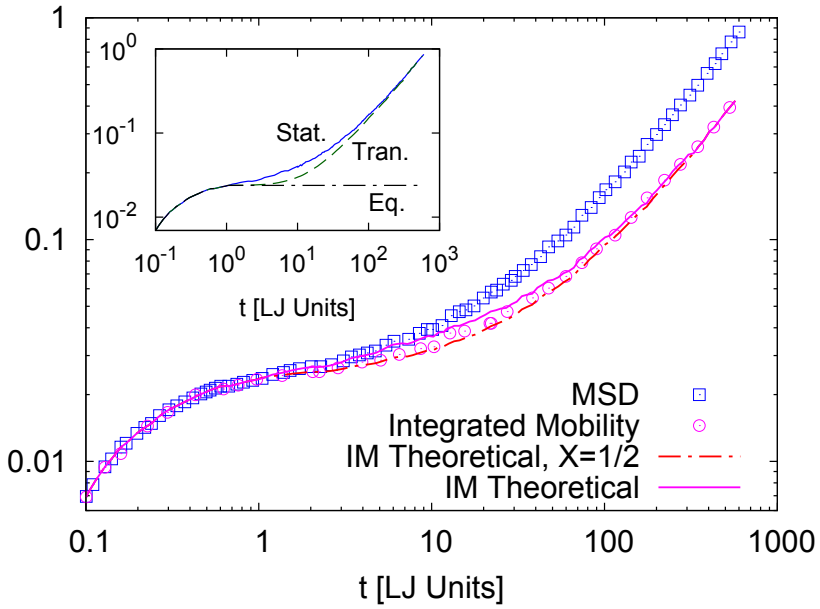

Figure 4.18: Comparison to simulation data for the diffusivity and the mobility in the neutral direction at temperature $T = 0.3$ ($T_c = 0.435$) and $\dot{\gamma} = 10^{-3}$. Circles and squares are the data (including units) from Fig. 16 in Ref. [1]. Lines are the integrated mobility calculated via Eq. (4.84). The dashed dotted line shows the approximation $\delta z^2(t) \approx \delta^{(\dot{\gamma})} z^2(t)$. For the other line, we used *the same value* for $\tilde{\sigma}$ as in Fig. 4.15. Note that the agreement between the long time part of the simulation results and the theoretical values for the mobility are independent of our construction of the un-sheared MSD and the value of $\tilde{\sigma}$. Inset shows the different MSDs, see main text.

Now we turn to the value of $X^{\infty}_{\mathrm{MSD}}$. As discussed in Sec. 3.8, we have to require that transient and stationary MSDs have equal time derivatives for long times ($\dot{\gamma}t \gg 1$). This leads to the interesting result that the FDR, as approximated in Eq. (4.84) takes the value $X^{\infty}_{\mathrm{MSD}} = \frac{1}{2}$ then. In Fig. 4.17, the lines fitted to the long time FDR at $\dot{\gamma}/\Gamma = 10^{-8}$ have slope $-\frac{1}{2}$, for both the ideal and the realistic case.

What about the subdominant terms we neglected? The second term in Eq. (4.61) is, in this case, the time derivative of the difference between stationary and transient MSDs. This difference vanishes at very long times. We already noted that this term is not important, since it does not influence the value of $X^{\infty}_{\mathrm{MSD}}$. In Eq. (4.79) we saw that only the last term in Eq. (4.61) leads to a deviation of the FDR from the value $\frac{1}{2}$. But setting the two terms equal leads in this case to the vanishing of both of them (since the first one vanishes), and the FDR for very long times is equal to $\frac{1}{2}$ according to Eq. (4.79). We do not have a reason to believe that the last term in Eq. (4.61) is actually zero in the MSD-case, but in the accuracy of our approach it takes this value.

Following this discussion, it is interesting to compare Eq. (4.84) directly to the simulation results in Ref. [1]. This is done in Fig. 4.18, following closely the analysis corre-

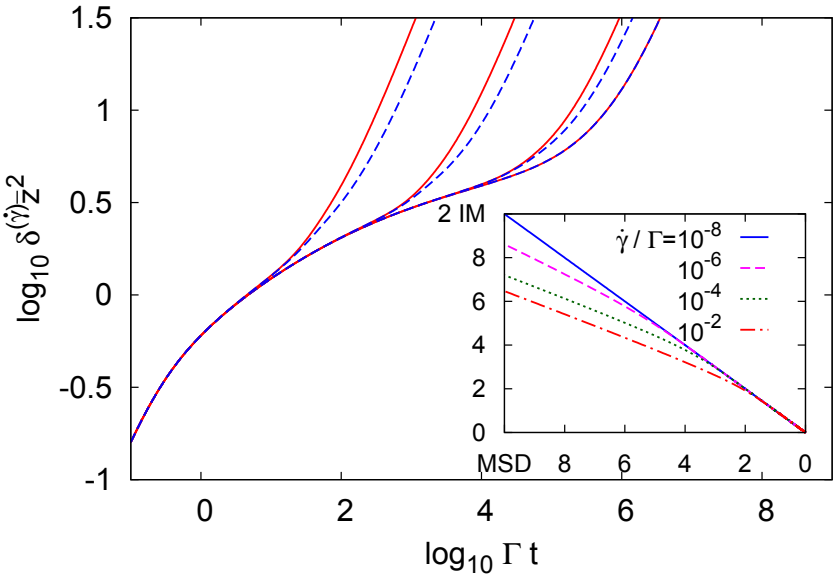

Figure 4.19: Stationary MSDs and integrated mobility perpendicular to the flow direction for a fluid state ($\varepsilon = -10^{-3}$). Shear rates are $\dot{\gamma}/\Gamma = 10^{-8,-6,-4,-2}$ from right to left. Inset shows the parametric plot for the different shear rates. For the smallest shear rate, it is almost indistinguishable from the equilibrium-FDT line.

sponding to Fig. 4.15. We construct a quiescent MSD which is constant for long times and calculate the transient one via Eq. (3.100). These are shown in the inset. Note that we use the same value of $\tilde{\sigma}$ as in Fig. 4.15, which appears slightly too large in the present case. The long time mobility fits very well to the simulation results. Note that this implies that the long time FDR takes the value of $\frac{1}{2}$ in the simulations within accuracy. The long time mobility as calculated from (4.84) is independent of our choice of the height of the non-ergodicity parameter and of the fitted value for $\tilde{\sigma}$. The agreement for long times is hence true without any fit parameter and gives strong support for Eq. (4.84).

Last, we consider the FDT violation for the MSDs on the fluid side. We find the expected behavior, i.e., for small shear rates, the equilibrium FDT is restored for all times, see Fig. 4.19.

4.7 Summary

We presented two independent approaches to investigate the relation between susceptibilities and correlation functions for colloidal suspensions at the glass transition. Both approaches lead to very similar results, namely a nearly time independent, positive FDR at long times smaller than unity. Let us summarize the second approach in more detail.

We find that the long time FDR is nearly isotropic in the plane perpendicular to the shear flow and takes the universal value $\hat{X}(\dot{\gamma}t) = \frac{1}{2}$ in glasses at small shear rates in the simplest approximation. This would agree with the interpretation of an effective temperature. Nevertheless, corrections arise from the difference of the stationary to the transient correlator and depend on the considered observable. They alter $\hat{X}_{\mathrm{f}}$ to values $\hat{X}_{\mathrm{f}} \leq \frac{1}{2}$ in the glass. Our findings are in great agreement with the simulations differing only in the dependence of the FDR on observable which contradicts the notion of an effective temperature.

Our finding of values close to the universal $\hat{X}(\dot{\gamma}t) = \frac{1}{2}$ points to intriguing connections to critical systems discussed in Sec. 4.2. Open questions concern establishing such a connection and to address the concept of an effective temperature, which was developed for ageing and driven mean field models.

Finally, we showed the connection of the dominant part of the violating term to the waiting time derivative of $C_{\mathrm{f}}(t, t_w)$, i.e., the connection of two completely different physical quantities. This connection can be tested in simulations. Because we identified all but one contributions of the violating term with independently measurable quantities, all our approximations are testable independently in simulations. The difference of the measured $\Delta\chi_{\mathrm{f}}$ in FDT simulations to the sum of the measured terms of $\Delta\chi_{\mathrm{f}}$ in waiting time simulations yields the contribution of the last term in $\Delta\chi_{\mathrm{f}}$.

5 Properties of the Stationary Correlator

In this chapter, some properties of the correlation function C_f in the stationary state shall be discussed. This is necessary because many known properties of the correlation function in equilibrium cannot be shown in non-equilibrium. We will also gain new insights into the susceptibility under shear, we will connect it to the dynamics in the frame comoving with the stationary probability current.

5.1 Properties in Equilibrium

The adjoined SO $\Omega_e^\dagger$ is Hermitian with respect to the equilibrium average [21], i.e.,

$$\left\langle f^* \Omega_e^\dagger g \right\rangle = \left\langle g \Omega_e^\dagger f^* \right\rangle = -\left\langle \sum_i \frac{\partial f^*}{\partial \mathbf{r}_i} \cdot \frac{\partial g}{\partial \mathbf{r}_i} \right\rangle . \tag{5.1}$$

Many important properties follow from this equation, as we will shortly sketch in order to be able to understand which mechanisms do not work in the steady state under shear. By choosing $g = f = \phi_n$, with ϕ_n being an eigenfunction of $\Omega_e^\dagger$, i.e.,

$$\Omega_e^\dagger \phi_n = \lambda_n \phi_n, \tag{5.2}$$

it follows from Eq. (5.1) that $\Omega_e^\dagger$ is negative semi-definite, $\lambda_n \leq 0$. One can also show with Eq. (5.1) that the eigenfunctions ϕ_n build an orthogonal set [22], i.e., for normalized functions holds

$$\langle \phi_n^* \phi_m \rangle = \delta_{nm}. \tag{5.3}$$

Using this, the auto-correlation of f can be written by expanding $\delta f = \sum_n c_n \phi_n$ as,

$$C_\mathrm{f}^{(e)}(t) = \left\langle \delta f^* e^{\Omega_e^\dagger t} \delta f \right\rangle = \sum_n c_n^* c_n e^{\lambda_n t}. \tag{5.4}$$

It is thus shown that $C_\mathrm{f}^{(e)}(t)$ is a sum of exponential functions with positive pre-factors, hence it is positive at all times and its n-th derivative has sign $(-1)^n$. Its spectrum, i.e., its Fourier transform is positive, too [124].

5.2 Smoluchowski Versus Newtonian Dynamics

We want to emphasize one more issue concerning the equilibrium state. The operator $\Omega_e^\dagger$ is Hermitian, while for Newtonian dynamics the time evolution operator iL, the Liouville

operator [125], is anti-Hermitian with respect to the corresponding average. This difference is important; in the literature, the correlation function under time translational invariance is often stated as [22, 125]

$$C^{(e)}_{\mathrm{f,t'}} = \left\langle \delta f^*(t')\delta f(t+t') \right\rangle , \tag{5.5}$$

with $\delta f(t)$ formally written as $\delta f(t) = e^{iLt} f$. The time t' is arbitrary in the time independent equilibrium state. With these definitions, it is immediately clear that Eq. (5.5) in Newtonian dynamics reduces to the definition of the correlation function

$$C^{(e)}_{\mathrm{f,t'}} = C^{(e)}_{\mathrm{f}} = \left\langle \delta f^* e^{iLt} \delta f \right\rangle . \tag{5.6}$$

In Smoluchowski dynamics, we would attempt to define $\delta f(t) = e^{\Omega^\dagger_e t}\delta f$. It follows that

$$C^{(e)}_{\mathrm{f,t'}} = \left\langle \delta f^*(t')\delta f(t+t') \right\rangle = \left\langle \delta f^* e^{\Omega^\dagger_e (t+2t')} \delta f \right\rangle = C^{(e)}_{\mathrm{f}}(t+2t'). \tag{5.7}$$

The last result is, of course, not useful and we conclude that the notation introduced with Eq. (5.5) cannot be used for Smoluchowski dynamics. The reason for this difference is probably that the Smoluchowski dynamics is not time reversible: If one inverts all velocities, the system does not go back in time.

5.3 Attempts to Show Properties for the Correlator under Shear

Recall the correlation function in the steady state

$$C_{\mathrm{f}}(t) = \left\langle \delta f^* e^{\Omega^\dagger t} \delta f \right\rangle^{(\dot\gamma)} . \tag{5.8}$$

The operator $\Omega^\dagger$ is not Hermitian in the stationary average. One can still perform an expansion of the function δf in eigenfunctions of $\Omega^\dagger$. But the eigenfunctions build only a biorthogonal set [21, 22, 126] and the pre-factors of the exponential functions corresponding to Eq. (5.4) cannot be shown to be positive, i.e., the correlator cannot be shown to be positive at all times.

Does the correlator have positive spectrum? There exists a proof for the positive spectrum based on time translational invariance in a notation as in Eq. (5.5) [124]. Since we cannot write our correlator like Eq. (5.5) for Smoluchowski dynamics, this proof does not work. The question remains, if time translational invariance is sufficient in order to have positive spectra.

5.4 Splitting the SO Into Hermitian and Anti-Hermitian Part

Subsequent to realizing that many proofs fail under shear due to the non–Hermiticity of the SO, we want to split it into its Hermitian and its anti–Hermitian part. Before

we can define the adjoined of an operator, we have to specify the corresponding scalar product. We have already introduced the SOs Ω and $\Omega^\dagger$. These two are adjoined in the unweighted scalar product defined as [20–22]

$$\int d\Gamma g(\Gamma)\,\Omega f^*(\Gamma) = \int d\Gamma f^*(\Gamma)\,\Omega^\dagger g(\Gamma). \tag{5.9}$$

As we saw above, the equilibrium operator $\Omega_e^\dagger$ is Hermitian in the scalar product containing the equilibrium distribution,

$$\int d\Gamma \Psi_e(\Gamma) g(\Gamma)\,\Omega_e^\dagger f^*(\Gamma) = \int d\Gamma \Psi_e(\Gamma) f^*(\Gamma)\,\Omega_e^\dagger g(\Gamma). \tag{5.10}$$

The SO for the system under shear is Hermitian with respect to no known scalar product [127], neither with respect to the equilibrium nor the stationary weight. To get some more insight, it therefore appears useful to derive the *adjoined of* $\Omega^\dagger$ *in the stationary average*, defined by

$$\left\langle g\,\Omega^\dagger\,f^*\right\rangle^{(\dot\gamma)} = \int d\Gamma \Psi_s(\Gamma) g(\Gamma)\,\Omega^\dagger f^*(\Gamma) = \int d\Gamma \Psi_s(\Gamma) f^*(\Gamma)\,\tilde\Omega^\dagger g(\Gamma) = \left\langle f^*\,\tilde\Omega^\dagger\,g\right\rangle^{(\dot\gamma)}. \tag{5.11}$$

We already stressed that it is neither identical to Ω nor $\Omega^\dagger$. It is given by

$$\tilde\Omega^\dagger = \sum_i \boldsymbol{\partial}_i^2 + 2\,(\boldsymbol{\partial}_i \ln \Psi_s)\cdot\boldsymbol{\partial}_i - \mathbf{F}_i\cdot\boldsymbol{\partial}_i - \boldsymbol{\partial}_i\cdot\boldsymbol{\kappa}\cdot\mathbf{r}_i. \tag{5.12}$$

Now we can split the SO into an Hermitian and an anti-Hermitian part with respect to stationary averaging,

$$\Omega^\dagger = \underbrace{\frac{1}{2}(\Omega^\dagger + \tilde\Omega^\dagger)}_{\Omega_H^\dagger} + \underbrace{\frac{1}{2}(\Omega^\dagger - \tilde\Omega^\dagger)}_{\Omega_A^\dagger}. \tag{5.13}$$

The two parts are found to be

$$\Omega_H^\dagger = \sum_i \boldsymbol{\partial}_i^2 + (\boldsymbol{\partial}_i \ln \Psi_s)\cdot\boldsymbol{\partial}_i\,, \tag{5.14a}$$

$$\Omega_A^\dagger = \sum_i -(\boldsymbol{\partial}_i \ln \Psi_s)\cdot\boldsymbol{\partial}_i + \mathbf{F}_i\cdot\boldsymbol{\partial}_i + \boldsymbol{\partial}_i\cdot\boldsymbol{\kappa}\cdot\mathbf{r}_i\,. \tag{5.14b}$$

$\Omega_H^\dagger$ is very similar to the equilibrium SO $\Omega_e^\dagger$, but the forces $\mathbf{F}_i = \boldsymbol{\partial}_i \ln \Psi_e$ are replaced by the non-equilibrium forces $\boldsymbol{\partial}_i \ln \Psi_s$. In the following section we will show the intriguing connection of $\Omega_H^\dagger$ to the susceptibilities discussed in Chap. 4. As expected, the anti-Hermitian part contains the shear part $\delta\Omega^\dagger$ as well as the difference between equilibrium and non-equilibrium forces. It is easy to show that the eigenvalues of $\Omega_A^\dagger$ are imaginary and the eigenvalues of $\Omega_H^\dagger$ are real. This holds for any anti-Hermitian or Hermitian

operator, respectively [22]. In the given case, $\Omega_H^\dagger$ can furthermore be shown to have negative semi-definite spectrum as does the equilibrium operator, because we have[1]

$$\left\langle f^* \Omega_H^\dagger g \right\rangle^{(\dot\gamma)} = -\left\langle \frac{\partial f^*}{\partial \mathbf{r}_i} \cdot \frac{\partial g}{\partial \mathbf{r}_i} \right\rangle^{(\dot\gamma)} . \tag{5.15}$$

If the correlation function is real for all times, $C_\mathrm{f}(t) = C_\mathrm{f}^*(t)$, which can be shown e.g. for density fluctuations [60], we can show that the initial decay rate is negative since the anti-Hermitian part does not contribute,

$$\mathcal{R}\left\{ \left\langle f^* \Omega^\dagger f \right\rangle^{(\dot\gamma)} \right\} = \left\langle f^* \Omega_H^\dagger f \right\rangle^{(\dot\gamma)} = -\left\langle \frac{\partial f^*}{\partial \mathbf{r}_i} \cdot \frac{\partial f}{\partial \mathbf{r}_i} \right\rangle^{(\dot\gamma)} \leq 0. \tag{5.16}$$

This has not been shown before. For higher order terms in t, such an argument is not possible since they contain contributions of $\Omega_A^\dagger$. We have thus shown that a real correlator initially always decays, i.e., the external shear does not enhance the fluctuations in some way.

5.5 Connection to the Susceptibility – The Comoving Frame

In the previous section, we saw that the adjoined SO can be split up into an Hermitian and an anti-Hermitian part. While this is not surprising, because it is possible for every operator, the result for the Hermitian part is indeed surprising in the given case. First, it intriguingly appears in the susceptibility defined in (4.20), which can be exactly written as

$$\chi_\mathrm{fg} = -\left\langle f^* \Omega_H^\dagger \, e^{\Omega^\dagger t} g \right\rangle^{(\dot\gamma)} . \tag{5.17}$$

Let us spend some time to consider this relation. The response of the system is not given by the time derivative with respect to the full dynamics but by the time derivative with respect to the Hermitian, i.e., the "well behaved" dynamics. Our finding in Chap. 4, that the equilibrium FDT holds at $t = 0$, is found again comparing with Eq. (5.16).

There is another interesting coincidence which is connected to this. The system is out of equilibrium because of the stationary probability current[2] $\mathbf{j}_i^s$. This current is nontrivial since it has $3N$ components. Eq. (5.17) can be rewritten to

$$\chi_\mathrm{fg} = -\left\langle f^* (\Omega^\dagger - \Omega_A^\dagger) \, e^{\Omega^\dagger t} g \right\rangle^{(\dot\gamma)} . \tag{5.18}$$

Regarding now the anti-Hermitian part, (5.14b), in more detail, we see that it can be exactly expressed by the probability current,

$$\Omega_A^\dagger = \Psi_s^{-1} \sum_i \mathbf{j}_i^s \cdot \boldsymbol{\partial}_i . \tag{5.19}$$

[1] The stationary distribution Ψ_s must be positive and (5.15) is negative for $f = g$.
[2] See the definition of $\mathbf{j}_i^s$ before Eq. (4.30).

It follows that we can write the susceptibility,

$$\chi_{\mathrm{fg}} = -\left\langle f^* \left(\partial_t - \Psi_s^{-1} \sum_i \mathbf{j}_i^s \cdot \boldsymbol{\partial}_i \right) e^{\Omega^\dagger t} g \right\rangle^{(\dot\gamma)} . \tag{5.20}$$

The derivative in the brackets can be identified as the convective or comoving derivative which is often used in fluid dynamics [128]. It measures the change of the function in the frame comoving with the probability current. That means the *equilibrium FDT holds in the frame comoving with the probability current*. This was also found for the velocity fluctuations of a single driven particle in Ref. [92], as presented in Sec. 4.2. The difference in our system is that the probability current, i.e., the local mean velocity, speaking with the authors of Ref. [92], does not depend on the spatial position x, but on the relative position of the particles because it originates from particle interactions.

We see that the Hermitian part of the SO is the operator which governs the dynamics comoving with the $3N$ dimensional probability current. After these interesting insights, it might be worthwhile to study the correlator defined with the Hermitian operator, the comoving correlator,

$$C_{\mathrm{f}}^{(H)}(t) \equiv \left\langle \delta f^* e^{\Omega_H^\dagger t} \delta f \right\rangle^{(\dot\gamma)} . \tag{5.21}$$

Because $\Omega_H^\dagger$ is Hermitian in the stationary average with negative eigenvalues, just as the equilibrium SO in the equilibrium average, the comoving correlator has all the properties which were inferred from this fact in Sec. 5.1, i.e., it is real, positive and has positive spectrum. Its n-th derivative has sign $(-1)^n$. It seems to be one possibility for the definition of a proper correlator, since it is well behaved and is still connected to the full dynamics of the system. To find this connection would be a great achievement. With it, one would be able to study the properties of the correlator $C_{\mathrm{f}}(t)$. The problem is, that very desirable things are mostly very hard to find [129]. Up to the present, the author was only able to find this relation approximative. This shall not be reported, because we are only interested in exact relations in this chapter.

Let us finish with interpretations of the comoving correlator. X_{f} describes the tendency of particles to move with the stationary current. If $X_{\mathrm{f}} = 1$, the stationary current vanishes, and we have $C_{\mathrm{f}} = C_{\mathrm{f}}^{(H)}$. If the particle trajectories are completely constraint to follow the current, we have $X = 0$, because a small external force cannot change these trajectories and $\chi_{\mathrm{f}} = 0$. In this case, $C_{\mathrm{f}}^{(H)} = const.$ since the particles do not move in the comoving frame. As examples for the latter case serve the experiments in Refs. [130, 131]. They consider a rather dilute suspension of colloids in a highly viscous solvent. The bare diffusion coefficient is approximately zero, i.e., on the experimental timescale the particles do not move at all without shear. As far as the author can judge, this is the system of non-Brownian particles introduced in Sec. 3.1. Shearing this suspension, the particles move with the flow and one observes diffusion in the directions perpendicular to the shearing due to interactions. A very small external force does not change the trajectories of the particles (on the timescale of the experiment) due to the high viscosity. We expect $X_{\mathrm{f}} = 0$ in this case and that the comoving correlator

is constant, as is the equilibrium correlator in the un-sheared system. The studies in the references above do not consider the susceptibility, the focus is put on the question whether the system is chaotic or not.

6 FDT-Violation: Final Discussion

In this chapter, we gather the insights we gained in the previous chapters in order to understand the physical reasons for the violation of the equilibrium FDT. One can approach this discussion from various sides. We want to focus on the clearest approach. Afterwards, we will consider a simple toy model which helps us to understand many of the phenomena which we encountered in this thesis.

6.1 Deterministic versus Stochastic Motion

We saw in Chap. 5 that the susceptibility measures the fluctuations of the particles in the frame comoving with the probability current $\mathbf{j}_i^s$. We conclude that we can split the displacements of the particles into two meaningful parts. First, the stochastic motion in the frame comoving with the probability current. Second, the motion following the average probability current, which is deterministic. This is illustrated in Fig. 6.1. In Fig. 6.1 b), the red particle has moved *upwards*, this is also on average true for this time window. The movement upwards is hence deterministic. Fig. 6.1 refers to the low density limit because the dynamics is less illustrative at the glass transition. But the picture is similar. Due to the interactions, the particle displacements have a deterministic part which is not measured by the susceptibility. The susceptibility is thus smaller than expected from the equilibrium FDT because it measures only part of the dynamics. We have $X_{\rm f} \leq 1$. It is hard to imagine how a system must be built up in order to exhibit an FDR larger than unity. We want to stress that the mixing of deterministic and stochastic parts lead to random, un-deterministic displacements at long observation times. But given the particle positions at time t one can in principle calculate the deterministic part of the displacements up to time $t + \delta t$.

6.2 What Does $X(t \to \infty) \leq \frac{1}{2}$ Mean?

Let us quantify the above discussion as far as possible. For this we recall Eq. (5.20),

$$\chi_{\rm fg} = -\left\langle f^* \left(\Omega^\dagger - \Psi_s^{-1} \sum_i \mathbf{j}_i^s \cdot \boldsymbol{\partial}_i \right) e^{\Omega^\dagger t} g \right\rangle^{(\dot\gamma)} . \tag{6.1}$$

We see that we can formally split the time derivative of the stationary correlation function into two pieces, the stochastic one, measured by the susceptibility, and the deterministic one due to the probability current,

$$\partial_t C_{\rm f}(t) = \left\langle f^* \Omega_H^\dagger \, e^{\Omega^\dagger t} g \right\rangle^{(\dot\gamma)} + \left\langle f^* \Omega_A^\dagger \, e^{\Omega^\dagger t} g \right\rangle^{(\dot\gamma)} \equiv \partial_t^{(sto)} C_{\rm f}(t) + \partial_t^{(det)} C_{\rm f}(t). \tag{6.2}$$

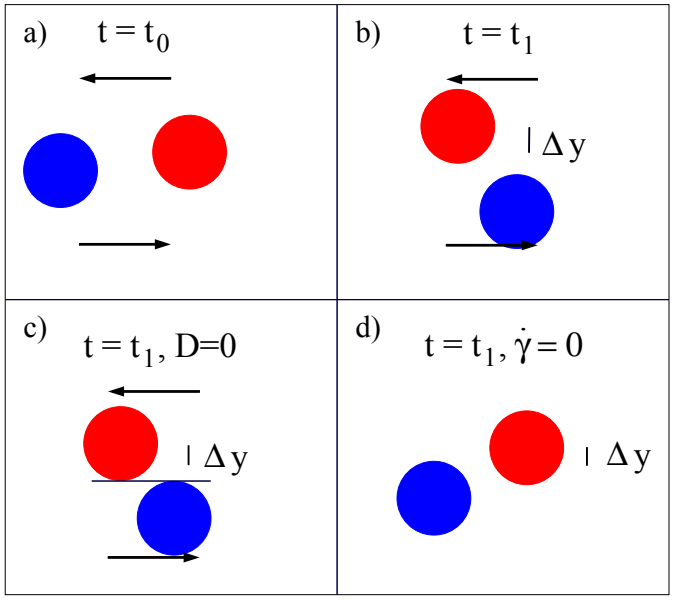

Figure 6.1: The two parts of the displacement of the particles. a) depicts the situation at the starting time. b) shows the full time evolution of a randomly picked trajectory after some time. In c), only the deterministic part (diffusivity is zero) is observed. The final positions can in principle be calculated from the initial conditions. d) shows only the stochastic part without shear. Note that b) is different from the sum of c) and d).

The inequality $X_{\mathrm{f}} \leq \frac{1}{2}$ now translates into an inequality for the two derivatives above,

$$|\partial_t^{(det)} C_{\mathrm{f}}(t)| \geq |\partial_t^{(sto)} C_{\mathrm{f}}(t)|. \tag{6.3}$$

In completely shear governed decay of glassy states, the deterministic displacements of the particles due the probability current are larger than the stochastic fluctuations around this average current. In other words, if the stochastic motion was faster than the deterministic one, the decay would not be completely shear governed.

It is likely that with increasing density, the particles are more and more confined to follow the probability current and the FDR gets smaller and smaller and might eventually reach zero.

6.3 The Thesis in Short: A Toy Model

Trap models have been repeatedly used to study the slow dynamics of glassy systems and to investigate the violation of the equilibrium FDT [99, 132–137]. They have to be considered critically because in a real system, the particles themselves form the traps for each other and the potential landscape is not constant in time. It is therefore not possible to map the problem onto a single particle problem. Nevertheless, we want to employ a simple toy model which will give us more insight into many of the topics

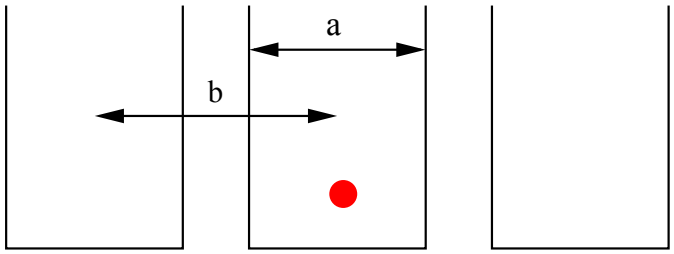

Figure 6.2: The toy model: The particle is trapped in wells of width a with infinitely high potential barriers. The center-to-center distance of the wells is denoted b.

discussed in this thesis. As far as the author knows, this model has not been introduced before. The model for glassy states is depicted in Fig. 6.2: The particle, surrounded by solvent (diffusivity $D_0 = k_B T \mu_0$), is trapped in an infinite potential well of width a. This potential well is one in a row of infinitely many with center-to-center distances b. Since these potential wells look very much like water glasses, the particle is literally "in the glass". The particle performs a stochastic motion in this well, and a very long time after we measured its position, its probability distribution $P(x)$ is constant within the well and zero outside. We neglect the dimensions of the particle and restore physical units.

6.3.1 Shear Melts the Glass

Now we introduce the shear, i.e., a mechanism which lifts the particle over the potential barriers; At time $t = \tau, 2\tau, 3\tau, \ldots$, we introduce shear steps; The particle is put into one of the neighboring wells according to its current position: If it is on the left side of the well, it gets to the well on the left hand side, if it is on the right hand side, it gets into the well on the right hand side. We hence consider a direction perpendicular to the shear flow, where its influence is symmetric. The position at which the particle enters the new well is not important, it shall be distributed randomly. The resulting dynamics has some similarities to a Cauchy process [138].

6.3.2 Dynamics

The dynamics in our model shares many properties of colloidal suspensions. We regard the limit of small shear rates, it corresponds to $\tau \gg a^2/D_0$, i.e., the time between two shear steps is much longer than it takes the particle to relax in the well.

Short Times

At short times, the mean squared displacement of the particle is the one of a free particle,

$$\lim_{t \to 0} \langle (x - x(0))^2 \rangle = 2 D_0 t. \tag{6.4}$$

Intermediate Times

For times $\tau > t \gg a^2/D_0$, the dynamics of the particle is glassy, i.e., the MSD is constant on the plateau. This plateau value can be derived from the constant probability distribution of the particle in the well, $P(x) = 1/a$,

$$\langle (x - x(0))^2 \rangle = \frac{1}{a^2} \int_{-a/2}^{a/2} dx(0) \int_{-a/2}^{a/2} dx (x - x(0))^2 = \frac{a^2}{6}, \qquad \tau > t \gg a^2/D_0. \quad (6.5)$$

We notice that in accordance with the glassy dynamics of colloidal suspensions, the plateau value is independent of D_0 and temperature. Note that the average over initial conditions is important in Eq. (6.5). The initial conditions are distributed with $P(x)$ as well.

Long Times

At every shear step the particle jumps to the left or right with equal probability, performing a random walk with step-length b and number of steps t/τ [1]. After many steps, the contribution of the plateau value to the MSD becomes negligible,

$$\langle (x - x(0))^2 \rangle = b^2 \frac{t}{\tau}, \qquad t \gg \tau. \quad (6.6)$$

The long time dynamics is independent of temperature and short time diffusivity D_0, as is the long time decay of the density correlator for colloidal glasses, compare the discussion in Sec. 1.6. The timescale is set by the period τ.

6.3.3 Mobility

To calculate the fluctuation dissipation ratio X, we have to find the mobility $\mu(t)$ of the particle in response to a small test force F acting on the particle. We assume that this test force does not influence the game rules defined above: At the shear step, the particle gets to the left if it is on the left hand side of the well, and to the right, if it is on the right hand side of the well. Recall the FDT (the Einstein relation) in equilibrium,

$$\mu(t) = \frac{1}{2k_BT} \frac{\partial}{\partial t} \langle (x - x(0))^2 \rangle. \quad (6.7)$$

It is more convenient to study the integrated version,

$$\frac{1}{F} \langle (x - x(0)) \rangle^{(F)} = \frac{1}{2k_BT} \langle (x - x(0))^2 \rangle. \quad (6.8)$$

$\langle \dots \rangle^{(F)}$ denotes an average under the influence of the external force.

[1] We ignore the fact that the movement is discontinuous.

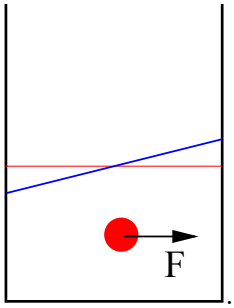

Figure 6.3: The long time probability distribution of the particle in the well without (red) and with external force (blue). This probability function for the real hard sphere system is calculated as function of external force within mode coupling theory in Ref. [118].

Short Times

At short times the particle obeys the FDT (6.8) and the mean traveled distance is

$$\lim_{t\to 0} \frac{1}{F} \langle (x - x(0)) \rangle^{(F)} = \mu_0 t = \frac{1}{k_B T} D_0 t. \tag{6.9}$$

Intermediate Times

The external force influences the probability distribution of the particle in the well, see Fig. 6.3. It is more likely to find the particle in the right hand side of the well than on the left hand side. The probability distribution $P_F(x)$ for $\tau > t \gg a^2/D_0$ follows the Boltzmann distribution [20], which, in linear order of the external force, reads,

$$P_F(x) = \begin{cases} \frac{1}{a}\left(1 + \frac{F\,x}{k_B T}\right) & -a/2 < x < a/2, \\ 0 & \text{else}, \end{cases} \qquad \tau > t \gg a^2/D_0. \tag{6.10}$$

The mean traveled distance is easily derived,

$$\frac{1}{F} \langle (x - x(0)) \rangle^{(F)} = \frac{1}{a} \int_{-a/2}^{a/2} dx(0) \int_{-a/2}^{a/2} dx P_F(x)(x - x(0)) = \frac{a^2}{12 k_B T}. \tag{6.11}$$

Comparing with Eq. (6.5), the Einstein relation (6.8) holds for all times $t < \tau$ as expected.

Long Times

Due to the distorted probability distribution $P_F(x)$ in Eq. (6.10), the particle will more likely jump to the right at the shear step at $t = \tau$. The rate R for jumps to the right minus the rate for jumps to the left follows,

$$R = \frac{\int_0^{a/2} P_F(x)dx - \int_{-a/2}^{0} P_F(x)dx}{\int_0^a P_F(x)dx} = \frac{a}{4}\frac{F}{k_B T} + \mathcal{O}(F^2). \tag{6.12}$$

At every shear step, the particle travels on average the distance bR. For $t \gg \tau$, the initially traveled distance in the well is negligible and we have

$$\frac{1}{F}\langle (x - x(0)) \rangle^{(F)} = \frac{a\,b}{4k_BT}\frac{t}{\tau}, \qquad t \gg \tau. \tag{6.13}$$

The mobility of the particle is finite at long times and independent of the diffusivity D_0.

6.3.4 Long Time FDR

Comparing Eqs. (6.13) and (6.6), we see that the Einstein relation does not hold for long times. The long time FDR $X(t \gg \tau)$ is different from unity,

$$X(t) = \begin{cases} 1 & t < \tau, \\ \frac{1}{2}\frac{a}{b} & t \gg \tau. \end{cases} \tag{6.14}$$

The FDT violation at long times comes from the fact that the shear steps are 'unbendable', i.e., their step-length is not influenced by the external force. Once the position of the particle in the well has been identified at the shear step, the dynamics is deterministically going to the appointed well. In some cases even to the left well, i.e., *against* the external force. The external force has no means to prevent this. We believe that the same happens in the real system under shear.

We note that $X(t \gg \tau)$ is independent of temperature because the potential barriers are infinitely high. We found the same for the hard sphere system in Chap. 4. In simulations of soft spheres, this is not true because the temperature also governs the glass transition. We observe that the FDR in our model depends on the ratio of "stochastic diffusion length" a and "deterministic diffusion length" b. This illuminates our interpretation in Sec. 6.1.

We note that $X(t \gg \tau)$ reaches $\frac{1}{2}$ if b goes to a. $b < a$ (leading to $1 > X > \frac{1}{2}$) is physically not reasonable, therefore there is an excluded region for the value of the FDR in the glass, as we found for the real system. This range coincides with the one we found in Chap. 4.

The model allows to discuss two more effects: In the real system at increasing density, the cages become smaller and smaller, i.e., in our model we have a decreasing value of $\frac{a}{b}$ and $X(t \gg \tau)$ decreases in accordance with the real system in Fig. 4.13. In the toy model, it eventually reaches zero being always positive.

For increasing shear rates, i.e., decreasing τ, the particle has less time to relax in the well and the effect of the external force decreases, this leads to a decreasing value of X. This is also in agreement with our calculation in Chap. 4, see Fig. 4.13 and the simulations in Ref. [1]. We believe that the decrease in the real colloidal system has the same origin, i.e., the particle has less time to adjust its distribution in the cage in response to the force.

6.3.5 The Comoving Frame

Our simple model also allows to illustrate the dynamics in the frame comoving with the probability current because the latter is simply given by the shear steps between the

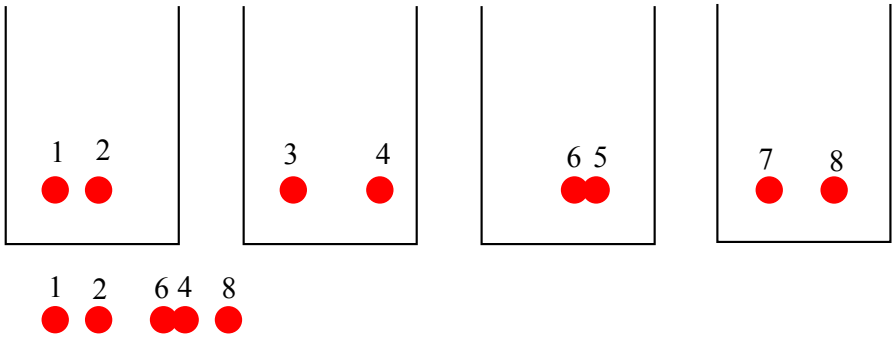

label	1	2	3	4	5	6	7	8
time	0	$\tau - \delta t$	$\tau + \delta t$	$2\tau - \delta t$	$2\tau + \delta t$	$3\tau - \delta t$	$3\tau + \delta t$	$4\tau - \delta t$

Figure 6.4: The real dynamics (top) and the dynamics in the comoving frame (bottom). The positions correspond to times given in the table. The particle diffuses in the well and is at position 2 when the shear step happens. This shear step takes the particle to position 3 from where it diffuses to position 4 from where it is taken away by the next shear step and so on. On the bottom, we show the movement in the comoving frame. Positions 2 and 3, 4 and 5, and 6 and 7 coincide. The traveled distance is shorter, but the particle will get infinitely far away in contrast to the case without shear steps.

potential wells. Fig. 6.4 illustrates the dynamics in the comoving frame. It is slower than in the rest-frame but still ergodic in contrast to the case without shear steps. We see that in the comoving frame, the position of the well is changed at every shear step. It is clear that the mobility of the particle obeys the FDT at all times in this system.

6.3.6 The Waiting Time Derivative

Our relation for the waiting time derivative in Eq. (2.18) is the central approximation of this thesis. The toy model can give further insight into this approximation although it does not contain the difference between stationary or transient dynamics. How can we introduce a small waiting time t_w in the toy model? For $t_w = \delta t$, we simply have shear steps at $t = \tau - \delta t$, $2\tau - \delta t, \ldots$, i.e., they are shifted by $-\delta t$. This is in agreement to the real system, where for $t_w = \delta t$ the cages break at $t_{\text{break}} - \delta t$ if they break at t_{break} for $t_w = 0$. With this and Sec. 6.3.2 we find

$$\lim_{\delta t \to 0} \left\langle (x - x(0))^2 \right\rangle (t, t_w = \delta t) = \begin{cases} \left\langle (x - x(0))^2 \right\rangle (t, t_w = 0) & t < \tau - \delta t, \\ \left\langle (x - x(0))^2 \right\rangle (t + \delta t, t_w = 0) & t \gg \tau. \end{cases} \tag{6.15}$$

The derivative with respect to waiting time at $t_w = 0$ is zero for $t < \tau$ and equal to the time derivative for $t \gg \tau$, i.e., it is the long time derivative in accordance to our approximation in Chap. 2. Of course, the way we introduced the waiting time into the model was chosen such that this result is achieved, but it still illustrates our intuitive argument in Sec. 2.5.3.

7 Summary and Outlook

In this thesis, different properties of colloidal suspensions near the glass transition under shear are analyzed. We saw that the difference between the transient and the stationary correlator is largest at intermediate times. This effect is attributed to the fact that in the case of the transient correlator, all particles are mobilized simultaneously at a certain strain, whereas in the steady state, the particles escape their cages every now and then, uncorrelated to the correlation time t. Hence, the steady correlator decays earlier from the glassy plateau. We saw that the dependence on waiting time after switch-on can be very accurately described for small waiting times. This prediction awaits experimental tests. The same is true for our formula for long waiting times, which one might also be able to improve in the future.

A tagged particle shows anisotropic dynamics under shear. This anisotropy is very simple near the critical plateau, it shows the expected "quadrupole"-behavior: Two opposite poles on the unit sphere in wavevector space have slightly faster dynamics, the other two poles have slightly slower dynamics. This prediction also awaits experimental tests. We saw that the mean squared displacement of the tagged particle is anisotropic as well. In the direction of the shear flow it shows a term that grows cubically in time. The amplitude of this term is connected to the diffusivity in the gradient direction as is the case for low densities where the phenomenon is known as Taylor dispersion. This holds even for glassy states where all terms show the characteristic yield scaling with shear rate. We found agreement to recent simulations.

Focus was put on the violation of the fluctuation dissipation theorem. We saw that the largest of the terms that violate the FDT can be related to the difference between transient and stationary correlators. This led us to a universal non-equilibrium ratio between response and fluctuations in the simplest approximation, namely an FDR of $X = \frac{1}{2}$ for glassy states at long times. This is in agreement with the notion of an effective temperature proposed previously. Intriguingly, this value was also found in different spin models before. Looking more closely, we find corrections to this value which depend on observable and which alter X to values smaller than $\frac{1}{2}$ in glassy states. This dependence on observable contradicts the notion of an effective temperature. We identified all but one of the terms that violate the fluctuation dissipation theorem with well defined measurable quantities. With this, all our approximations can in principle be tested independently. It would be a great joy for the author if someone would identify the last one of the violating terms with a measurable quantity in the future.

Studying the microscopic form of the susceptibility, we found that it contains not the full Smoluchowski operator (SO) in front of the time evolution exponential, which would give the time derivative, but only part of it. The SO is not Hermitian under shear and it is exactly its Hermitian part which enters the susceptibility. The Hermitian part can

be shown to represent the dynamics in the frame comoving with the $3N$-dimensional probability current. We concluded that the equilibrium FDT holds in the comoving frame.

Finally we attributed the violation of the equilibrium FDT to the deterministic part of the dynamics to which the susceptibility is not sensitive. The deterministic part is given by the dynamics following the average probability current. This led us to the conclusion that the deterministic part is as large as the stochastic part at $X = \frac{1}{2}$, illuminating the specialty of this value. We argued that the FDR must always be less than unity. In a very simple toy model, which shares many properties of the real colloidal system, we were able to study the FDT violation more closely. We saw that the violation appears due to the deterministic part of the dynamics and we were able to visualize the dynamics in the comoving frame.

8 Zusammenfassung

In der vorliegenden Arbeit werden Eigenschaften von kolloidalen Gläsern unter dem Einfluß von Scherung untersucht. Dieses System ist im Nichtgleichgewicht und erreicht einen stationären Zustand, wenn man ausreichend lang eine konstante Scherung anlegt. Insbesondere wird das Fluktuations-Dissipations-Theorem (FDT) studiert. Dieses gilt im Gleichgewicht und verbindet die Antwort des Systems auf eine kleine externe Kraft mit den thermischen Fluktuationen des ungestörten Systems. Im Nichtgleichgewichtssystem unter Scherung ist das FDT verletzt. In Computersimulationen [1] wurde gefunden, dass das FDT in gescherten Gläsern auf sehr spezielle Weise verletzt ist. Das Gleichgewichts-FDT scheint zu gelten wenn man die Temperatur des Systems durch einen anderen Wert ersetzt, die so genannte effektive Temperatur.

Die Arbeit beginnt mit der Analyse verschiedener Korrelationsfuntionen. Dies ist nötig, da sich die Kenntnis der Unterschiede zwischen diesen als erforderlich für das Studium des FDT herausstellte. Der transiente Korrelator beschreibt thermische Fluktuationen, deren Messung beim Einschalten der externen Scherung beginnt. Beginnt die Messung eine Zeitspanne nach dem Einschalten der Scherung, d.h. nach der sogenannten Wartezeit, so wird der Zwei-Zeiten-Korrelator gemessen. Im Limes großer Wartezeiten erreicht dieser den stationären Korrelator, der die Fluktuationen im stationären Zustand beschreibt. Der Unterschied zwischen diesen Korrelatoren wird untersucht, wobei insbesondere eine sehr genaue Beschreibung der Abhängigkeit des Korrelators von der Wartezeit für kurze Wartezeiten erreicht wird. Diese Beschreibung für kurze Wartezeiten kann in Computersimulationen getestet werden.

Im dritten Kapitel wird die Dynamik eines einzelnen markierten Teilchens studiert, eine Erwartungsgröße, die im Bezug auf die Verletzung des FDTs im vierten Kapitel von Bedeutung sein wird: In den Computersimulationen wird besonders die Verletzung des FDT für einzelne markierte Teilchen untersucht. Unsere Untersuchungen ergeben, dass das mittlere Verschiebungsquadrat des Teilchens in Richtung des Scherflusses für lange Zeiten nicht wie in Diffusionsprozessen linear in der Zeit wächst, sondern kubisch. Dies ist für kolloidale Lösungen niedriger Dichte bekannt als Taylor Dispersion. Wir finden, dass der kubische Term mit der Diffusion des Teilchens in Gradientenrichtung verknüpft ist. Diese Verknüpfung ist identisch zu derjenigen, die bei niedrigen Dichten auftaucht. Dies gilt sogar für Gläser, wo alle Diffusionskonstanten die charakteristische lineare Skalierung mit der Scherrate zeigen.

Das Studium der Verletzung des FDTs unter Scherung ergibt, dass der Term, der den größten Beitrag zur Verletzung liefert, mit der Abhängigkeit des Zwei-Zeiten-Korrelators von der Wartezeit verknüpft ist. Wir verbinden somit zwei völlig verschiedene experimentelle Meßgrößen. Das führt uns auf ein universelles Nichtgleichgewichts-Verhältnis von Antwortfunktion und Fluktuationen in der einfachsten Näherung, das Fluktuations-

Dissipations-Verhältnis (FDR) X nimmt den Wert $X = \frac{1}{2}$ an. Dies ist in Übereinstimmung mit der vorgeschlagenen Beschreibung mithilfe einer effektiven Temperatur. Der Wert $X = \frac{1}{2}$ wurde interessanterweise vorher auch in kritischen Spin-Modellen gefunden. Wenn man genauer hinschaut, gibt es Korrekturen zu diesem Wert, die von der studierten Observablen abhängen. Diese Abhängigkeit widerspricht der Interpretation einer effektiven Temperatur. Es ergibt sich, dass das FDR in Gläsern kleiner als $\frac{1}{2}$ ist.

Anschließend untersuchen wir die mikrospkopische Form der Suszeptibilität genauer. Wir finden, dass die Antwortfunktion nicht durch die volle Zeitableitung der Korrelationsfunktion gegeben ist, wie das im Gleichgewicht der Fall ist, sondern nur durch einen Teil der Ableitung. Dieser Teil kann interpretiert werden als Ableitung im System, das sich mit dem stationären Wahrscheinlichkeitsstrom mitbewegt. Dieser Wahrscheinlichkeitsstrom hat $3N$ Komponenten, wobei N die Teilchenzahl ist. Wir folgern, dass man die Dynamik des Systems in einen stochastischen und einen deterministischen Teil (gegeben durch den Wahrscheinlichkeitsstrom) aufteilen kann, wobei die Antwortfunktion nur den stochastischen Teil misst. Sie ist damit kleiner, als man vom Gleichgewichts-FDT erwarten würde. Der spezielle Wert von $X = \frac{1}{2}$ kann damit so interpretiert werden, dass stochastischer und deterministischer Teil genau gleich groß sind. Zuletzt betrachten wir ein einfaches Spielzeug-Modell, das viele Eigenschaften glasartiger kolloidaler Suspensionen teilt. Es erlaubt uns, die Verletzung des FDTs zu studieren. Wir sehen, dass diese Verletzung vom deterministischen Anteil der Dynamik verursacht wird.

A β-Analysis

For $0 \leq \varepsilon \ll 1$ and $\dot{\gamma}t \ll 1$, the correlators are expanded near the critical plateau

$$\Phi_{\mathbf{q}}(t) = f_q^c + (1-f_q^c)^2 \mathcal{G}_q(t), \tag{A.1a}$$
$$\Phi^s_{\mathbf{q}}(t) = f_q^{sc} + (1-f_q^{sc})^2 \mathcal{G}^s_{\mathbf{q}}(t), \tag{A.1b}$$

where the isotropic $\mathcal{G}_q(t)$ for the coherent correlator is known, $\mathcal{G}_q = \mathcal{G} e_q$, with e_q the eigenvector with eigenvalue unity of the stability matrix of the coherent memory function [10, 27]. Eq. (3.42) is recovered by $(1-f_q^c)^2\, e_q = h_q$. We rename the incoherent memory function in traditional MCT notation[1],

$$m^s_{\mathbf{q}}(t,t') = \mathcal{F}_{\mathbf{q}}(t,t',\Phi_{\mathbf{k}},\Phi^s_{\mathbf{p}}). \tag{A.2}$$

It is for $\dot{\gamma}=0$ given by $\mathcal{F}^e_q(\Phi^{(e)}_k, \Phi^{s(e)}_p)$. Expanding it around the critical value, where superscripts c and e denote critical parameters and equilibrium respectively, one has

$$\begin{aligned}\mathcal{F}_{\mathbf{q}}(t,t',\Phi_{\mathbf{k}},\Phi^s_{\mathbf{p}}) &= \mathcal{F}^{c,e}_q(f^c,f^{sc}) + \sum_k C^{c,e}_{q,k}\mathcal{G}_k(t-t') + \sum_{\mathbf{k}} C^{c,e,s}_{q,k}\mathcal{G}^s_{\mathbf{k}}(t-t') \\ &\quad + \Delta\mathcal{F}^{(\dot{\gamma})}_{\mathbf{q}}(t,t',f^c_q,f^{sc}_p) + \ldots .\end{aligned} \tag{A.3}$$

The last term, $\Delta\mathcal{F}^{(\dot{\gamma})}_{\mathbf{q}}$, is the contribution in lowest order in $\dot{\gamma}t$ and $\dot{\gamma}t'$ of the advection in the vertices. The Taylor coefficients read

$$C^{c,e}_{q,k} = \left.\frac{\partial \mathcal{F}^{c,e}_q(f,f^s)}{\partial f}\right|_{f^c,f^{sc}} (1-f^c_k)^2, \tag{A.4a}$$
$$C^{c,e,s}_{q,k} = \left.\frac{\partial \mathcal{F}^{c,e}_q(f,f^s)}{\partial f^s}\right|_{f^c,f^{sc}} (1-f^{sc}_k)^2. \tag{A.4b}$$

Only the critical Taylor coefficients appear in Eq. (A.3), because higher order terms are of order ε [10] and hence of order $\mathcal{G}^2$. With Eq. (A.3), the equation of motion, Eq. (3.38) becomes for long times (divided by $(1-f^{sc}_q)$),

$$\begin{aligned}\frac{f^{sc}_q}{1-f^{sc}_q} - \mathcal{F}^{c,e}_q(f^c,f^{sc}) + \mathcal{G}^s_{\mathbf{q}}(t) &= \sum_k C^{c,e}_{q,k}\mathcal{G}_k(t) + \sum_{\mathbf{k}} C^{c,e,s}_{q,k}\mathcal{G}^s_{\mathbf{k}}(t) \\ &\quad + \Delta\mathcal{F}^{(\dot{\gamma})}_{\mathbf{q}}(t,0,f^c_q,f^{sc}_p) + \ldots .\end{aligned} \tag{A.5}$$

[1] $\mathcal{F}_{\mathbf{q}}$ is different from the function introduced in Eq. (1.25). We do not want to use the superscript s here because of the many superscripts it will carry below.

The first two terms cancel each other since they fulfill the equation for the plateau value f_q^s [77],

$$\frac{f_q^s}{1-f_q^s} = \mathcal{F}_q^e(f, f^s). \tag{A.6}$$

Eq. (A.5) is not singular at the critical density [10] and we can solve the linear equation for $\mathcal{G}_{\mathbf{q}}^s$,

$$\sum_{\mathbf{k}} (\delta_{\mathbf{q},\mathbf{k}} - C_{q,k}^{c,e,s}) \mathcal{G}_{\mathbf{k}}^s(t) = \sum_k C_{q,k}^{c,e} \mathcal{G}_k(t) + \Delta\mathcal{F}_{\mathbf{q}}^{(\dot\gamma)}(t, 0, f_q^c, f_p^{sc}). \tag{A.7}$$

We notice that the anisotropic part of $\mathcal{G}_{\mathbf{k}}^s(t)$ is eigenfunction of the eigenvalue zero of the matrix $C_{q,k}^{c,e,s}$, because it is antisymmetric in q_x and q_y as we will see below. The isotropic and the anisotropic part of the equation separate. We find that the solution of the isotropic part is given by the coherent β-correlator with a q-dependent pre-factor, $\mathcal{G}_q^{(s,iso)}(t) = e_q^s \mathcal{G}(t)$. The equation for this pre-factor is given by

$$\sum_k (\delta_{q,k} - C_{q,k}^{c,e,s}) e_k^s = \sum_k C_{q,k}^{c,e} e_k. \tag{A.8}$$

Eq. (A.8) is identical to the corresponding equation for the equilibrium case in Ref. [77]. The critical amplitude for the incoherent correlator is thus given by its equilibrium value,

$$h_q^s = (1 - f_q^{sc})^2 e_q^s. \tag{A.9}$$

Eq. (3.47) for the anisotropic term follows with (we insert the pre-factor of $(1-f_q^{sc})^2/h_q^s$ to be able to compare the anisotropic part directly to $\mathcal{G}(t)$),

$$\frac{(1-f_q^{sc})^2}{h_q^s} \Delta\mathcal{F}_{\mathbf{q}}^{(\dot\gamma)}(t, 0, f_q^c, f_p^{sc}) \equiv \mathcal{G}_{\mathbf{q}}^{(s,aniso)}(t) = G(\mathbf{q})\, \dot\gamma t + \mathcal{O}(\dot\gamma t)^2. \tag{A.10}$$

B Approximations for $n_{\mathbf{q}}(t)$

We show the derivation of the expressions for the memory functions used in Sec. 4.5 in detail. The time dependent pair density projector is given by [60],

$$P_2(t) = \sum_{\mathbf{k}>\mathbf{p},\mathbf{k}'>\mathbf{p}'} \frac{\varrho_{\mathbf{k}(t)}\varrho_{\mathbf{p}(t)}\rangle\langle\varrho^*_{\mathbf{k}'(t)}\varrho^*_{\mathbf{p}'(t)}}{\langle\varrho^*_{\mathbf{k}(t)}\varrho^*_{\mathbf{p}(t)}\varrho_{\mathbf{k}'(t)}\varrho_{\mathbf{p}'(t)}\rangle} \approx \sum_{\mathbf{k}>\mathbf{p}} \frac{\varrho_{\mathbf{k}(t)}\varrho_{\mathbf{p}(t)}\rangle\langle\varrho^*_{\mathbf{k}(t)}\varrho^*_{\mathbf{p}(t)}}{N^2 S_{\mathbf{k}(t)} S_{\mathbf{p}(t)}}. \tag{B.1}$$

The triple density projector is used less often in the literature [139–141]. It follows directly from the pair projector,

$$\begin{aligned} P_3(t) &= \sum_{\mathbf{k}>\mathbf{p}>\mathbf{n},\mathbf{k}'>\mathbf{p}'>\mathbf{n}'} \frac{\varrho_{\mathbf{k}(t)}\varrho_{\mathbf{p}(t)}\varrho_{\mathbf{n}(t)}\rangle\langle\varrho^*_{\mathbf{k}'(t)}\varrho^*_{\mathbf{p}'(t)}\varrho^*_{\mathbf{n}'(t)}}{\langle\varrho^*_{\mathbf{k}(t)}\varrho^*_{\mathbf{p}(t)}\varrho^*_{\mathbf{n}(t)}\varrho_{\mathbf{k}'(t)}\varrho_{\mathbf{p}'(t)}\varrho_{\mathbf{n}'(t)}\rangle} \\ &\approx \sum_{\mathbf{k}>\mathbf{p}>\mathbf{n}} \frac{\varrho_{\mathbf{k}(t)}\varrho_{\mathbf{p}(t)}\varrho_{\mathbf{n}(t)}\rangle\langle\varrho^*_{\mathbf{k}(t)}\varrho^*_{\mathbf{p}(t)}\varrho^*_{\mathbf{n}(t)}}{N^3 S_{\mathbf{k}(t)} S_{\mathbf{p}(t)} S_{\mathbf{n}(t)}}. \end{aligned} \tag{B.2}$$

The memory function $n^{(1)}_{\mathbf{q}}$ has only one time evolution operator and can hence be approximated via "standard" routes with the projector $P_2(t)$ [60],

$$n^{(1)}_{\mathbf{q}}(t) \approx \frac{\dot\gamma}{2N S^{(\dot\gamma)}_{\mathbf{q}} \Gamma_{\mathbf{q}}} \left\langle \sigma_{xy} \varrho^*_{\mathbf{q}} Q P_2(-t) U(t) P_2 \Omega^\dagger \varrho_{\mathbf{q}} \right\rangle. \tag{B.3}$$

For the appearing time dependent four point correlation function, the MCT factorization approximation is used

$$\langle \varrho^*_{\mathbf{k}'(-t)} \varrho^*_{\mathbf{k}'(-t)-\mathbf{q}} U(t) \varrho_{\mathbf{k}} \varrho_{\mathbf{k}-\mathbf{q}} \rangle \approx N^2 S_{k(-t)} S_{k(-t)-q} \Phi_{\mathbf{k}(-t)}(t) \Phi_{\mathbf{k}(-t)-\mathbf{q}}(t) \delta_{\mathbf{k},\mathbf{k}'}. \tag{B.4}$$

At the left hand side appears the expression

$$V^{(1)}_{\mathbf{qk}} = \frac{\left\langle \sigma_{xy} \varrho^*_{\mathbf{q}} Q \varrho_{\mathbf{k}} \varrho_{\mathbf{q}-\mathbf{k}} \right\rangle}{N S_q} \approx k_x (k_y - q_y) \frac{S'_{q-k}}{q-k} S_k + k_x k_y \frac{S'_k}{k} S_{q-k}. \tag{B.5}$$

On the right hand side, we have the standard vertex

$$V^{(2)}_{\mathbf{qk}} = \frac{\left\langle \varrho_{\mathbf{k}} \varrho_{\mathbf{q}-\mathbf{k}} Q \Omega^\dagger \varrho_{\mathbf{q}} \right\rangle}{N S_{k-q} S_k} = \mathbf{q} \cdot ((\mathbf{k}-\mathbf{q}) n c_{k-q} + \mathbf{k} n c_k). \tag{B.6}$$

In the derivation of Eqs. (B.5) and (B.6), the convolution approximation for the static three point correlation function was used [10],

$$\langle \varrho_{\mathbf{q}} \varrho_{\mathbf{k}-\mathbf{q}} \varrho_{\mathbf{k}} \rangle \approx N S_q \, S_{k-q} \, S_k. \tag{B.7}$$

Improvements for this formula have been discussed in Refs. [61, 142, 143]. The approximation for the function $m_{\mathbf{q}}(t)$ is achieved in a similar way, the vertex (B.6) appearing on both sides of the time evolution operator [60]. The term of order $\dot{\gamma}$, which appears in the left vertex when approximating Eq. (4.37), is neglected.

The treatment of $n_{\mathbf{q}}^{(2,3)}$ is more involved. We first separate the time evolution operator in t with pair projectors to get,

$$n_{\mathbf{q}}^{(2)}(t) \approx \frac{\dot{\gamma}}{2NS_{\mathbf{q}}^{(\dot{\gamma})}\Gamma_{\mathbf{q}}} \int_0^\infty ds \left\langle \sigma_{xy} e^{\Omega^\dagger s} \varrho_{\mathbf{q}}^* \Omega^\dagger \, Q \, P_2 U(t) P_2(t) Q \Omega^\dagger \varrho_{\mathbf{q}} \right\rangle, \tag{B.8}$$

$$n_{\mathbf{q}}^{(3)}(t) \approx \frac{-\dot{\gamma}}{2NS_{\mathbf{q}}^{(\dot{\gamma})}\Gamma_{\mathbf{q}}} \int_0^\infty ds \left\langle \sigma_{xy} e^{\Omega^\dagger s} (\Omega^\dagger \varrho_{\mathbf{q}}^*) \, Q \, P_2 U(t) P_2(t) Q \Omega^\dagger \varrho_{\mathbf{q}} \right\rangle. \tag{B.9}$$

After doing this, we are on the left hand side of the projectors left with the two respective expressions,

$$\left\langle \sigma_{xy} e^{\Omega^\dagger s} \varrho_{\mathbf{q}}^* \Omega^\dagger \, Q \, \varrho_{\mathbf{q}-\mathbf{k}} \varrho_{\mathbf{k}} \right\rangle, \tag{B.10}$$

and

$$\left\langle \sigma_{xy} e^{\Omega^\dagger s} (\Omega^\dagger \varrho_{\mathbf{q}}^*) \, Q \, \varrho_{\mathbf{q}-\mathbf{k}} \varrho_{\mathbf{k}} \right\rangle. \tag{B.11}$$

Writing Q as $1 - P$, we realize that the term containing P is identical for both terms (they are real),

$$\left\langle \sigma_{xy} e^{\Omega^\dagger s} (\Omega^\dagger \varrho_{\mathbf{q}}^*) \, \varrho_{\mathbf{q}} \right\rangle \frac{1}{NS_q} \left\langle \varrho_{\mathbf{q}}^* \varrho_{\mathbf{q}-\mathbf{k}} \varrho_{\mathbf{k}} \right\rangle, \tag{B.12}$$

with opposite sign. These terms cancel each other. We are left with the two expressions,

$$\left\langle \sigma_{xy} e^{\Omega^\dagger s} \varrho_{\mathbf{q}}^* \Omega^\dagger \varrho_{\mathbf{q}-\mathbf{k}} \varrho_{\mathbf{k}} \right\rangle, \tag{B.13}$$

and

$$\left\langle \sigma_{xy} e^{\Omega^\dagger s} (\Omega^\dagger \varrho_{\mathbf{q}}^*) \varrho_{\mathbf{q}-\mathbf{k}} \varrho_{\mathbf{k}} \right\rangle. \tag{B.14}$$

Now there is in principal more than one option to treat these terms, but we will argue that only one option is applicable. The standard way, i.e., the usage of P_2 right and left of the time evolution operator is not preferable since it would not preserve the derivative with respect to s. As already mentioned, this derivative is necessary for the correct $\dot{\gamma}$-dependence. Also, this treatment would lead to a static five point correlation, whose further treatment would be delicate. Another option would be to use only one pair projector on the left hand side of the evolution operator. This would lead us to a time dependent five point correlation which is even more delicate. That is why we chose to use the triple densities projector P_3. The first of the expressions, Eq. (B.13) is written as

$$\left\langle \sigma_{xy} e^{\Omega^\dagger s} \varrho_{\mathbf{q}}^* \Omega^\dagger \varrho_{\mathbf{q}-\mathbf{k}} \varrho_{\mathbf{k}} \right\rangle \approx \left\langle \sigma_{xy} P_3(-s) e^{\Omega^\dagger s} \varrho_{\mathbf{q}}^* \Omega^\dagger \varrho_{\mathbf{q}-\mathbf{k}} \varrho_{\mathbf{k}} \right\rangle. \tag{B.15}$$

It is now clear that we have to demand that the wavevectors in the triple projector take the values of the wavevectors on the right hand side. Due to this constraint,

the summation over wavevectors in Eq. (B.2) contains only one term and no counting factor appears. The left hand side is just the Vertex $V^{(1)}_{\mathbf{qk}}$ in Eq. (B.5) for s–dependent wavevectors. Note that in (B.5), the projector Q does not make any difference. The appearing six point s-dependent correlation function is approximated as,

$$\frac{\langle \varrho^*_{\mathbf{q}} \varrho^*_{\mathbf{k}(-s)} \varrho^*_{\mathbf{k}(-s)-\mathbf{q}} e^{\Omega^\dagger s} \varrho_{\mathbf{q}} \Omega^\dagger \varrho_{\mathbf{k}} \varrho_{\mathbf{k}-\mathbf{q}} \rangle}{N^3 S_q S_{k(-s)-q} S_{k(-s)}} \approx \Phi_{\mathbf{q}}(s) \left(\left[\frac{\partial}{\partial s} - \mathbf{k}(-s) \cdot \frac{\partial}{\partial \mathbf{k}} \right] \Phi_{\mathbf{k}(-s)}(s) \Phi_{\mathbf{k}(-s)-\mathbf{q}}(s) \right). \tag{B.16}$$

This approximation rests on the observation that the operator $\Omega^\dagger$ acts as an s derivative. $\Phi_{\mathbf{k}(-s)}(s)$ and $\Phi_{\mathbf{k}(-s)-\mathbf{q}}(s)$ depend on s via the decay of the correlator and via the s–dependent wavevectors. Since $\Omega^\dagger$ in (B.16) represents the s–derivative with respect to correlator dynamics, we have to subtract the change in s due to the change of the wavevectors. The term in Eq. (B.14) is treated analogously with the triple density projector. Here, the approximation for the appearing six point correlation function is more straight forward, since $\Phi_{\mathbf{q}}(s)$ has no wavevector advection,

$$\frac{\langle \varrho^*_{\mathbf{q}} \varrho^*_{\mathbf{k}(-s)} \varrho^*_{\mathbf{k}(-s)-\mathbf{q}} e^{\Omega^\dagger s} (\Omega^\dagger \varrho_{\mathbf{q}}) \varrho_{\mathbf{k}} \varrho_{\mathbf{k}-\mathbf{q}} \rangle}{N^3 \, S_q \, S_{k(-s)-q} \, S_{k(-s)}} \approx \left(\frac{\partial}{\partial s} \Phi_{\mathbf{q}}(s) \right) \Phi_{\mathbf{k}(-s)}(s) \Phi_{\mathbf{k}(-s)-\mathbf{q}}(s). \tag{B.17}$$

The expressions in Eqs. (4.51a – 4.51c) follow.

C Approximations for $n^s_{\mathbf{q}}(t)$

The terms in Eq. (4.60) are approximated similarly to the coherent analogues, using the pair density projector in Eq. (3.34). The approximation for $n^{(s,1)}_{\mathbf{q}}(t)$ is then straight forward following Eqs. (B.3-B.5). Regarding the vertex, there occur simplifications,

$$V^{(s,1)}_{\mathbf{qk}} = \left\langle \sigma_{xy} \varrho^{s*}_{\mathbf{q}} Q^s \varrho_{\mathbf{k}} \varrho^s_{\mathbf{q}-\mathbf{k}} \right\rangle = k_x k_y \frac{S'_k}{k}. \tag{C.1}$$

The right hand side of the vertex is identical to Eq. (3.37),

$$V^{(s,2)}_{\mathbf{qk}} = \frac{\left\langle \varrho^s_{\mathbf{k}-\mathbf{q}} \varrho_{-\mathbf{k}} Q^s \, \Omega^\dagger_e \varrho^s_{\mathbf{q}} \right\rangle}{S_k} = \mathbf{k} \cdot \mathbf{q} \, n \, c^s_k. \tag{C.2}$$

For the memory functions $n^{(s,2)}_{\mathbf{q}}(t)$ and $n^{(s,3)}_{\mathbf{q}}(t)$ we first use the projector P^s_2 according to Eqs. (B.8) and (B.9). We note that the term corresponding to Eq. (B.12), which cancels, vanishes here in both terms independently, see the discussion around Eq. (3.55). We arrive at the expressions equivalent to Eqs. (B.13) and (B.14), reading

$$\left\langle \sigma_{xy} e^{\Omega^\dagger s} \varrho^{s*}_{\mathbf{q}} \Omega^\dagger \varrho^s_{\mathbf{q}-\mathbf{k}} \varrho_{\mathbf{k}} \right\rangle, \tag{C.3}$$

and

$$\left\langle \sigma_{xy} e^{\Omega^\dagger s} (\Omega^\dagger \varrho^{s*}_{\mathbf{q}}) \varrho^s_{\mathbf{q}-\mathbf{k}} \varrho_{\mathbf{k}} \right\rangle. \tag{C.4}$$

On first sight, it seems not necessary to use the triple density projector here, since the densities on the right hand side might reduce to a pair density and the dependence on $\varrho^s_{\mathbf{q}}$ might drop out. The author did not find a way to perform this simplification while conserving the interpretation of the derivative with respect to s, which is necessary to achieve the correct $\dot{\gamma}$-dependence. We hence use the triple density projector

$$P^s_3(t) \approx \sum_{\mathbf{k}>\mathbf{p}>\mathbf{n}} \frac{\varrho^s_{\mathbf{k}(t)} \varrho^s_{\mathbf{p}(t)} \varrho_{\mathbf{n}(t)} \rangle \langle \varrho^s_{\mathbf{k}(t)} \varrho^s_{\mathbf{p}(t)} \varrho_{\mathbf{n}(t)}}{N S_{n(t)}}, \tag{C.5}$$

according to Eq. (B.15). The discussions around Eqs. (B.16) and (B.17) hold. We finally arrive at

$$n_{\mathbf{q}}^{(s,1)}(t) = \frac{\dot\gamma}{2nq^2}\int\frac{d^3k}{(2\pi)^3}V^{(s,1)}_{\mathbf{qk}(-t)}V^{(s,2)}_{\mathbf{qk}}\Phi_{\mathbf{k}(-t)}(t)\Phi^s_{\mathbf{k}(-t)-\mathbf{q}}(t), \tag{C.6a}$$

$$n_{\mathbf{q}}^{(s,2)}(t) = \frac{\dot\gamma}{2nq^2}\int_0^\infty ds\int\frac{d^3k}{(2\pi)^3}V^{(s,1)}_{\mathbf{qk}(-s)}V^{(s,2)}_{\mathbf{qk}(t)}\Phi^s_{\mathbf{q}}(s) \left(\left[\frac{\partial}{\partial s}-\mathbf{k}'(-s)\cdot\frac{\partial}{\partial\mathbf{k}}\right]\Phi_{\mathbf{k}(-s)}(s)\Phi^s_{\mathbf{k}(-s)-\mathbf{q}}(s)\right)\Phi_{\mathbf{k}}(t)\Phi^s_{\mathbf{k}-\mathbf{q}}(t), \tag{C.6b}$$

$$n_{\mathbf{q}}^{(s,3)}(t) = \frac{-\dot\gamma}{2nq^2}\int_0^\infty ds\int\frac{d^3k}{(2\pi)^3}V^{(s,1)}_{\mathbf{qk}(-s)}V^{(s,2)}_{\mathbf{qk}(t)}\left(\frac{\partial}{\partial s}\Phi^s_{\mathbf{q}}(s)\right) \Phi_{\mathbf{k}(-s)}(s)\Phi^s_{\mathbf{k}(-s)-\mathbf{q}}(s)\Phi_{\mathbf{k}}(t)\Phi^s_{\mathbf{k}-\mathbf{q}}(t). \tag{C.6c}$$

We evaluate these expressions numerically, using the approximation (4.54) for the coherent correlator and a similar approximation for the incoherent one, motivated by the solution for the correlator near the critical plateau in Eq. (3.53). We neglect the anisotropic part and write for long times in glassy states

$$\Phi^s_{\mathbf{q}}(t)\approx\Phi^s_q(t)=f^s_q\exp\left(-\frac{h^s_q}{f^s_q}c\,|\dot\gamma|t\right). \tag{C.7}$$

We use again $c=3$. We consider the case where the tagged particle has the same size as the bath particles, for which $c^s_q=(S_q-1)/(nS_q)$ holds. For the numerical evaluation of (C.6), we use the grid $k_{max}=25$, $\Delta k=0.2$, $\Delta\theta=\pi/40$ and $\Delta\phi=\pi/20$ (z-direction) and $\Delta\theta=\pi/20$ and $\Delta\phi=\pi/64$ (y-direction) or smaller to account for the different symmetries in the different directions. The time was discretized as in the coherent case.

Bibliography

[1] L. Berthier and J.-L. Barrat. *J. Chem. Phys.* **116**, 6228 (2002).

[2] R. G. Larson. *The Structure and Rheology of Complex Fluids* (Oxford University Press, New York, 1999).

[3] P. N. Pusey and W. Van Megen. *Nature* **320**, 340 (1986).

[4] P. N. Pusey and W. van Megen. *Phys. Rev. Lett.* **59**, 2083 (1987).

[5] W. van Megen and P. N. Pusey. *Phys. Rev. A* **43**, 5429 (1991).

[6] W. van Megen and S. Underwood. *Phys. Rev. Lett.* **70**, 2766 (1993).

[7] W. van Megen and S. Underwood. *Phys. Rev. E* **49**, 4206 (1994).

[8] W. van Megen, T. C. Mortensen, J. Müller, and S. R. Williams. *Phys. Rev. E* **58**, 6073 (1998).

[9] P. Hébraud, F. Lequeux, J. Munch, and D. J. Pine. *Phys. Rev. Lett.* **78**, 4657 (1997).

[10] W. Götze. *Liquids, freezing and glass transition* ed J.-P. Hansen, D. Levesque and J. Zinn-Justin (Amsterdam, 1991) p 287.

[11] *Soft and fragile Matter* ed M. E. Cates and M. R. Evans (Scottish Universities Summer School in Physics & Institute of Physics Publishing, Bristol & Philadelphia).

[12] R. Besseling, E. R. Weeks, A. B. Schofield, and W. C. K. Poon. *Phys. Rev. Lett.* **99**, 028301 (2007).

[13] J. J. Crassous, M. Siebenbürger, M. Ballauff, M. Drechsler, D. Hajnal, O. Henrich, and M. Fuchs. *J. Chem. Phys.* **128**, 204902 (2008).

[14] J. Zausch, J. Horbach, M. Laurati, S. Egelhaaf, J. M. Brader, Th. Voigtmann, and M. Fuchs. *J. Phys.: Condens. Matter* **20**, 404210 (2008).

[15] J. K. G. Dhont. *Phys. Rev. E* **60**, 4534 (1999).

[16] J. Bender and N. J. Wagner. *J. Rheol.* **40**, 899 (1996).

[17] C. B. Holmes, M. E. Cates, M. Fuchs, and P. Sollich. *J. Rheol.* **49**, 237 (2005).

[18] M. Fuchs. *Advances in Polymer Science* Submitted, ArXiv:0810.2505 (2008).

[19] J. Bergenholtz. *Current Opinion in Colloid & Interface Science* **6**, 484 (2001).

[20] J. K. G. Dhont. *An Introduction to Dynamics of Colloids* (Elsevier science, Amsterdam, 1996).

[21] M. Fuchs and M. E. Cates. *J. Phys.: Cond. Mat.* **17**, 1681 (2005).

[22] H. Risken. *The Fokker-Planck Equation* (Springer, Berlin, 1984).

[23] E. D. Elrick. *Austral. J. Phys.* **15**, 283 (1962).

[24] G. I. Taylor. *Proc. Roy. Soc. A* **219**, 186 (1953).

[25] G. I. Taylor. *Proc. Roy. Soc. A* **223**, 446 (1954).

[26] G. I. Taylor. *Proc. Roy. Soc. A* **225**, 473 (1954).

[27] M. Fuchs and M. E. Cates. *Faraday Discuss.* **123**, 267 (2003).

[28] M. Fuchs and M. E. Cates. *Phys. Rev. Lett.* **89** (2002).

[29] J.-P. Hansen and I. R. McDonald. *Theory of Simple Liquids – 2nd ed.* (Academic press limited, London, 1986).

[30] R. Zwanzig. *J. Chem. Phys.* **33**, 1338 (1960).

[31] R. Zwanzig. *Phys. Rev.* **124**, 983 (1961).

[32] H. Mori. *Phys. Rev.* **112**, 1829 (1958).

[33] H. Mori. *Prog. Theor. Phys.* **33**, 423 (1965).

[34] R. Zwanzig. *Nonequilibrium Statistical Mechanics* (Oxford University Press, 2001).

[35] U. Bengtzelius, W. Götze, and A. Sjölander. *J. Phys. C.: Solid State Phys.* **17**, 5915 (1984).

[36] E. Leutheusser. *Phys. Rev. A* **29**, 2765 (1984).

[37] W. Götze and L. Sjögren. *Rep. Prog. Phys.* **55**, 241 (1992).

[38] M. Fuchs. *Transp. Theory Stat. Phys.* **24**, 855 (1995).

[39] H. Z. Cummins. *J. Phys.: Condens. Matter* **11**, A95 (1999).

[40] M. E. Cates. *Annales Henri Poincaré* **4**, 647 (2003).

[41] S. P. Das. *Rev. Mod. Phys.* **76**, 785 (2004).

[42] D. R. Reichman and P. Charbonneau. *J. Stat. Mech.* page P05013 (2005).

[43] K. Miyazaki and D. R. Reichman. *Phys. Rev. E* **66**, 050501 (2002).

[44] K. Miyazaki, D. R. Reichman, and R. Yamamoto. *Phys. Rev. E* **70**, 011501 (2004).

[45] T. Franosch, M. Fuchs, W. Götze, M. R. Mayr, and A. P. Singh. *Phys. Rev. E* **55**, 7153 (1997).

[46] W. Götze. *Z. Phys. B* **60**, 195 (1985).

[47] M. Fuchs and M. Ballauff. *J. Chem. Phys.* **122**, 094707 (2005).

[48] M. Fuchs and M. Ballauff. *J. Chem. Phys.* **125**, 204906 (2006).

[49] R. Kubo, M. Toda, and N. Hashitsume. *Statistitical Physics 2* (Springer, Berlin, 1985).

[50] J. M. Brader, Th. Voigtmann, M. E. Cates, and M. Fuchs. *Phys. Rev. Lett.* **98**, 058301 (2007).

[51] J. M. Brader, M. E. Cates, and M. Fuchs. *Phys. Rev. Lett.* **101**, 138301 (2008).

[52] W. Götze. *Z. Phys. B* **56**, 139 (1984).

[53] Th. Voigtmann. *Schematische Modelle der Modenkopplungstheorie mit Hoppingterm* (Diploma Thesis, Technische Universität München, 1998).

[54] M. Fuchs, W. Götze, I. Hofacker, and A. Latz. *J. Phys.: Condens. Matter* **3**, 5047 (1991).

[55] Th. Voigtmann and M. Fuchs, unpublished.

[56] D. Hajnal. *Scaling laws in the Rheology of Colloidal Dispersions* (Diploma Thesis, Universität Konstanz, 2007).

[57] A. W. Lees and S. F. Edwards. *J. Phys. C.: Solid State Phys.* **5**, 1921 (1972).

[58] M. Fuchs and K. Kroy. *J. Phys.:Condens. Matter* **14**, 9223 (2002).

[59] W. Götze and A. Latz. *J. Phys.:Condens. Matter* **1**, 4169 (1989).

[60] M. Fuchs and M. E. Cates. *J. Rheol.* Submitted (2008).

[61] O. Henrich, O. Pfeifroth, and M. Fuchs. *J. Phys: Condens. Matter* **19**, 205132 (2007).

[62] D. Hajnal, O. Henrich, J. J. Crassous, M. Siebenbürger, M. Drechsler, M. Ballauff and M. Fuchs. *AIP Conference Proceedings* **1027**, 674 (2008).

[63] Th. Voigtmann, private communication.

[64] M. Krüger and M. Fuchs. *Phys. Rev. Lett.* **102**, 135701 (2009).

[65] F. Varnik. *Complex Systems* ed M. Tokuyama and I. Oppenheim (Amer. Inst. of Physics, 2008) p 160.

[66] F. Weysser, private communication.

[67] D. R. Foss and J. F. Brady. *J. Fluid. Mech.* **410**, 243 (1999).

[68] A. Sierou and J. F. Brady. *J. Fluid. Mech.* **506**, 285 (2004).

[69] A. M. Leshansky and J. F. Brady. *J. Fluid. Mech.* **527**, 141 (2005).

[70] J. F. Morris and J. F. Brady. *J. Fluid. Mech.* **312**, 223 (1996).

[71] K. Kawasaki and J. D. Gunton. *Phys. Rev. A* **8**, 2048 (1973).

[72] M. Fuchs. *Die α-Relaxation einfacher Flüssigkeiten* (PhD Thesis, Technische Universität München, 1993).

[73] K. Kawasaki. *Physica A* **215**, 61 (1995).

[74] B. Cichocki and W. Hess. *Physica A* **141**, 475 (1987).

[75] F. G. Tricomi. *Integral Equations* (Interscience Publishers, New York, 1957).

[76] T. Franosch and W. Götze. *J. Phys.: Condens. Matter* **6**, 4807 (1994).

[77] M. Fuchs, W. Götze, and M. R. Mayr. *Phys. Rev. E* **58**, 3384 (1998).

[78] W. Götze and L. Sjögren. *J. Math. Anal. Appl.* **195**, 230 (1995).

[79] M. Fuchs, private communication.

[80] J. Bergenholtz, J. F. Brady, and M. Vivic. *J. Fluid Mech.* **456**, 239 (2002).

[81] Th. Voigtmann, A. M. Puertas, and M. Fuchs. *Phys. Rev. E* **70**, 061506 (2004).

[82] J. Zausch, private communication.

[83] G. Doetsch. *Einführung in Theorie und Anwendung der Laplace-Transformation* (Birkhäuser, Stuttgart, 1970).

[84] L. Sjögren. *Phys. Rev. A.* **33**, 1254 (1986).

[85] D. Forster. *Hydrodynamic Fluctuations, Broken Symmetry, and Correlation Functions* (Benjamin, Reading, MA, 1975).

[86] A. Einstein. *Annalen der Physik* **17**, 459 (1905).

[87] F. Schwabl. *Statistische Mechanik* (Springer, Berlin, 2000).

[88] F. Schwabl. *Quantenmechanik für Fortgeschrittene* (Springer, Berlin, 2000).

[89] H. Nyquist. *Phys. Rev.* **32**, 110 (1928).

[90] A. Crisanti and F. Ritort. *J. Phys. A* **36**, R181 (2003).

[91] G. S. Agarwal. *Z. Physik* **252**, 25 (1972).

[92] T. Speck and U. Seifert. *Europhys. Lett.* **74**, 391 (2006).

[93] V. Blickle, T. Speck, C. Lutz, U. Seifert, and C. Bechinger. *Phys. Rev. Lett.* **98**, 210601 (2007).

[94] L. Berthier, J.-L. Barrat, and J. Kurchan. *Phys. Rev. E* **61**, 5464 (2000).

[95] C. Godrèche and J. M. Luck. *J. Phys. A: Math. Gen.* **33**, 1151 (2000).

[96] C. Godrèche and J. M. Luck. *J. Phys. A: Math. Gen.* **33**, 9141 (2000).

[97] P. Calabrese and A. Gambassi. *Phys. Rev. E* **65**, 066120 (2002).

[98] P. Mayer, L. Berthier, J. P. Garrahan, and P. Sollich. *Phys. Rev. E* **68**, 016116 (2003).

[99] P. Sollich, S. Fielding, and P. Mayer. *J. Phys.: Condens. Matter* **14**, 1683 (2002).

[100] F. Corberi *et al. J. Phys A: Math. Gen.* **36**, 4729 (2003).

[101] P. Calabrese and A. Gambassi. *J. Stat. Mech.: Theo. Exp.* page P07013 (2004).

[102] R. J. Glauber. *J. Math. Phys.* **4**, 294 (1963).

[103] L. Berthier and J.-L. Barrat. *Phys. Rev. Lett.* **89**, 095702 (2002).

[104] J.-L. Barrat and L. Berthier. *Phys. Rev. E* **63**, 012503 (2000).

[105] C. S. O'Hern, A. J. Liu, and S. R. Nagel. *Phys. Rev. Lett.* **93**, 165702 (2004).

[106] T. K. Haxton and A. J. Liu. *Phys. Rev. Lett.* **99**, 195701 (2007).

[107] F. Zamponi, G. Ruocco, and L. Angelani. *Phys. Rev. E* **71**, 020101 (2005).

[108] I. K. Ono, C. S. O'Hern, D. J. Durian, S. A. Langer, A. J. Liu, and S. R. Nagel. *Phys. Rev. Lett.* **89**, 095703 (2002).

[109] J.-L. Barrat. *J. Phys.: Condens. Matter* **15**, S1 (2003).

[110] J.-L. Barrat and W. Kob. *Europhys. Lett.* **46**, 637 (1999).

[111] W. Kob and J.-L. Barrat. *Eur. Phys. J. B* **13**, 319 (1999).

[112] A. Latz. *J. Phys.: Condens. Matter* **12**, 6353 (2000).

[113] P. Ilg and J.-L. Barrat. *Europhys. Lett.* **79**, 26001 (2007).

[114] J. S. Langer and M. L. Manning. *Phys. Rev. E* **76**, 056107 (2007).

[115] N. Greinert, T. Wood, and P. Bartlett. *Phys. Rev. Lett.* **97**, 265702 (2006).

[116] B. Abou and F. Gallet. *Phys. Rev. Lett.* **93**, 160603 (2004).

[117] C. Maggi, R. d. Leonardo, J. C. Dyre, and G. Ruocco ArXiv:0812.0740 (2009).

[118] I. Gazuz, A. M. Puertas, Th. Voigtmann, and M. Fuchs. *Phys. Rev. Lett.* Submitted, ArXiv 0810.2627 (2008).

[119] P. Habdas, D. Schaar, A. C. Levitt, and E. R. Weeks. *Europhys. Lett.* **67**, 477 (2004).

[120] T. Harada and S. i. Sasa. *Phys. Rev. Lett.* **95**, 130602 (2005).

[121] G. Szamel. *Phys. Rev. Lett.* **93**, 178301 (2004).

[122] F. Varnik. *J. Chem. Phys.* **125**, 164514 (2006).

[123] H. Zhang and G. Nägele. *J. Chem. Phys.* **117**, 5908 (2002).

[124] J. A. McLennan. *Introduction to Non-equilibrium Statistical Mechanics* (Prentice Hall, New York, 1988).

[125] B. J. Berne and R. Pecora. *Dynamic Light Scattering: With Applications to Chemistry, Biology and Physics* (Dover Publications, Mineola, NY, 2000).

[126] M. Morse and H. Feshbach. *Methods of Theoretical Physics, part 1* (McGraw-Hill, New York, 1953).

[127] R. Graham. *Z. Physik B - Cond. Mat.* **40**, 149 (1980).

[128] L. D. Landau and E. M. Lifshitz. *Course of Theoretical Physics, Volume 6: Fluid Mechanics* (Pergamon Press, Oxford, 1959).

[129] Monty Python, *Monty Python and the Holy Grail*, Scotland 1975.

[130] D. J. Pine, J. P. Gollub, J. F. Brady, and A. M. Leshansky. *Nature* **438**, 997 (2005).

[131] J. P. Gollub and D. J. Pine. *Physics Today* **59**, 8 (2006).

[132] J. P. Bouchaud. *J. Phys. I* **2**, 1705 (1992).

[133] A. Barrat and M. Mézard. *J. Phys. I* **5**, 941 (1995).

[134] C. Monthus and J. P. Bouchaud. *J. Phys. A* **29**, 3847 (1996).

[135] B. Rinn, P. Maass, and J. P. Bouchaud. *Phys. Rev. Lett.* **84**, 5403 (2000).

[136] S. Fielding and P. Sollich. *Phys. Rev. Lett.* **88**, 050603 (2002).

[137] S. M. Fielding, P. Sollich, and M. E. Cates. *J. Rheol.* **44**, 323 (2000).

[138] C. W. Gardiner. *Handbook of Stochastic Methods* (Springer, Berlin, 1985).

[139] J. Schofield and I. Oppenheim. *Physica A* **181**, 89 (1992).

[140] J. Schofield and I. Oppenheim. *Physica A* **187**, 210 (1992).

[141] W. Götze and L. Sjögren. *J. Phys. C: Solid State Phys.* **17**, 5759 (1984).

[142] R. J. Baxter. *J. Chem. Phys.* **41**, 553 (1964).

[143] J.-L. Barrat, J.-P. Hansen, and G. Pastore. *Phys. Rev. Lett.* **58**, 2077 (1987).